ADDIS ABABA UNIVERSITY

COLLEGE OF NATURAL AND COMPUTATIONAL SCIENCES

SCHOOL OF EARTH SCIENCES

ASSESSING IMPACT OF LAND USE/COVER PRACTICES ON RESERVOIR CAPACITY THROUGH EROSION AND SEDIMENTATION IN GILGEL GIBE III DAM, SOUTHWESTERN ETHIOPIA

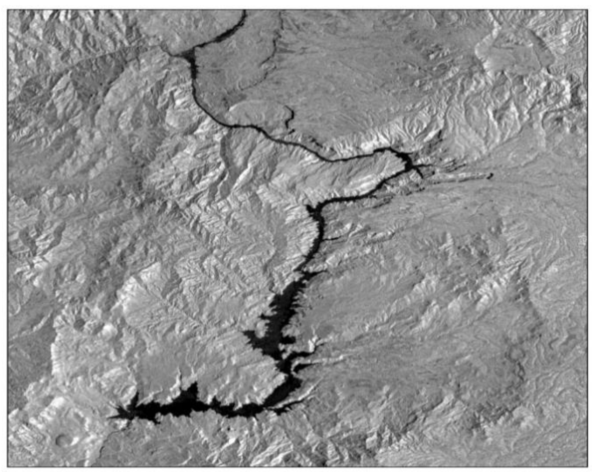

A Thesis Submitted to the School of Graduate Studies of Addis Ababa University in Partial Fulfillment of the Requirements for the Degree of Masters of Science In Remote Sensing and Geo-Informatics.

By:

Ayele Akirso

ID No. GSR/2019/12

ADVISER: Dr. DAGNACHEW LEGESSE

CO-ADVISER: Dr. BINYAM TESFAW

JUNE, 2021

ASSESSING IMPACT OF LAND USE/COVER PRACTICES ON RESERVOIR CAPACITY THROUGH EROSION AND SEDIMENTATION IN GILGEL GIBE III DAM, SOUTHWESTERN ETHIOPIA

AYELE AKIRSO

A Thesis Submitted to

School of Earth Sciences

Presented in Partial Fulfillment of the requirements for the Degree of Master of Science in

(Remote sensing and Geo-informatics)

Addis Ababa, Ethiopia

June, 2021

DECLARATION

I hereby declare that the research entitled: "Assessing impact of land use/cover practices on reservoir capacity through erosion and sedimentation in Gilgel Gibe III dam, Southwestern Ethiopia" is being submitted by me in the partial fulfillment of the requirements for the degree of Master of Science in (Remote sensing and Geo-informatics). The matter embodies in this study has not been submitted to any other Universities or institutions for the award of degree. The thesis work is my original work and it has not been presented earlier in this manner. All sources of materials used for the thesis have been duly acknowledged.

Ayele Akirso Adugna

Signature ________________________________ Date__________________________

School of Earth Sciences

June, 2021

SIGNATURE PAGE

Addis Ababa University

Graduate Studies

This is to certify that the thesis prepared by AYELE AKIRSO, entitled: "Assessing impact of land use/cover practices on reservoir capacity through erosion and sedimentation in Gilgel Gibe III dam, Southwestern, Ethiopia" and submitted in partial fulfillment of the requirements for the Degree of Masters of Science in Remote sensing and Geo-informatics complies with the regulations of the University and meets the accepted standards with respect to the originality and quality.

Signed by The Examining Committee:

Advisor: Dr. Dagnachew Legesse Signature ___________________ Date ______________

Co-Advisor Dr. Binyam Tesfaw Signature ___________________ Date ______________

Examiner: Dr. K.V.Suryabhagavan Signature __________________Date________________

Examiner: Dr. Tibebu Kassawmar Signature____________________ Date ______________

Chairperson: Dr. K.V.Suryabhagavan Signature________________ Date___________________

____

Chair of School or Graduate Program Coordinator

ACKNOWLEDGEMENTS

Thanks to the Almighty God ‘for all thing that happens to have happened through my life!

First of all, I would like to express my deep sense of gratefulness to my advisors Dr. Dagnachew Legesse and Dr.Binyam Tesfaw for their leading and constructive comments, generous support, continuous guidance and feedback throughout the thesis process made this study possible.

I am glad to Wolaita Sodo University for sponsoring me to pursue my post-graduate study at Addis Ababa University. This is a great opportunity to thank Addis Ababa University School of Earth Sciences staff members directly or indirectly for their support during my study period.

I would like to express my warm thankfulness to Regional Centre for Mapping of Resources for Development/ Global Monitoring for Environment and Security RCMRD/GMES and Africa Scholarship Grants who helped to achieve this work on time and motivating to use European Space Agency (ESA) free SAR, and optical Remote Sensing Data. They give the grant to access field logistics, to use my full time on this work, and other supportive materials for my thesis, free data access, software access, and unbelievable limitless guidance. Generally, they helped me to learn and conduct my research work. I also like to acknowledge the United Geological Survey, Ethiopian Metrological Agency, Ethiopian Electrical Power, Ethiopian Basin Development Authority, Geological Survey of Ethiopia, for providing the necessary data and information to carry out this research.

Finally, I would like to express my special thanks to my instructors, family, and friends they were close to me in all aspect of my life. All names could not be mentioned separately because of their independent encouragement and cooperation and my friends. Thanks!

TABLE OF CONTENTS

LIST OF FIGURES

LIST OF TABLES

APPENDICES

LIST OF ACRONYMS

ALOS PALSAR	Advanced Land Observation Satellite Phased Array type L-band Synthetic Aperture Radar
ASF	Alaska Satellite Faculty
BMC	Billion Cubic Meters
CHRS	Center for Hydrometeorology and Remote Sensing
cumyr	Cubic Meter per year
DEM	Digital Elevation Model
EMA	Ethiopian Metrological Agency
ENVI	Environment for Visualizing Images
EOS	Earth Observation System
ERDAS	Earth Resource Data Analysis System
EBDA	Ethiopian Basin Development Authority
EEPOW	Ethiopian Electric Power
ESA	European Space Agency
ETM+	Enhanced Thematic Mapper plus
FAO	Food and Agriculture Organization
GGIIID	Gilgel Gibe Three Dam
GIIE	Geospatial Information Institute of Ethiopia
GIS	Geographic Information System
GSNS	Global Satellite Navigation systems
GPS	Global Position Space Elevation
GRD	Ground Range Detected
GSE	Geological Survey of Ethiopia
ha	Hectare
HEC-GeoHMS	Hydrological Engineering Center Geospatial Hydrologic Modeling System
HEC-RAS	Hydrological Engineering Center for River Analysis System
HEP	Hydroelectric Power

HWDB	Harmonized World Soil Database
LULC	Land use land cover
MSI	Multispectral Instrument
MUSLE	Modified Universal Soil Loss Equation
MNDWI	Modified Normalized Difference Water Index
MRSE	Mean Rate of Soil Erosion
MRSY	Mean Rate of Sediment Yield
MW	Mega Watts
NDWI	Normalized Difference Water Index
OLI	Operational Land Imagery
OGRBDMP	Omo-Gibe River Basin Development Master Plan
RADAR	Radio Detection And Ranging
RUSLE	Revised Universal Soil Loss Equation
SAR	Synthetic Aperture Radar
SE	Soil Erosion
SNAP	Sentinel Application Platform
SNNPR	Southern Nations and Nationality of Peoples Region
SDR	Sediment Delivery Ratio
SY	Sediment Yield
USDA	United States Department of Agriculture
USGS	United States Geological Survey
USLE	Universal Soil Loss Equation
WGS	World Geodetic System

ABSTRACT

Assessing the impact of land use/cover practices on reservoir capacity through erosion and sedimentation in Gilgel Gibe III dam, Southwestern Ethiopia.

Ayele Akirso Adugna MSc. Thesis

Addis Ababa University, June 2021

Land use/cover change practice and the conversion of the natural vegetation cover into cropland, in particular, are major human-induced problems in Ethiopia. This has played a substantial role in increasing the rate of soil erosion, sediment yield, and reducing the designed reservoir storage capacity of hydroelectric power in the country. The study evaluates various land cover change and their impact on the reservoir capacity, through erosion and sedimentation. Time series Landsat images of (2001–2015) and Sentinel-2A of (2020) besides Sentinel-1 data were used to assess land cover change and reservoir area dynamics. Both supervised and unsupervised land use classification technique; Kappa statistics assessment for accuracy of the classification; post-classification method for change evaluation; Integrated model of the revised universal soil loss equation (RUSLE) and the sediment delivery ratio (SDR) along streamline to estimate soil erosion and sediment yield; threshold approach of Radar and normalized difference water index (NDWI) delineated water spread area for the water year of 2016-20; the Trapezoidal and Mid Area system was applied to estimate the live storage capacity of a reservoir with the elevation. Five land cover maps (2001-2020) were undertaken and six classes were classified. Over all accuracy and Kappa coefficient were above eighty percent agreed with classified land cover. Land cover change assessment resulted that 15 percent change took place between grassland and cropland which is the highest conversion. The mean rate of soil erosion (t/ha/yr) rises from 1093.9 in 2001 to 4222.7 in 2020 while the corresponding sediment yield along streamlines increased from 573.3 to 609t/ha/yr for the same period. Grassland accounts for the highest soil erosion (t/ha/yr.) 1085 and 770.5 in 2001 and 2020. The area (sq. km) of Gilgel Gibe III reservoir augmented starting from 121.5 in 2016 to 195.8 in 2020. The original live storage capacity (2015) was 11750 Mm3 at a normal operating level of 855m. The estimated live storage capacity was 9511.4 Mm^3 at 889. 9 m and has reduced from 11750 Mm^3 (2015) to 9511.4 Mm^3. Finally, the percentage coverage of cropland area is 43 following grassland 41.8 in 2020 and the mean rate of soil erosion and analogous sediment yield in the same year of the catchment were 4,222.7 and 609 t/ha/yr. respectively. The study advocates watershed management by planting tries and land controlling practices from erosion.

Keywords: Land use/cover, Revised Universal Soil Loss Equation; Normalized Difference Water Index, Trapezoidal, Gilgel Gibe III Dam, Radar

CHAPTER-1 INTRODUCTION

1.1 Background of the study

Globally, human activities have been changing the terrestrial environment at an alarming rate, magnitude, and spatial scales (Turner, 1994; Schneider, 2001). Such modifications are linked to economic development, population growth, and/or technological advancements, while human use of land relates to the cultivation of various forms, livestock grazing, settlement, protected lands, or timber extraction. Land-use/ cover (LULC) has two separate terminologies that are often used interchangeably (Rawat *et al*., 2015). Land cover refers to the biophysical characteristics of the earth's surface, including the distribution of vegetation, water, soil, and other physical features of the land. While land use refers to how the land has been used by humans and their habitat, usually with an emphasis on the functional role of land for economic activities (McConnell *et al*., 2015). Mapping and detecting land-use/cover and its change is the most significant, as well as the most widely researched, topic in remote sensing. Land-use/cover has been used extensively to derive many biophysical variables, such as vegetation index, biomass, and carbon content. More importantly, land-use/ cover pattern and its change reflect the underlying natural and/or social processes, thus providing essential information for modeling and understanding many different phenomena on the Earth. It is possible to establish a model to predict the trends in land-use/cover in a certain time through the study of past land-use changes, which could provide some basis for scientific and effective land-use planning, management, and ecological restoration in a study area and guidance for regional socio-economic development (Yogendra *et al*., 2019). Knowledge of land-use/cover and its change is also critical to effective planning and management of natural resources (Lam, 2008).

Reservoir sedimentation is the filling up of a dam with sediment, which leads to a loss in the capacity of the reservoir. Sedimentation is an unstoppable process but can only be controlled through suitable measures of upstream reservoir catchment. Particles may eventually find their way to the lake or river bed where they become deposited; this is known as Sedimentation. Soil Erosion is a common term that is often confused with soil degradation as a whole but refers only to absolute soil losses in terms of topsoil or sediment and nutrients (FAO, 2008). Sedimentation in reservoirs is the major constraint on the safety of dams, energy production, and flood threat. Its estimation is very much important to know the changing elevation and reservoir capacity. Estimation of reservoir capacity through conventional surveys such as hydrographic surveys is tedious; time and money-consuming (Prasad *et al*., 2018). Reservoirs are normally constructed across rivers and have crucial roles such as water supply, irrigation, discharge regulation, Electric power generation, and flood control. As the hydraulic process, rivers and streams within a catchment are continuously provided with sediment from run-off, rainfall, snowmelt, and the erosion of river channel, which get deposited in the reservoir (Merina *et al*., 2016). A reservoir is typically positioned at the end of a catchment and so collects inflows from various major rivers (Jorgensen *et al*., 2005).

According to the geospatial awareness hub, (2020), Geospatial Technology is one of the evolving fields that involve Remote Sensing, Geographic Information Systems (GIS), and Global Satellite Navigation systems (GSNS). It enables to access data about the earth and makes informed decisions depending on the significance and priority of the resources. Geospatial technology provides a plentiful opportunity in this field through the availability of high-resolution satellite data from sensors such as Sentinel, Indian Remote Sensing Satellite, Landsat, and SPOT all of which can be used to calculate the water spread area of the reservoir (Prasad *et al*., 2018). Since the water flows within a reservoir with a very low velocity, reservoirs tend to be very efficient sediment traps leading to a reduction in transport capacity and increment in the sedimentation deposition in the reservoir (Merina *et al*., 2016).

Human activities and the interventions in the upstream watershed also contribute to accelerated reservoir sedimentation. Although there is the fact that soil erosion results from the geomorphologic process, accelerated soil erosion is primarily favored by human activities (Foteh *et al*., 2018). Rapid population growth, deforestation, unsuitable land cultivation, and uncontrolled overgrazing have caused accelerated soil erosion in the world principally in developing countries (Abebe and Sewnet, 2014; Tamene, 2006). According to Merina *et al*., (2016), most of the reservoirs accompanying dams on natural rivers are vulnerable to some level of sediment deposition and inflow. Approximately 40,000 large reservoirs around the world are facing sedimentation issues, and it is predicted that their total storage capacity is being lost between 0.5 and 1% per year (Merina *et al*., 2016). Therefore, it is essential to estimate or quantify the sedimentation of the project for the whole of its life, so that an appropriate conservation strategy can be implemented.

Many of Ethiopia's hydroelectric power and irrigation reservoirs such as Aba-Samuel, Koka, Angerib, Melka Wakena, Borkena, Adarko, and Legedadi has been threatened by heavy sedimentation (Gelagay *et al*., 2016). According to the Free Encyclopedia (2020), The Gilgel Gibe III dam construction began in 2006 and opened for service in October 2015. It is the third-largest hydroelectric plant in Africa with a total construction cost of US$1.8 billion and the purpose was to generate hydroelectric power of 1870 megawatt (MW). It is part of a cascade, a series of dams including the existing, Gibe I dam (184MW) and Gibe II power station (which produce 420MW) as well as the planned and under construction Gibe IV (1472MW) and Gibe V (560MW) dams. The Gilgel Gibe III Dam is a 610 m-long and 243 m high roller-compacted concrete dam. The reservoir has a capacity of 14.7cu. Km and a surface area of 200 sq. km, with a catchment area of 34,150 sq. km. The reservoir's live (active or "useful") storage is 11.75 Cu.km and dead storage 2.95cu. Km. The normal operating level of the reservoir is 892 m above sea level with a maximum of 893 m and a minimum of 800 m a.s.l. The dam's spillway is 108 m long and floodgate-controlled with a maximum discharge capacity of 18,000 cubic meters per second. Water above 873 m above sea level can be discharged through its gates. Feeding the dam's powerhouse are two penstocks that each branch into five separate tunnels for each turbine. The powerhouse contains ten 187 MW generators supported by Francis turbines for a total installed capacity of 1,870 MW.

1.2 Statement of the problem

Dam reservoirs are man-made water bodies that to keep functioning and to be considered volumetrically healthy for a designed lifespan need constant assessment (Borghero, 2018). Sedimentation processes related to watershed activities, river characteristics, and reservoir design are lowering the water storage capacity and threaten reservoir functionality (Pandey *et al*., 2016). Sedimentation is a major problem in reservoirs and dams as it reduces water storage capacity, thus indirectly reducing electricity production besides shortening the lifetime and increasing the maintenance cost (Devi *et al*., 2008). Unfortunately, numerous reservoirs stop performing their designed functions due to sediment deposition (Ijam and Al-Mahamid 2012; Merina *et al*., 2016). Eventually, the transported sediments can be deposited at various levels of a reservoir leading to a reduction in the storage capacity of the reservoir (Foteh *et al*., 2018).

According to Abreham, (2020) Sediment delivery to a given watercourse is increasing as catchments are progressively modified by human activities such as deforestation, agriculture expansion, construction, and urbanization. This in turn affects the life expectancy of the reservoirs.

1.3 Research questions

- ✔ What land use/cover practices are causing erosion and sedimentation in reservoir catchment?
- ✔ What are the areal dynamics of the reservoir?
- ✔ What are the temporal dynamics of the storage capacity of the reservoir?
- ✔ What is the rate of soil erosion and sediment yield of the catchment?

1.4 Objectives of the study

1.4.1 The general objective of the study

- ❖ The main objective of the study is to assess the various land use/cover practices and their impact on the reservoir capacity, through erosion and sedimentation on the Gilgel Gibe III Dam by using satellite images, soil erosion modeling, and hydrographic data.

1.4.2 Specific objectives of the study

- ➢ To conduct land use/cover change detection in the Dam's catchment over the recent decades using various satellite images.
- ➢ To estimate soil erosion with RUSLE modeling, sediment yield with SDR, and assess the impact of land use/cover changes on the dam catchment.
- ➢ To analyze the areal dynamics of the reservoir with both Sentinel -1 RADAR and Optical images.
- ➢ To analyze bathymetry of the reservoir capacity with a designed storage capacity

1.5 Significance of the study

The significance of this study will be to increase the habit of sediment controlling from going down to reservoir area filling and to use the proposed lifespan of the reservoir. The proposed study will identify the most vulnerable places to erosion in the study area. Currently, the reservoir serves for fish farming; recreation, and transportation in addition to HEP, which are further incentives to control the area from excessive sedimentation. Moreover, the country Gebeta Project and the long-lived Kawo Halala Kela (King Halal stone Wall) are found in the study area and that will benefit from the study.

Generally, after the completion of the study will have the following significances:

- Enables to identify Erosion prone places in the study area
- Enables to know the dynamic storage capacity of the reservoir
- Enables to know the rate of the sediment in the catchment
- Provide relevant information that will contribute to the environmental management and erosion controlling the activity
- It will serve as an input for further studies

1.6 The scope of the study

The study focused on the land-use/cover practices assessment for recent decades and estimation of reservoir capacity from years 2016-2020 in the Gilgel Gibe III dam of the lower Gibe river (middle Omo basin) catchment. The rate of sediment loss (erosion) estimation was another part of the study that will be analyzed.

Generally, the scope of the study covers the following:

- Estimation of reservoir level from hydrography and satellite data for five years
- Assessing land use/land cover practices impact on reservoir capacity from satellite data for consecutive twenty-year of five-year interval.
- Estimation of the rate of sediment in the reservoir catchment per year
- Assessment of the applied RUSLE model for sediment loss (Soil erosion)

1.7 Limitation of the study

The limitations of the study were the lack of precise secondary data for sediment yield validation in the study area. The extent of the study area that covers a large area of the Omo river basin, that challenges the analysis of all data in the catchment and to get validated data. Another was a lack of historical data of the study area and previous research work. In addition, meteorology data interpolation for the whole study area having two gauging stations in the catchment and has also incompleteness of the data record. Furthermore, challenge was occurred to process huge radar image processing which could propagate errors in the result. Nevertheless, this study provides valuable information and insight that can be of great importance for the relevant information regarding the impact of land use land cover change assessment, soil erosion, sediment yield, and reservoir capacity assessment, but the study was not much affected by the limitations.

1.8 Thesis Chapters organization

This thesis is composed of six chapters. The first chapter is about an introduction to the subject and presents the statement of the problem, research objectives, and scope of the study. Chapter two gives an overview of remote sensing and GIS technology in land-use/cover studies, soil erosion, sediment yield, reservoir capacity assessment and it introduces the previous studies ‘in the Omo basin of Ethiopia as well as the study area in the basin. Chapter three presents a detailed description of the study area, the datasets that were used, and the overall explanation, applied to conduct the research, materials used, and methods applied to perform the study. Chapter four explains results and chapter is about the discussion of the study, the results, which mainly introduces the results and findings primarily leading to a map of land-use/cover, accuracy assessment, soil erosion, and sediment yield, and reservoir capacity of the study area. The discussion parts of this work talk about findings and previous work of the same work. Finally, chapter six addresses the conclusion and recommendations.

CHAPTER-2 LITERATURE REVIEW

Preamble

Global measurements of reservoir water levels are crucial for understanding Earth's hydrological dynamics, especially in the context of global industrialization and climate change (Park *et al*., 2020). At present, retention basins, reservoirs and polder systems, inundation plains, discharge channels, and river regulation are still the main methods used for flood control, irrigation, navigation, and Hydropower (Jorgensen *et al*., 2005). The time of the estimate is important since new reservoirs are continuously being constructed, while the volumes of some lakes are diminishing significantly because of mismanagement and unsustainable use (e.g., Aral Sea, Lake Chad). Anthropogenic disturbances have direct impacts on ecosystem health. One such impact is the depletion of soil resources. The hydrological behavior of a watershed in the basin has multiple biophysical factors interplaying diversely in time and space. Land-use/cover (LULC) dynamics, and the modification of the natural vegetation cover replacing with cultivation practice, in particular, are major human-induced problems in Ethiopia, which have played a significant role in increasing the rate of soil erosion and altering the hydrological balance in the country (Ajanaw Negese, 2021). Over generations, dams and reservoirs have work for multi-purposes including energy production, domestic water supply, flood control, agriculture, industry, recreation, and fishing. However, the construction and operation of a reservoir often cause considerable ecological disturbances within the streamflow network. As a result, reservoirs frequently drive serious environmental concerns (Clement, 2017; Zhang *et al*., 2009).

2.1 Sedimentation and Omo basin

Sedimentation is an important parameter to assess the life span of a reservoir. Seventy-eight years ago, Cook was the first to identify mathematically, the three major factors disturbing soil erosion in the catchment of a reservoir. As sedimentation is dependent on sediment yield and sediment yield be contingent on soil erosion, it is required to predict all three parameters to estimate the functionality of a reservoir (Dutta, 2016).

2.1.1 Sedimentation and soil erosion

The problem of sedimentation is a common concern for reservoirs as it affects the storage capacity and depletes the water quality (Clement, 2017; Fan and Morris, 1992; Palmieri and Dinar, 2001). Reservoir sedimentation is, in utmost cases, caused by water erosion occurring at the watershed scale. However, the amount of sediment losses varies from one location to another depending on the watershed's biophysical characteristics (Clement, 2017; Williams, 1975).

Soil erosion is the wearing away of land topsoil by the natural physical forces of water (rainfall, glacial), gravity, and wind or through forces associated with farming activities such as tillage. The three distinct actions involved during soil erosion are: – soil detachment, movement, and deposition. Soil erosion has an adverse impact in the world that considered as the most critical issues resulting in both on-site and off-site effects (Rediet and Eshetu, 2020); Zhou *et al*., 2014); (Aiello *et al*., 2015; Zhou and Wu, 2008). Soil erosion in catchment areas and the following deposition in rivers, lakes, and reservoirs are of great concern for two reasons. First, fertile soil is worn from the catchment areas. Secondly, there is a drop in reservoir capacity as well as degradation of downstream water quality (Aiello et al., 2015; Zhou and Wu, 2008); European Environment Agency, 1995).

Soil erosion is a big challenge to natural resource management in semi-arid and arid areas, which is expressed as land degradation (Amiya *et al*., 2019). At a given location of the watershed, soil erosion depends on several factors including the local rainfall patterns, the surface runoff, the type of soil, the land cover, the soil management practices, the slope, and the watershed shape (Clement, 2017). Universally, sediment losses are often estimated and interpreted using the Universal Sediment Loss equation or its Revised and modified formulations model (Clement, 2017; Williams, 1975).

Modeling soil erosion can provide a quantitative and consistent estimation of the phenomenon under various conditions. However, these models differ greatly in terms of complexity, processes considered, and data required for model calibration and model use (Aiello *et al*., 2015; Merritt *et al*., 2003). The most appropriate model depends on several factors, such as the intended use and the characteristics of the catchment considered; data requirements; capability, accuracy, validity, and reliability of the model; the objectives of the model users; the ease of use of it; the scales at which model outputs are required; and hardware requirements. The assessment of soil erosion typically involves the use of empirical models such as the USLE (Wischmeier and Smith, 1978);

the MUSLE (Williams, 1975); the RUSLE (Renard *et al*., 1997); the RUSLE3D (Mitasova and Mitas, 1999b); the Unit Stream Power-based Erosion Deposition (USPED) (Mitas and Mitasova, 1998; Mitasova *et al*., 1996; Mitasova and Mitas, 1999a), or physically-based models such as the Areal Nonpoint Source Watershed Environmental Resources Simulation (ANSWERS) (Beasley *et al*., 1980), the Water Erosion Prediction Project (WEPP) (Nearing *et al*., 1989), and the EUROSEM (Morgan *et al*., 1998). Physically-based models attempt to reproduce the real processes and require several parameters related to each involved process such as hydrology, hydraulics, meteorology, and soil mechanics. Thus, lack of data is one of the main problems of those models. They are benefitting only on a small scale. On the contrary, empirical models are the most commonly used methods because of their simplicity of application thanks to their least data required and ease of use (Bhattarai and Dutta, 2006; Demirci and Karaburun, 2011). In the last ten years, estimation of soil erosion using empirical models has long been an active research topic. Nevertheless, their application over large areas is still a challenge. The valuation of soil erosion requires the specific soil parameters (susceptibility of soils to erosion, soil protection, etc.), as well as physical parameters (precipitation, temperature, slope, surface areas), all highly variable in space and time. Although empirical models are centered on the key factors of soil erosion processes, they differ in the processing of data and the accuracy of results. Successful monitoring can be realized with the integration of ancillary data and remotely-sensed data in a GIS environment. Soil erosion, movement, and deposition are part of natural hydrological processes, but the rate of sedimentation is fast-tracked due to environmental degradation, lack of conservation events, change in land use, deforestation, etc. (NIHRCB and WRDGCR, 2013). In following a drop of runoff down the hillslope, three distinct forms of erosion are seen in the upland areas. These are sheet erosion, rill erosion, and gully erosion (Hussen Muhammed, 2020; Marcelo *et al*., 2008).

Sheet erosion is also known as interrill erosion, occurs uniformly between rills or gullies and results primarily from raindrop impact. The washing away of a thin layer of the land surface and erosive potential of this impact depends on raindrop size, fall velocity, and total mass at impact, but can be devastating. In the absence of vegetation, mulch, or other covers to absorb the impact, raindrops can detach tremendous quantities of soil.

On the other way, if more sediment is added from the upstream areas, then the channel flow can transport significant deposition, and storage of upland sediment may occur within the channel system, in which case the channel is said to be degrading. In a stable channel, very little net erosion occurs because of equilibrium between the sediment transported out of the channel system and that added by the upland erosion processes. Rainfall causes increasing water saturation or the formation of a seal on the soil surface. Because of both processes, infiltration into the soil is decreased. Water on the soil surface occurs as soon as rain intensity begins to exceed the infiltration rate (Nill, 1996). The potential for soil erosion varies from watershed to watershed depending on the arrangement of the watershed, the soil characteristics, the local climatic conditions, and the land use and management practices implemented on the watershed. The Universal Soil Loss Equation (USLE), a plot- or field-scale model, incorporates most of these factors to estimate long-term soil erosion areas (Wischmeier *et al*., 1978). A revised form of this model (RUSLE) further enhanced its capability to predict water erosion by incorporating new information that has become available through the last 40 years of research (Renard *et al*., 1997). RUSLE, with great acceptance and wide use, is simple and easy to parameterize, and requires less data and time to run than most other models dealing with rill and inter rill erosion (Jones *et al*., 1996).

2.1.2 Sediment yield and sediment delivery ratio

Sediment yield refers to the amount of eroded sediment discharged by a stream at any given point over a period, which is also the amount that will enter a reservoir located downstream of its watershed (Vanoni, 2006). The most common unit for sediment yield is tons/year. The specific sediment yield is the yield per unit of land area which is most commonly given in tons/km2/year and (t/ha/yr.). Long-term sediment yield estimates have been used for sizing storage reservoirs and estimating reservoir life span (Morris and Fan, 1998).

Accurate estimation of sediment yield is very important to plan a reservoir and efficiently manage its sediment so that the reservoir can meet its requirements. Sediment yield is affected by geology, slope, climate, drainage density, and patterns of human disturbance and therefore, no single parameter explains the wide variability in sediment yields (Morris and Fan, 1998); (Vanoni, 2006; Lustig, 1965). Sediment yield from drier areas tends to be limited because of low runoff and yield in wetter areas is limited by the defending soil cover and reduced erodibility of humid zone soils (Vanoni, 2006).

The **sediment delivery ratio (SDR)** connects the weight of sediments eroded and transported from slopes of a watershed to the weight that eventually enters streams and rivers ending at the watershed outlet. For watershed management activities, the estimation of annual sediment yield

(SY) and sediment delivery has been the topmost priority due to the influence that sedimentation has on the holding capacity of reservoirs and the annual economic cost of sediment-related disasters (Thomas *et al*., 2020). The sediment delivery ratio was established as the relationship between the SY and the gross erosion.

2.2 Land-use and land cover

In African countries, land-use/cover changes, in general, and conversion of the natural land cover into agricultural land, in particular, are major continuous phenomena mainly caused by anthropogenic activities (Nasche *et al*., 2019).

Remote sensing is one of the tools which is very significant for the production of land use/cover maps through a process called image classification. The processing and classification of land use/cover of remote sensing data need accuracy assessment or validation for obtaining corresponding ground truth data (Rwanga and Ndambuki, 2017). Remote sensing provides broad, precise, impartial, and easily available information for quantifying the location, extent, and variability of change; the causes and processes of change; and the responses to and consequences of change. Land use has a direct link between land cover and the actions of people in their environment (Assefa Nigussie, 2017; FAO, 2021). The relevant assessment of land use/cover impact information helps to understand the state of human activities on the environmental change (Tibebu *et al*., 2016)

Catchments of the dam are sensitive to land use dynamics induced by human activities (Kidane and Bogale, 2017; Bosch and Hewlett, 1982). Land cover changes are predicted to have an important effect on river flows and sediment yields from specified catchment (Kidane and Bogale, 2017; Xing *et al*., 2009). Hydrological response dynamics (an integrated indicator of watershed conditions) and water response in different river basins are attracted by changes in land use and climate (Kidane and Bogale, 2017; Wang *et al*., 2007). Land-use/cover activities, development, and management of water resources are interdependent. Sedimentation in water resources is the outcome of land erosion in its catchment area. Land erosion fundamentally has an impact on the physical and chemical characteristics of soils and causes on-site nutrient loss and off-site sedimentation and nutrients enrichment of water resources (Kidane and Bogale, 2017; Upadhya *et al*., 2012).

To identify, prioritize and compare watersheds that are sensitive to change and to help management attempt to minimize undesired effects requires improved assessment and understanding of the relationship among habitat change, land-use change, runoff, and water quality at the landscape scale (Chhabra et al., 2006). Watershed processes are highly dynamic in both space and time (Bloschl and Sivapalan, 1995).

Disasters from land degradation such as deforestation, floods, poor agricultural practices, and inappropriate land-use systems, among others, can cause devastating effects. They disrupt the socio-economic activities, ecological systems, and general development of the region. The potential effects on water resources due to land use/cover change and global climate change in the past few decades have been of great concern. Land clearing, agricultural activities, dam construction, mining, urban and industrial development, and similar activities can have a major impact on the quantity and rate of surface runoff, and on the rates of erosion and sediment transport that take place.

The human and livestock population, different agricultural activities, urbanization, drought prevalence, and poor land-use planning have been reported as the main drivers of LULCC in Ethiopia. However, different land cover places have different driving factors and consequences. For example, overgrazing and charcoal productions are the dominant driving factors in the Afar and Somali regions of Ethiopia (Wakijra *et al.*, (2020)) while forest grabbing for investments (coffee and tea plantation and, agriculture), settlements, poor law enforcement, shifting cultivation and land tenure policy has been significant drivers in southwestern Ethiopia (Muke, 2019).

Land-use/cover change (LULCC) is commonly grouped into two broad categories conversion and modification (Meyer and Turne, 1994).

I. Conversion refers to a change from one cover or use category to another (e.g. from forest to grassland).

II. Modification, on the other hand, represents a change within one land use or land cover category (e.g. from rained cultivated area to irrigated cultivated area) due to changes in its physical or functional attributes. These changes in land use/cover techniques have important environmental consequences through their impacts on soil and water, biodiversity, and microclimate (Lambin *et al.*, 2003). The anthropogenic and natural modification of the land surface implies land use land cover change (Moges *et al.*, 2019)

2.3 Omo river basin

The causes for soil erosions are a lack of an effective basin or watershed management system and poor land-use practices in Ethiopia (Bagegnehu and Yenealem, 2020).

Ethiopia has 12 river basins with an annual runoff volume of 122 BMC of water and an estimated 2.6 - 6.5 BMC of groundwater potential, which makes an average of 1575 m3 of physically available water per person per year, a relatively large volume (Seleshi *et al.*, 2007). The Omo-Gibe River basin is one of the Ethiopian river basins and has an area of 79,000 km2, covering parts of two national regional states, the Southern Nations and Nationality Peoples Region (SNNPR) and Oromia Region. The total mean annual flow from the river basin is estimated at 16.6 billion cubic meters (BMC) (Shiferawn *et al.*, 2016). The Gibe River is known as the Omo River in its lower reaches, south-westwards from the confluence with the Gojeb River. The main tributaries of Omo-Gibe River Basin are from north-east Walga, Wabe, Wariness, and Derghe and south-west Tunjo (called Gilgel Gibe as a station) and Gilgel Gibe Rivers and the west Gojeb River. From the eastern side of the middle and lower Omo-Gibe catchment, the Sana, Soke, Wabe, Deme, and Zage rivers are the main tributaries. It flows into Lake Turkana in Kenya, which forms its southern boundary. The western watershed boundary of the Omo basin is the range of hills and mountains that separate the Omo-Gibe basin from the Baro-Akobo basin. To the north and north-west, the basin is bounded by the Blue Nile basin with a small area in the northeast bordering the Awash basin. There are four hydropower stations at Omo Gibe River Basin three of them constructed and one ongoing (Under construction), those are Gibe I, Gibe II, Gibe III, and Gibe IV (Koysha Hydropower project).

The Gibe III dam was the third sequence of water resource schemes of Gilgel Gibe/ Gibe I, and Gibe II in operation on the main Gibe/Omo River Basin. One further hydropower scheme – known as Gibe IV is under completion downstream on the Omo River Basin (EEPCO, 2009) (Figure. 2.1).

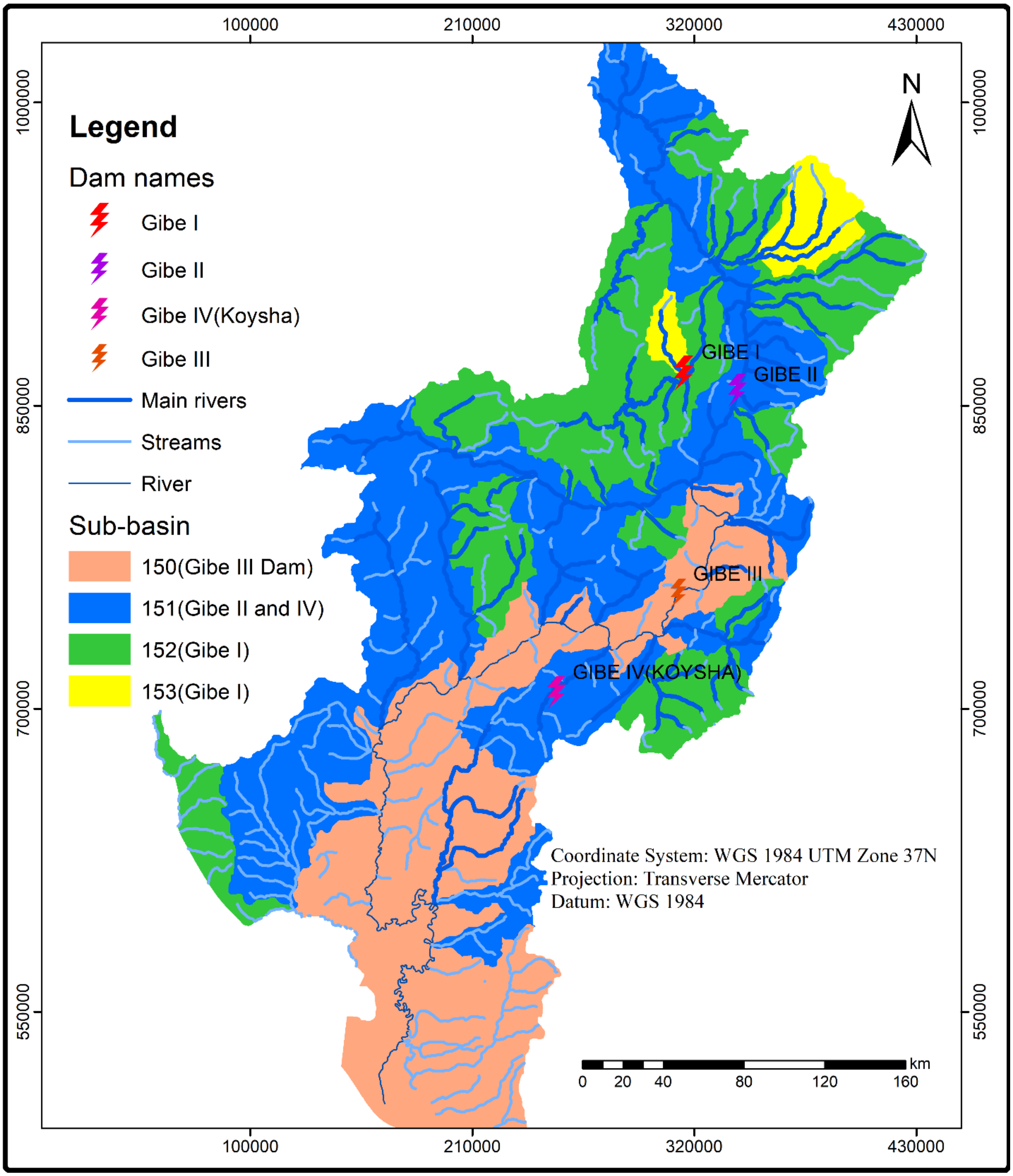

Figure 2. 1: Gibe I, II, III, and IV in the Omo river basin

Administratively, the Gilgel Gibe III dam reservoir stretches over five zones and twelve weredas (Fig. 2.2). Omo river below the Gilgel Gibe III dam traverses through the four woredas of the

South Omo Zone. The scheme, from the root of its reservoir to its tailrace outfall, extends over a corridor some 155km long (EEPCO, 2009).

According to the Omo Gibe river basin development master plan (OGRBDMP, 1995) most of the northern catchment is under widespread cultivation with the expansion of cultivated lands at the expense of woodlands. The Gibe, Gojeb, and Omo gorges are relatively abandoned and support a cover of open woodland and bush land with grasses through inaccessible lands.

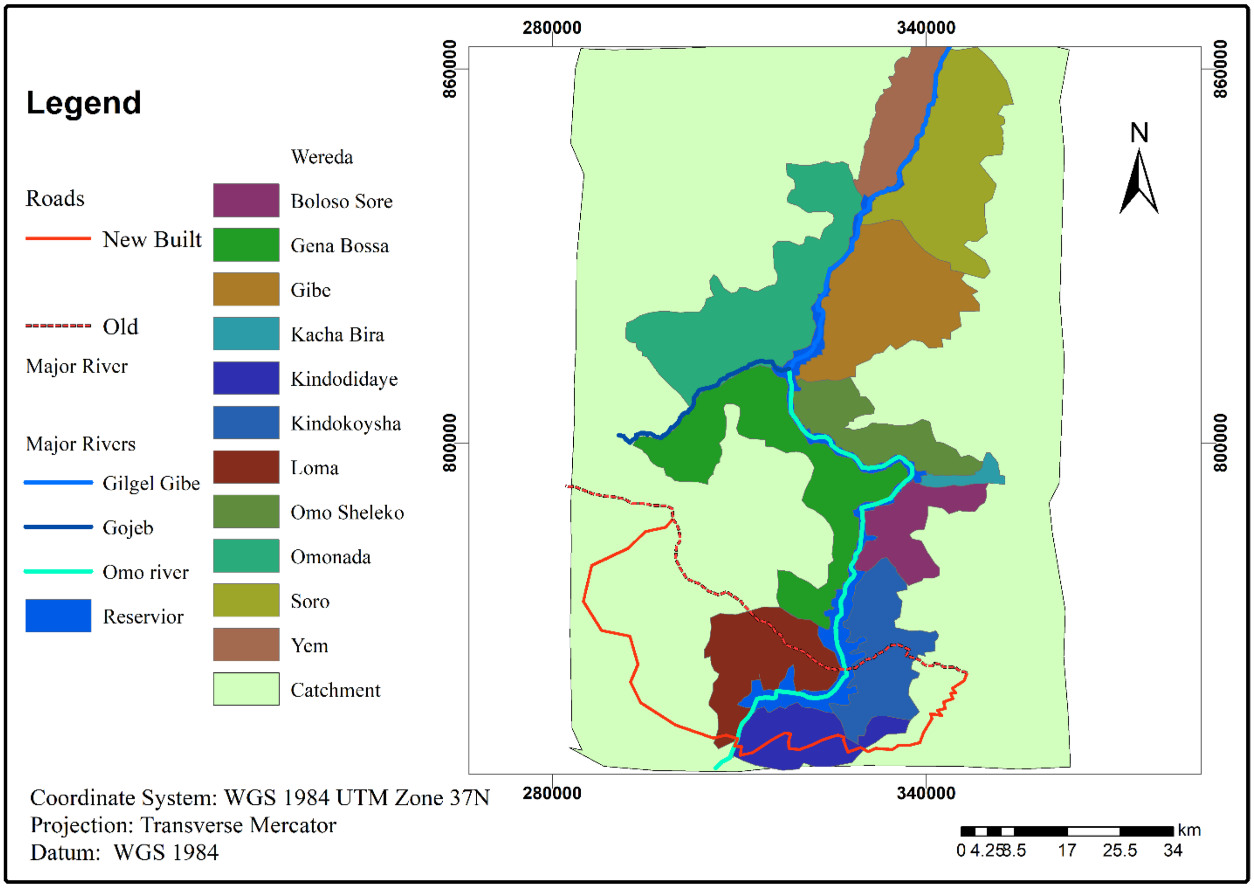

Figure 2. 2: Administration map of GGIIID around the reservoir area (source: EEPOW, 2009, p.3)

According to Ethiopian Electrical power (EEPow) (2021), Gibe IV (Koysha) (2200 MW, under construction) is the fourth hydropower plant of the Omo/Gibe river cascade in Ethiopia, comprising Gilgel Gibe I (184 MW), Gibe II (420 MW) and Gibe III (1,870 MW), all currently in operation. The project includes two 6 m diameter middle level outlets embedded in the dam body allowing controlling the reservoir level during the first impounding, releasing artificial/ecological flows, and lowering the reservoir level for inspection/maintenance needs. The river diversion layout includes two concrete culverts on the right side of the river, aimed to divert the river during the dam construction and designed to discharge up to 3'000 cubic meters per second, and an upstream composite RCC/rockfill cofferdam. Both the river diversion layout and the energy-generation operating rules of Koysha have been optimized taking advantage of the large flow regulation capacity of the upstream Gibe III project. Cyclic operations of the two projects allow maximizing energy generation and providing great flexibility guaranteeing power supply during both dry season and peak-demand period. The powerhouse is located on the left side of the river, housing eight Francis turbines generating 2'160 MW, together with erection bays and control building. Step-up transformers are located behind the powerhouse.

2.4 Role of remote sensing and GIS in reservoir capacity assessment

Remote sensing is the science, and art of acquiring information from or about an object, area, or phenomenon through the analysis of data obtained by a device that is not in contact with the object, area, or phenomenon under investigation. Using various sensors, data collected remotely may be analyzed to obtain information about the objects, areas, or phenomena being examined. The remotely collected data can be of many forms, including variations in force distributions, acoustic wave distributions, or electromagnetic energy distributions (Lillesand *et al*., 2015). Remotely sensed data characterization, classification, and accuracies; land resources monitoring, modeling, and mapping with remote sensing; and remote sensing of water resources, disasters, and urban studies were the overarching goal of Remote Sensing (Prasad, 2015).

Remote sensing is one of the tools and science which is very important for the production of Land use and land cover maps through a process called image classification (Rwanga and Ndambuki, 2017). The accelerated usage of remote sensing data and techniques has made the geospatial process faster and powerful, although the increased complexity also creates increased possibilities for error (Murty and Tiwari, 2015).

The assessment of Reservoir water, both in terms of quantity (e.g., surface area) and quality (e.g., turbidity) is a goal often sought by researchers by using remote sensing techniques. Various methods of analyzing remotely-sensed data have been used to achieve this goal (McFetters, 1996; Work and Gilmer, 1976; Lathrop and Lillesand, 1986; Han *et al*., 1994). The Normalized Difference Water Index (NDWI) is a new method for analyzing data for water resource assessment. Most common remote sensing systems operate in one or several of the visible, infrared, or microwave portions of the spectrum. The Copernicus program and its Sentinel satellites, a growing source of satellite remote sensing data are publicly available at no charge.

2.4.1 Optical remote sensing and normalized difference water index (NDWI)

The field of optical remote sensing has a wide-ranging number of applications. It is also possible to consider optical remote sensing from a variety of scales. Environmental remote sensing typically refers to detailed field-based measurements (e.g., field spectrometry); airborne imagery; and satellite imagery. Specifically, the type of data acquired in optical remote sensing makes use of the visible, near-infrared (NIR), and shortwave infrared (SWIR) parts of the electromagnetic radiation (EMR) spectrum. A sensor is termed panchromatic if it acquires data in a single region or waveband of the spectrum. A multispectral sensor will acquire several (up to ten) broad spectral bands, while a hyperspectral sensor will acquire many more narrow bands. The increasing availability of high-quality optical satellite images enables, in principle, the continuous monitoring of Earth ‘s surface changes (Tewabe Melkamu, 2019; Leprince *et al.*, 2008).

Normalized difference water indices (NDWIs) derived from satellite images are commonly and successfully utilized in surface water body detection and mapping. These applications have involved the delineation of open water using thematic information extraction techniques. There are various methods for the extraction of water information from remote sensing imagery, which, according to the number of bands used, are generally divided into two categories, i.e. single-band and multi-band methods (Hanqiu, 2006). Satellite altimetry is an important method for gauging reservoir water levels from space, but can only measure water levels along a fixed orbital track and, thus, is limited in geographical coverage (Park *et al*., 2020).

A. Landsat 7

Landsat data have been used widely for global monitoring, due to their free availability and regular revisit capabilities. The Landsat 5 satellite equipped with Thematic Mapper (TM) sensor was launched in 1984, but the TM sensor stopped transmitting in November 2011. As the successor of Landsat 5, the Landsat 7 satellite was launched in April 1999. In May 2003, however, the scan-line corrector (SLC) of the Landsat 7 Enhanced Thematic Mapper Plus (ETM+) sensor failed permanently, resulting in SLC-off images with around 22% dead pixels from May 2003 to present (Arvidson *et al*., 2006).

B. Landsat 8

To cope with the scan line corrector (SLC-off) issue of the Landsat 7 ETM+ sensor, the new generation Landsat 8 satellite equipped with Operational Land Imager (OLI) and Thermal Infrared Sensor (TIRS) sensors was launched in February 2013 and the sensors are now in operation routinely acquiring global remote sensing data (Roy *et al*., 2014)

C. Sentinel-2

Sentinel-2 is a European wide-swath, high-resolution, multi-spectral imaging mission designed for data continuity and enhancement of the Landsat and other missions. The full mission specification of the twin satellites flying in the same orbit but phased at 180°, is designed to give a high revisit frequency of 5 days at the Equator. sentinel-2 will carry an optical instrument payload that will sample 13 spectral bands: four bands at 10 m, six bands at 20 m, and three bands at 60 m spatial resolution. The orbital swath width will be 290 km. Each of the satellites in the sentinel-2 mission carries a single payload; the Multispectral Instrument (MSI) (ESA, 2020).

2.4.2 Microwave remote sensing

Due to the larger wavelength compared to visible and infrared radiation, microwaves (wavelength between 1 cm and 1 m) exhibit the important property of penetrating clouds, fog, and possible ash or powder coverage (for example, in case of an erupting volcano or a collapsed building). This important property provides an imaging capability in any weather condition or environment, although some atmospheric disturbances can affect both the amplitude and, more importantly, the phase of SAR images.

Microwave remote sensing has been mainly used in moist and cloudy zones in inter tropical or temperate regions to compensate for the impossibility of acquiring data in the visible and near-infrared bands.

A. Sentinel -1: Sentinel-1 is a space mission funded by the European Union and carried out by the ESA within the Copernicus Program, consisting of a constellation of two satellites, Sentinel-1A and sentinel-1B. The first satellite, sentinel-1A, launched on 3 April 2014, and Sentinel-1B was launched on 25 April 2016. The payload of Sentinel-1 is a Synthetic Aperture Radar in C- Band that provides continuous imagery (day, night, and all-weather) (Zheng and Shao, 2018).

B. Synthetic aperture radar (SAR)

Synthetic aperture radar (SAR) and optical sensors with high spatial resolution are very useful for obtaining detailed water body information of reservoir areal dynamics (Abileah and Vignudelli, 2011). SAR data with both the two features of high spatial resolution and cloud penetration are very attractive to water body monitoring (Delmeire, 1997; Liao *et al*., 2004; Lv *et al*., 2005; Juval *et al*., 2016), and the high spatial resolution optical data provide the ideal data source for water detection under the clear sky (Tholey *et al*., 1997; Profeti and Macintosh, 1997). Comprehensive using the SAR and optical remote sensing data both can enhance the all-weather satellite observing capability and data processing efficiency. Synthetic Aperture Radar (SAR) methods have shown promise for gauging and measuring the water level in lakes and reservoirs (Park *et al*., 2020).

2.4.3 Geographical information system (GIS)

Eighty percent of big data are associated with spatial information and are big spatial data. Big data refers to extremely large data sets that may be analyzed, retrieved, managed, and stored computationally to reveal patterns, trends, and associations with human behavior and interactions with the environment (Huang and Wang, 2020).

Different types of GIS definitions exist in different areas and disciplines. But all GIS definitions recognize the use of spatial data. Many alternative definitions of GIS have been suggested, but a simple definition is that a GIS is a computer-based system for the capture, storage, retrieval, analysis, and display of spatial data (Skidmore, 2002).

An influential set of tools for collecting, storing, retrieving at will, transforming, and displaying spatial data from the real world (Burrough, 1987)

"A geographic information system (GIS) is a computer-based tool for mapping and analyzing things that exist and events that happen on earth. GIS technology integrates common database operations such as query and statistical analysis with the unique visualization and geographic analysis benefits offered by maps (ESRI, 2020).

According to University Consortium for Geographic Information Science (UCGIS, 2003) suggests that "Geographic information Science and technology should not be defined by merely linking segments of the traditional domains (e.g., cartography, remote sensing, statistical analysis, locational analysis, etc.), but rather by placing the emphasis directly upon concepts and methods for geographic problem-solving in a computational environment."

A relatively simple geographic information science (GIS) solely based on operational remote sensing data is used to estimate water level dynamics at nearly global scales (Park *et al*., 2020).

2.5 Reservoir storage capacity of dam and stream flow

The overall reservoir capacity, comprises the active storage (for water supply and flow regulation), the dead storage (for sediment, recreation, and hydropower), and the flood control storage (required in the flood-prone seasons) (Nagy *et al*., 2002)

Sediment management practices for reservoir capacity are often as different as their physical and technical conditions and socio-economic and environmental aspects. Different researchers used to control the sedimentation of reservoirs by applying the mechanisms categorized in four general categories (Borounjeni, 2012). I) watershed rehabilitation (Structural and non- Structural Measures) ii) Sediment flushing, iii) Sediment routing, iv) Sediment removal and disposal.

River discharge is a fundamental hydrologic quantity that summarizes how a watershed transforms the input of precipitation into output as channelized **stream flow**. Accurate discharge measurements are critical for a wide range of applications including water supply, navigation, recreation, management of in-stream habitat, reservoir storage capacity assessment, and prediction and monitoring of floods and droughts (Legleiter *et al*., 2020).

CHAPTER-3 MATERIALS AND METHODS

3.1 Description of the study area

3.1.1 Location

The study area is a part of the Lower Gibe River basin commonly called Gilgel Gibe III Dam in the Omo river basin of Southwestern Ethiopia. Geographically it lies between 6° 38′ 21.78″ – 8° 16′ 20.91″ N latitude and 36° 31′ 10″ – 37° 58′ 9.90″ E Longitude (Fig. 3.1), covering total area of (1,119,085ha) and has an altitude range from 635 to 3315 m above mean sea level. It has an average distance of 550km Southwest of Addis Ababa and its administrative location is at the boundary of Wolaita and Dawuro Zone in the SNNPRS.

The hydropower plant is the third plant of the Gibe cascade developing the hydroelectric potential produce(1870MW) (Table 3.1) of the Omo-Gibe river including Gilgel Gibe or Gibe I and Gibe II operating since 2004 Omo-Gibe IV under construction and Gibe V projects, for hydropower and agricultural uses, currently being planned (EEPCO, 2006).

Table 3. 1: Basic feature of Gilgel Gibe III hydro power plant (EEPCo, 2008, 2009, 2014)

Hydrology		Unit
Catchment area	34160	km^2
Average annual runoff	438.2	m^3/s
Average Annual volume	13820	Mm^3
Reservoir		
Minimum operating level	800	m a.s.l
Normal operating level	855	m a.s.l
The maximum water level in the reservoir	892	m a.s.l
Live storage volume	11750	Mm^3
Surface area at the normal operating level	200	Km2
Reservoir length	155	Km
Dam		
Dam type	RCC Dam	
Foundation elevation	650	m a.s.l
Height above river bed elevation	243	m
Crest elevation	896	m .a.s.l
Crest length	580	m
Installed power	1870	MW

The study area is found in the Omo river basin that is bordered in the western watershed part, the range of hills and mountains that separate the Omo-Gibe basin from the Baro-Akobo basin. To the north and northwest, the basin is bounded by the Blue Nile Basin with a small area in the northeast bordering the Awash basin.

The whole of the eastern side borders the rift valley basin. The power house and the reservoir are located within the jurisdiction of the Loma, and Gana Wereda of the Dawro Zone and Kindo Didaye, and Kindo Koyisha Wereda of Wolaita zone of the Southern Nations and Nationalities People Regional State.

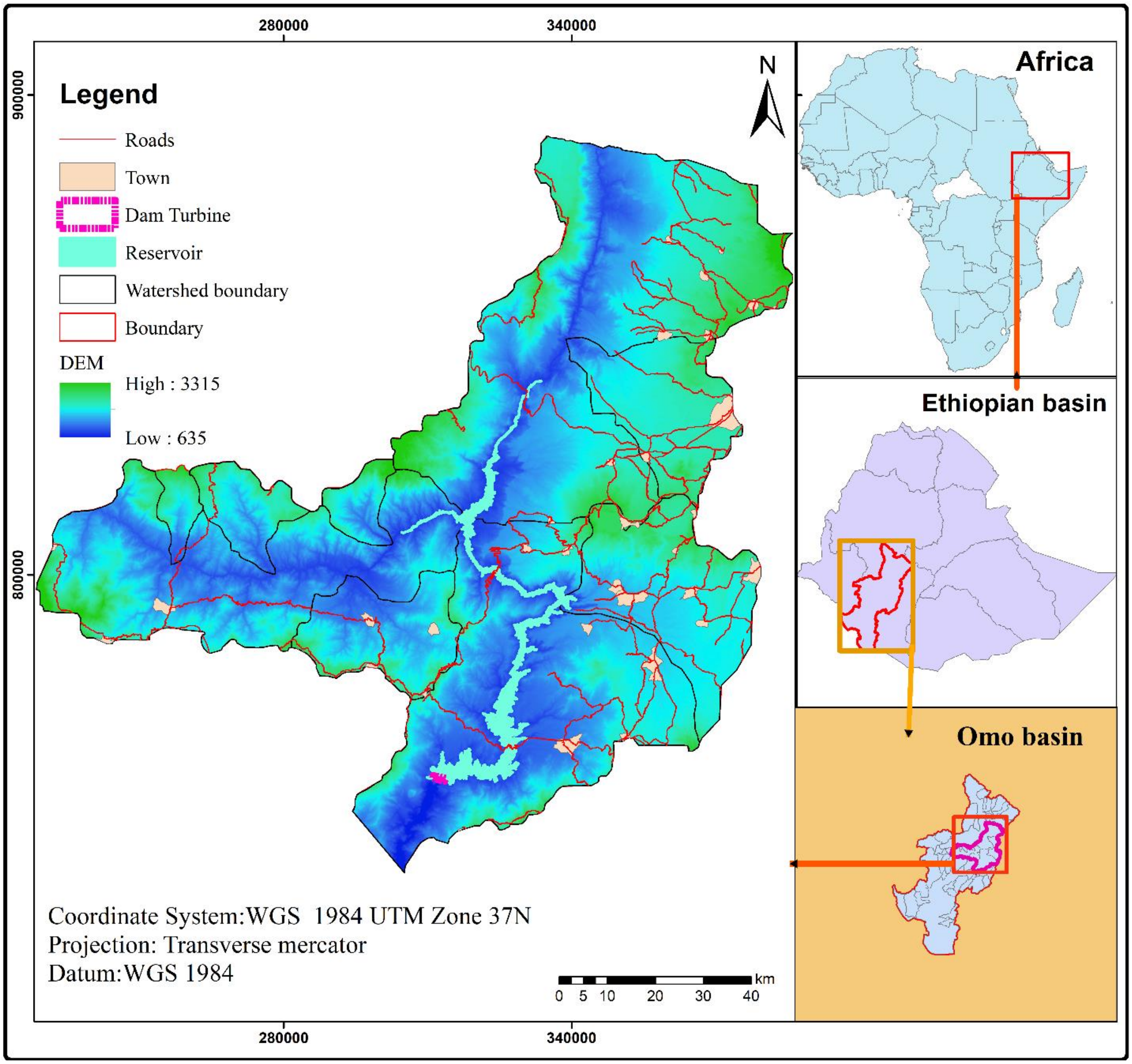

Figure 3. 1: Location of the study area

3.1.2 Topography and Drainage Pattern

3.1.2.1 Topography

The study area has variable altitude, ranging from very low land (635m) Valleys, very flat areas or plains (1000 m) to undulating plains (1500 m), hills (2000 m) to mountains (3000 m), and the highest elevation reaches up to (3315 m) or High ridges above mean sea level (Fig 3.2).

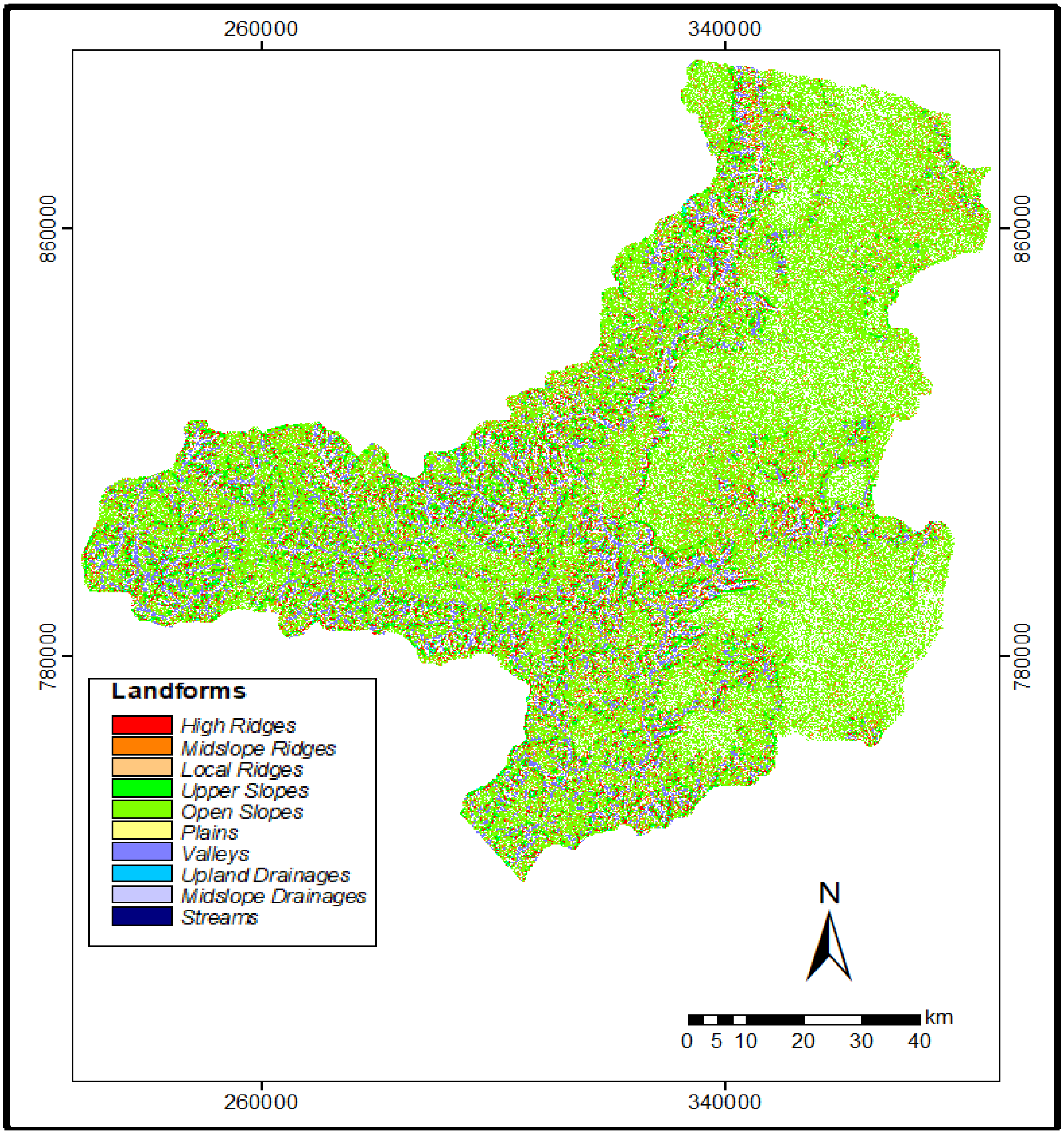

Figure 3. 2: Physiography map

The study area covers the upper and lower part of the Omo basin from the Ethio-basin. The Gibe River is known as the Omo river in its lower reaches, south-westwards from the confluence with the Gojeb river. The topography of the Omo-Gibe basin varies considerably (Jilo *et al*., 2017). The terrain in the northern two-thirds of the basin ranges from mountainous to hilly and is cut by the deeply incised gorges of the Omo, Gojeb, and Gilgel-Gibe rivers, while the southern one-third is a flat alluvial plain punctuated by hilly areas. Streams from the figure below include canyons, deeply incised streams. Local ridges, and hills in valleys consisted of local ridges and high ridges are mountain tops. The dominating terrain in the area was an Open slope (Fig. 3.3) that shows the higher area coverage in the catchment of the Gilgel Gibe III dam.

The elevation profile or topographic profile (Fig. 3.4) of the Study area varies from 3315 to 635m a.s.l changing abruptly from higher elevation to low and vice versa. In the area, the profile was taken from the Southwest to the northeast cross-sectional line by using 3D analysis in the ArcGIS and it shows variable topography or undulating terrain.

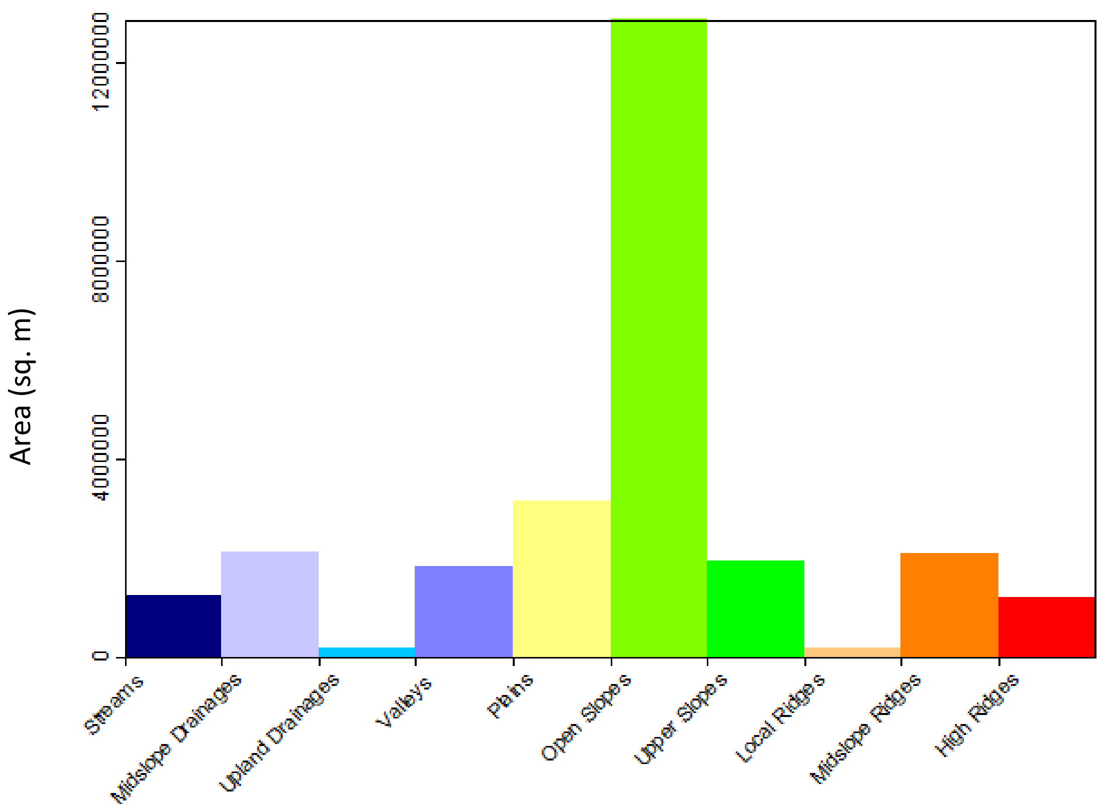

Figure 3. 3: Histogram of landforms in the study area generated in SAGA GIS

Contour lines are critical to understanding the profiles of elevation in the study area for particular land formations. In the catchment of Gilgel gibe III, dam contour lines are generated from the digital elevation model of ALOS PALSAR which has a 12.5m resolution and the contour has a 300-meter interval for the contour line. The study area is characterized as undulating topography with increasing and decreasing elevation in between 635 and 3315 m.

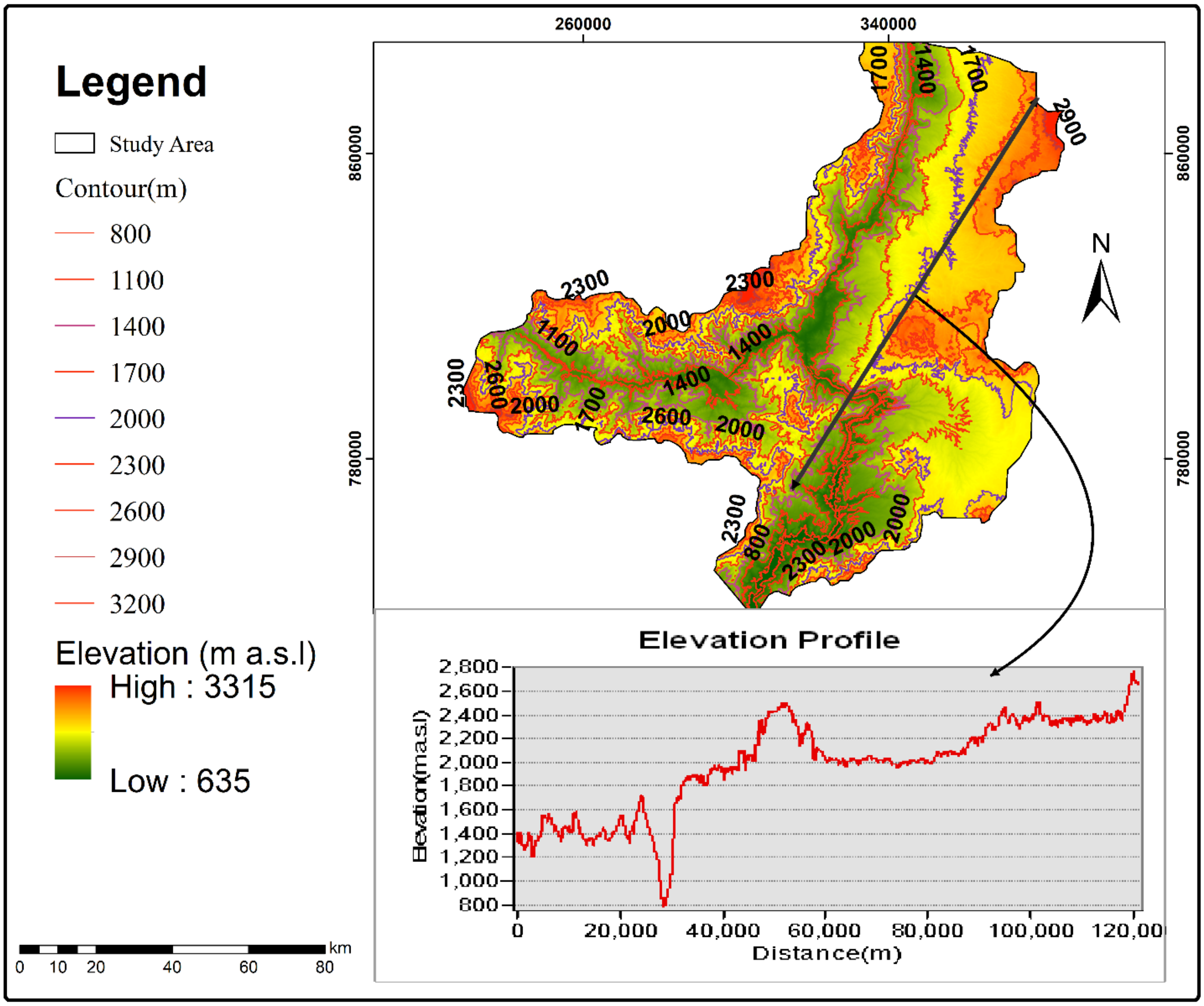

Figure 3. 4: Elevation profile and contour map

The landform of the study area dominantly covers Mesa which is an isolated, flat-topped hill or mountain with steep sides that are smaller in area than a plateau, and Butte which is also a flat-topped hill with steep sides, though smaller in area than a Mesa. The project area is characterized by hilly landforms on both sides of the Gilgel Gibe III dam either eastern or western, and canyon, which is a narrow, deep rocky, and steep-walled valley carved by a swift-moving river and long traveling river gorges.

3.1.2.2 Slope

The study area has a variable slope, ranging from Flat to Very gently sloping (Class 1), Gently sloping (Class 2), sloping (Class 3), strongly sloping (Class 4), Moderately steep (Class5), Steep (Class6), and very steep (Class7) gradient classification based on FAO listed slope gradient classes (Fig. 3.5).

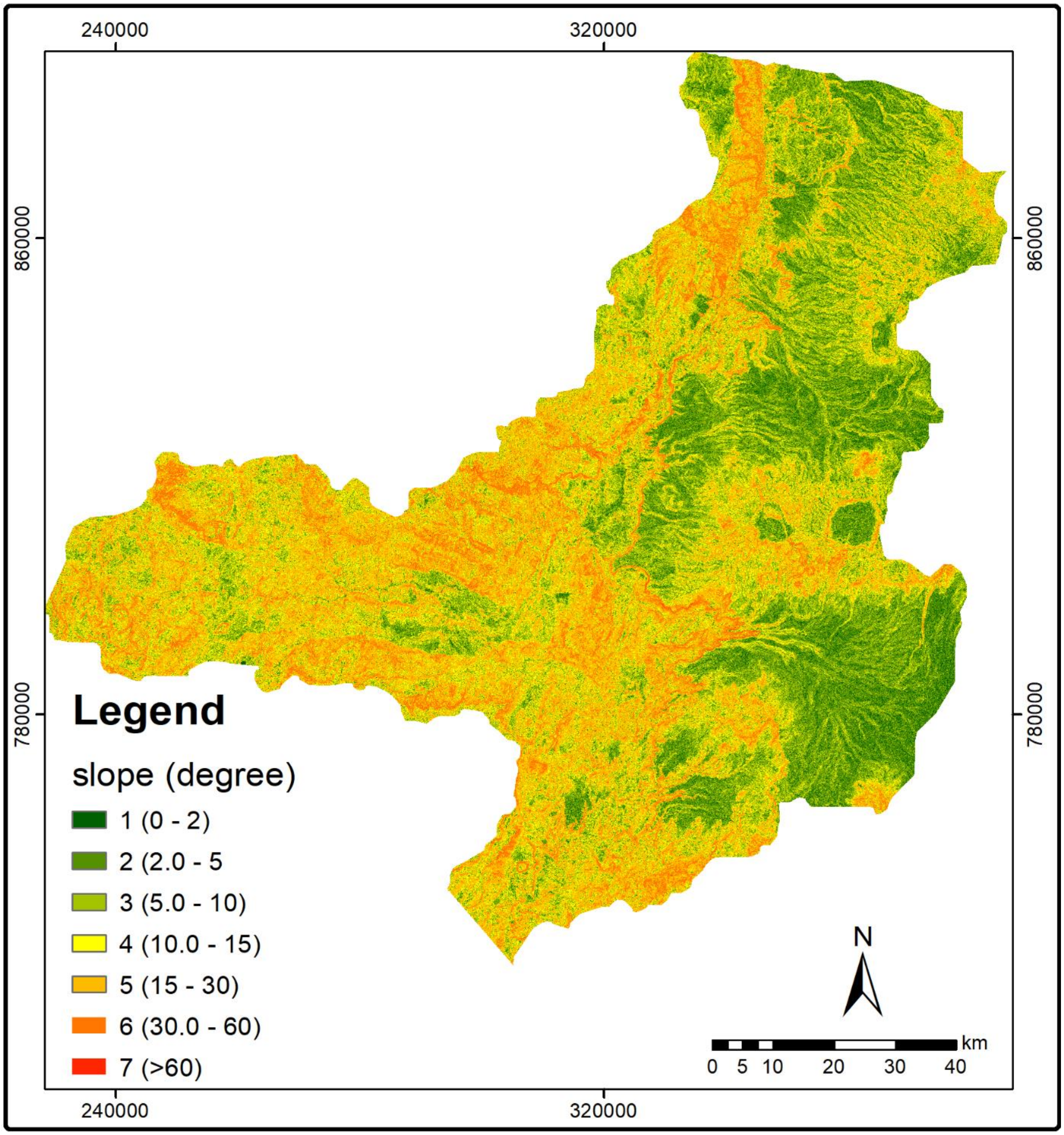

Figure 3. 5: Slope gradient map

However, 29.61 percent of the land area constitutes a moderately steep which is the dominant slope of the area and 25 percent is slopping whose gradient was 5−10 and it is the second dominating slope in the watershed. Generally, the study catchment characterizes by an undulating slope which is very commonly observed with varying area coverage (Table 3.2).

Table 3. 2: Slope gradient classes of Gilgel Gibe III dam watershed

Class*	Class description	Gradient (degree)	Area (sq. km)	Area (%)
1	Flat to very gently sloping	0−2	426.1	3.8
2	Gently sloping	2−5	1805.4	16.1
3	Sloping	5−10	2799.0	25.0
4	Strongly sloping	10−15	2009.4	18.0
5	Moderately steep	15−30	3312.5	29.6
6	Steep	30−60	829.3	7.4
7	Very steep	>60	5.5	0.1

3.1.2.3 Drainage pattern and drainage density

There are many rivers and streams which cross the watershed of the study area. These streams and rivers start from the NE, W, and E part of the study area and they drain to-wards S (south) where the Reservoir of GGIII Dam found and finally to the Lake Turkana (Kenya) where far south in the project site. Gojeb, Gilgel gibe, and Omo rivers are the major rivers; those can be mentioned at the first rank. Specifically, the Omo river is the most known river found in the South Western part of the Ethiopian basin. Rivers drained from North East and Western direction form a drainage pattern that is dominated by trills type and draining from the eastern direction is the dendritic type of drainage pattern (Fig. 3.6). Drainage density is the ratio of the total stream length of all orders to a unit area of a watershed (Clubb *et al.*, 2016).

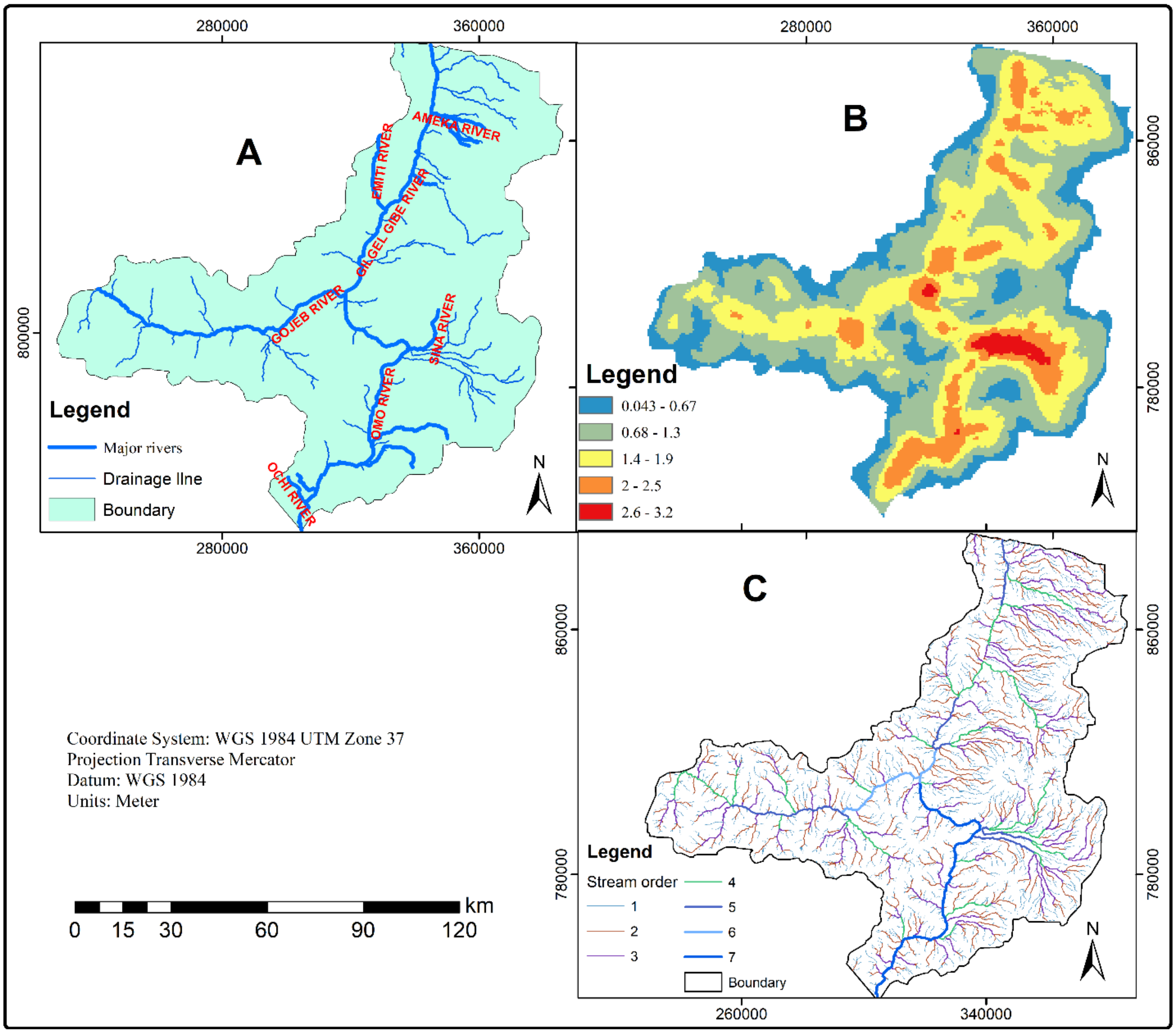

Figure 3. 6: Drainage pattern (A), drainage density (B), and stream order (C) of the study area

Drainage patterns are determined by regional and local geology and reflect control by structures, slope, and bedrock erosional characteristics. Combinations of these geologic controls lead to the formation of identifiable patterns. The geology of the Omo basin is dominated by a fault feature, filled with alluvial and lacustrine sediments of recent origin associated with the Great rift valley (Jilo *et al*., 2017).

3.1.3 Metrology of the study area

3.1.3.1 Rainfall

Based on the rainfall the study area divided into three climatic zones, those are Dega (cool to cold humid), Woyna dega (warm to cool, semi-humid), and Kola (warm to hot, semi-arid) based up on the annual rainfall they receive and altitude (EEPCO, 2009). The northern part of the study area, including Imdbir, Weliso, Welkite, and just north of Jima, has rainfall for about seven months, from March to September with a range of 1100-2500 mm per annum. The small rains are from March to May and the main from June to September with a marked increase in July and August. The North-western part of the catchment including Sekoru, Limu Genet, Jimma, and Wolkite has a more even distribution of rainfall over March to September without any peak in July and August in the year 2011. In the Gilgel Gibe III Dam catchment, the annual average rainfall was an increase from 2000 then decrease up to 2005 then increase up to 2010 which is the peak rainfall in the study area, and finally became decrease up to 2018(Fig.3.7). The southern part of the study area receives moderate annual rainfall and the western part receives the lowest annual rainfall and reflects the semi-arid climatic zone of the study. To sum up, the western part of the study area receives the higher av. annual rainfall from the years 2000- 2018 (Fig. 3.8).

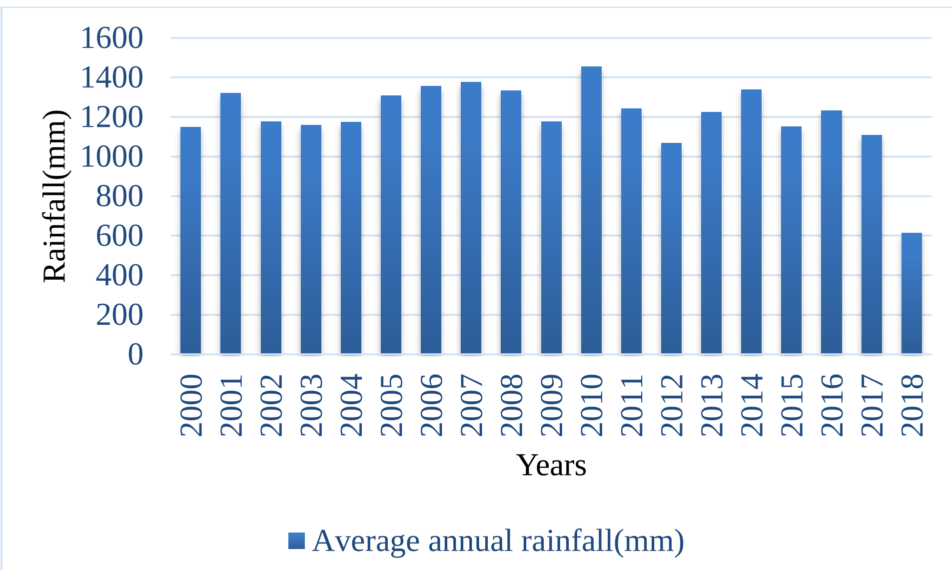

Figure 3. 7: Average annual rainfall from the year (2000 − 2018) (Data source: EMA)

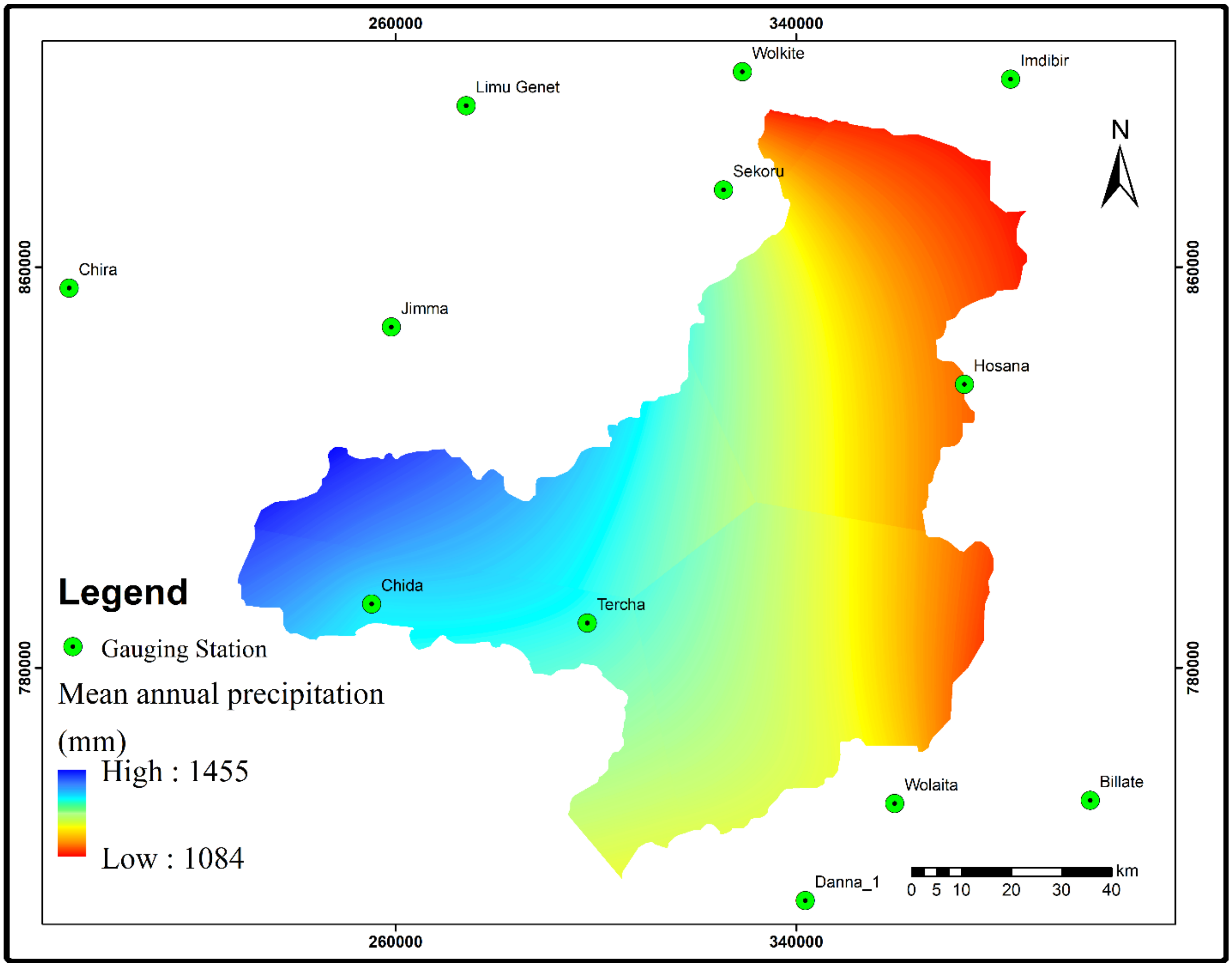

Figure 3. 8: Mean annual rainfall map of study area produced by kriging interpolation (2000−2019)

3.1.3.2 Temperature

The mean annual temperature in the study area (GGIII) varies from 14°C in the highlands to the north to over 22°C to the south, reflecting the correlation between temperature and elevation. There is little variation in the minimum temperature (around 10°C for most of the year) but the maximum drops markedly during July and August to 19°C compared to a maximum of 35°C in the year 2000 (Fig. 3.9). Arbaminch, to the north of the study area, shows a decreasing pattern with slightly slower values and less variation in the maximum. Toward the south of the catchment, has the highest average temperatures and shows increased variability in the period November to March when rainfall is the lowest. Lastly mean annual temperature, Average annual maximum temperature, and average annual minimum temperature of the study area vary from 2000 to 2019 (Fig. 3.10).

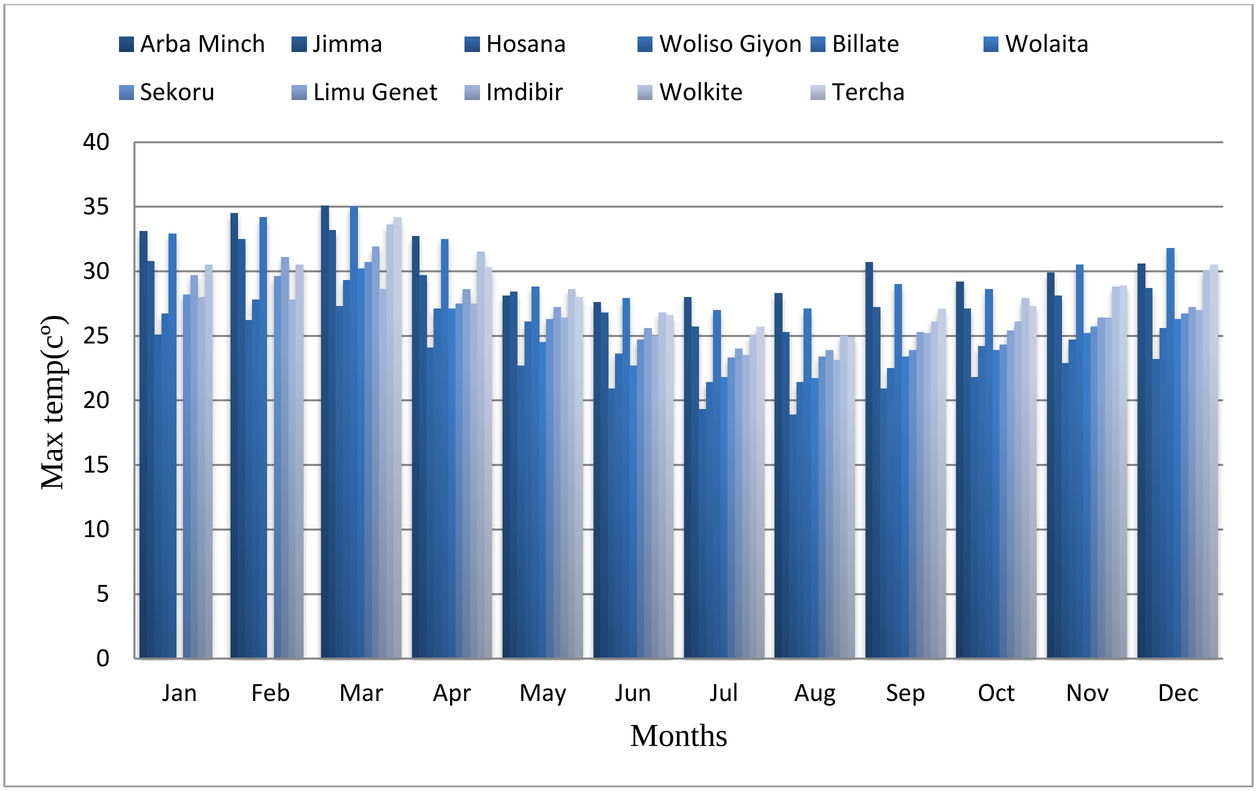

Figure 3. 9: Maximum monthly temperatures and gauging stations in the year (2000)

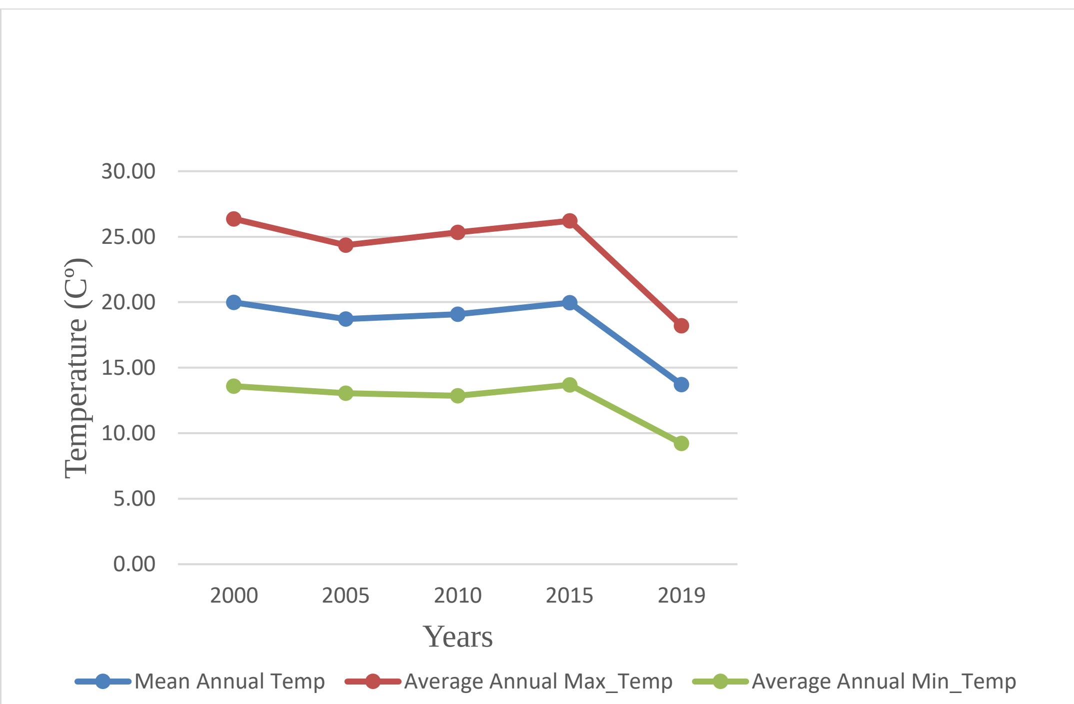

Figure 3. 10: Mean, max, and min average annual temperature of the study area

3.1.3.3 Relative humidity

The highest relative humidity occurs when the rainfall is the highest, reaching an average of over 80% on the high ground to the west of the study area. To the south of the Sub-basin, the average value drops below 65%. The seasonal variation in humidity follows a similar pattern to the rainfall.

3.1.3.4 Sunshine

As the major factor affecting the average daily hours of sunshine in the study area is the cloud factor, with relatively little effect due to the seasonal movement of the earth. Thus, there are relatively low sunshine levels in the west highlands to the west of the Sub-basin of the Omo River. There are marked minima for all stations in June and September. Wolaita has the longest hour of sunshine, with a minimum in June, July, and August, but this is less marked than for other stations.

3.1.4 Geology and hydrology of the study area

3.1.4.1 Geological setting

The geological history in the Omo Basin constructed by previous workers indicates that the region is built up of >1000 meter, and perhaps as much as 2000 m, thick successions of the volcanic lava flow, uncomfortably overlying scattered fluvial-lacustrine sediments and Precambrian crystalline basement rocks, as well as more widely distributed Tertiary 'flood basalts. Unlike conditions in northern and eastern Ethiopia, Mesozoic marine deposits have not, so far, been encountered in south-western Ethiopia including the study area instead, terrestrial sedimentation; rifting and volcanism seem to have dominated the geological process during the Mesozoic era. In general, several structural trends are recognized in and around the study area. Structural analysis suggests that N-S striking features are younger than NNE structures which in turn are younger than the NNW features. The facts that recent eruptive volcanic centers and a concentration of earthquake epicenters are associated with local basins bounded by N-S faults suggest that other NNE and NNW trends are older, (Richard and Associates, 1996).

The geology of the study area was classified based on the age of rocks across the geologic layer in the catchment (Table 3.3). For this study, the geology of the study area as shown in (Fig. 3.11) is classified into seven groups' geological survey of Ethiopia (GSE, 1983).

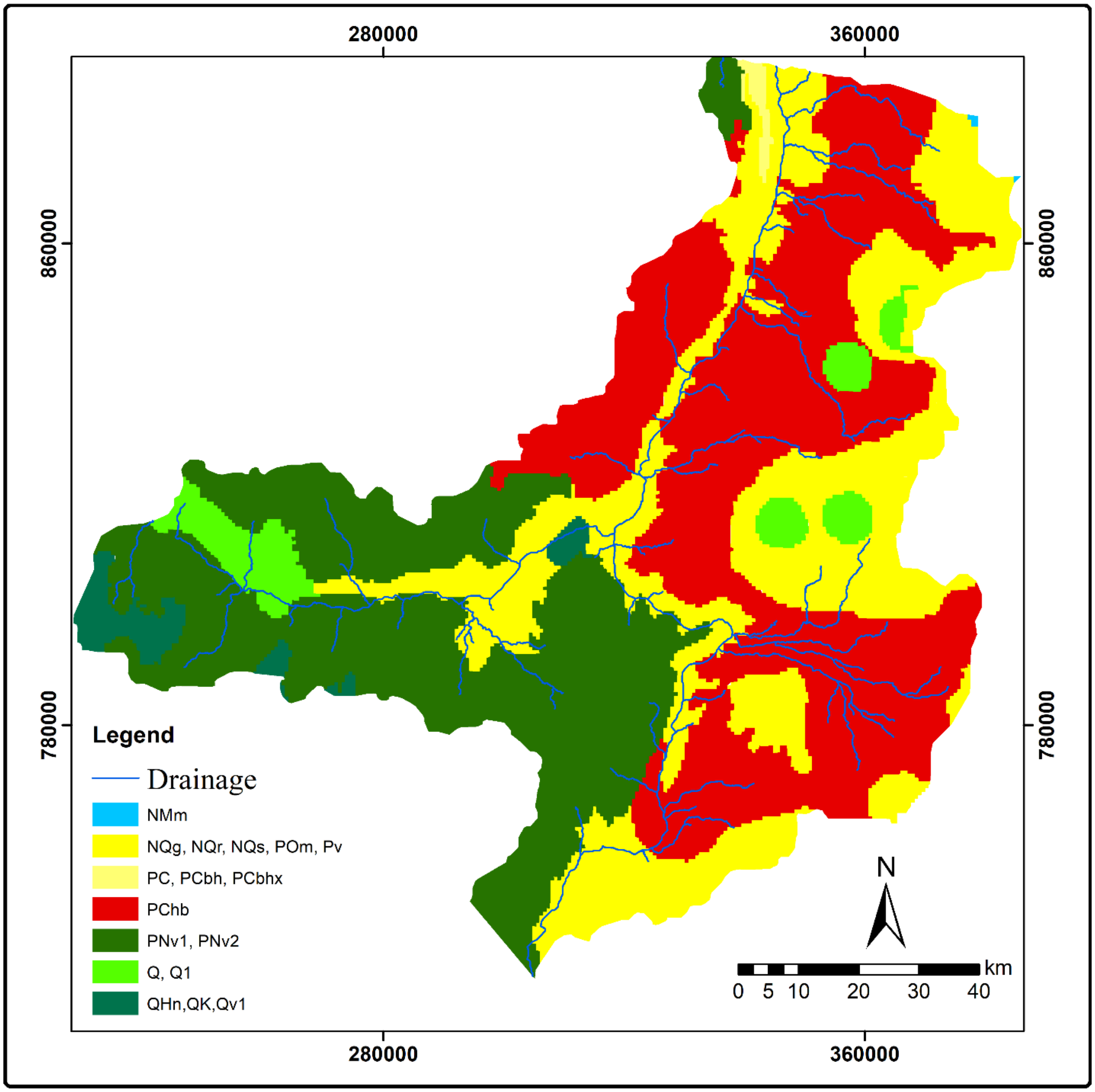

Figure 3. 11: Geological Map

Table 3. 3: Classification of lithologies and their stratigraphy

Age		Lithographic units	Symbol	Lithologies
PRECAMBR		Metamorphic rocks	Pcbhx	**-Surma Domain** – cataclastic gneiss derived from Pcbh with minor pegmatitic and granitoid orthogneiss, metasedimentary gneiss, amphibolite, and marble contains layers of derived ultracataclasite and mylonite
			Pcbh	**-Hamar Domain-** undivided gneiss includes predominantly biotite and hornblende gneiss, migmatitic in part, with minor meta-sedimentary gneiss, Quarzo-feldspathic gneiss, amphibolite, and granitoid orthogneiss.
			Pc	- **Akobo Domain** – Marble, Undifferentiated
			Pchb	- **Hamar Domain-** Layered Mafic Gneiss and Amphibolite
CENOZOIC	QUATERNARY	Igneous rock	QHn	-Nakwa Formation
	HOLOCENE		QVl	-Basalt, Basaltic Ejecta
		Sediments	Q	-Undivided alluvial, fluviatile and Lacustrine sediments
	PLEISTOCENE _HOLOCENE	Igneous rock	QK	-Kibish Formation
	PALAEOGENE		Ql	-Lacustrine silt, Clay
	PALAEOGENE		PNv	-Rhyolite, Trachyte, Ignimbrite, Minor Basalt, Tuff;
	OLIGOCENE	Igneous rock	PV	-Main volcanic sequence, Basalt, rhyolite, trachyte, tuff, ignimbrite
			POm	-Mekonen Basalt

The previous scholars classified the geology of the study area, tentatively into five groups of rocks according to their age relationships. These groups are:

- The pre-Cambrian crystalline basement rocks
- The early 'flood basalts' of late Eocene to early Miocene age

- A transitional series of intercalated basaltic and felsic volcanic of late Oligocene to early Miocene age
- A series of felsic volcanic ranging from early Miocene to late Miocene in age
- The post-rift sediments and volcanic, of Pliocene and Quaternary age

Nearly 11% of the study area is underlain by Precambrian metamorphic gneisses consisting of felsic meta-sediments and mafic meta-volcanic that represent the older 'cratonic' granite-gneiss terrain to the west and a younger 'oceanic' to the east. The younger oceanic 'greenstones' have been overthrust to the west onto the older craton. The main thrust zone, in the Sharma region west of the lower Omo river, is marked by intense shearing and cataclasis. Around 80% of the study area is underlain by Tertiary volcanic rocks. Also, the Basin occupies the combined Omo and Usno rift valleys which are failed north extension of the lake Turkana-Ethiopian Rift system. In the north part of the basin, the rivers have exploited the extensive fault zones to cut deep gorges. The eroded material has been deposited in the lower part of the basin as a thick sequence of quaternary alluvial deposits (Bogale, 2011).

3.1.5 Hydrology of the study area

Streamflow data of the study area were collected from seven River gauging stations and were used for comparisons against the modeled reservoir capacity in model calibration and validation. Daily streamflow data for Gilgel Gibe III watershed was collected from the basin development authority of Ethiopia (BDAE) from 2000 to 2017 G.C at Gibe nearby. Limu Genet, Gilgelghibe nr.Asendabo, Ghibe near Seka, Wabi near. Wolkite, Sokie near Areka, gojeb near.Shebe, Walga near. Wolkite, the station for RUSLE simulation, results in calibration and validation by using baseflow separation and runoff (Rof).

Water resource studies highly depend on streamflow data (Table 3.4). These data should be consistent, stationary, and homogenous. Annually streamflow data from a period of 2000 - 2017 were used for model calibration and were used for model validation. Unlike rainfall, streamflow shows a strong serial correlation; the value on one day is closely related to the value on the previous and following days especially during the period of low flow or recession. The runoff generated due to the small rainfall that occurs from December to April and heavy rainfall from Jun to September is the main cause of variation of flow in the study area (Source: Master plan study of

Omo Gibe river basin). The gauging station has good streamflow records with a small number of missing data in the area around the study.

Table 3. 4: Stream flow gauging stations and annual streamflow (Cumyr)

No.	Station_Name	X	Y	Annual streamflow (Cu.m.per year)
1	Ghibe near Limu Genet	895931.9	272263.1	9.70E+10
2	Gilgelgibe nearAsendabo	857088.5	299652.2	4.56E+11
3	Ghibe near Seka	840722.6	251754.2	6.37E+10
4	Wabi near Wolkite	912074.2	363560.3	1.21E+10
5	Sokie near Areka	781008.5	356661.3	1.48E+10
6	Gojeb near Shebe	820662.2	211152.7	7.22E+11
7	Walga near Wolkite	911667.9	367069.7	8.26E+10

3.1.6 The soil of study area

Soils that have predominantly available in the study area are eutric leptosols, eutric fluvisols, eutric cambisols, lithic leptosols, vertic cambisols, (Fig. 3.12) and (Table 3.5) (HWSDB (FAO, 2012). From these soil groups, eutric leptosols have a high potential for agricultural activity and are characterized by their very shallow depth over rock. They are <30cm deep, generally with medium textures and a range of colors. They are widespread throughout the Omo basin though they are prevalent in hilly and gorge topography associated with steep slopes and rock outcrops, because of their fertility, ease of cultivation, and ease of root penetration (Master plan study of OGRBD, 1995). In areas covered by such soils, there is less probability of the occurrence of erosion. Erosion is the greatest threat to leptosols. As a result, severe erosion problems may be observed in lithic leptosols under high anthropogenic effects. The erosion risk of fluvisols is high on hilly sides, where there are no proper land use management practices.

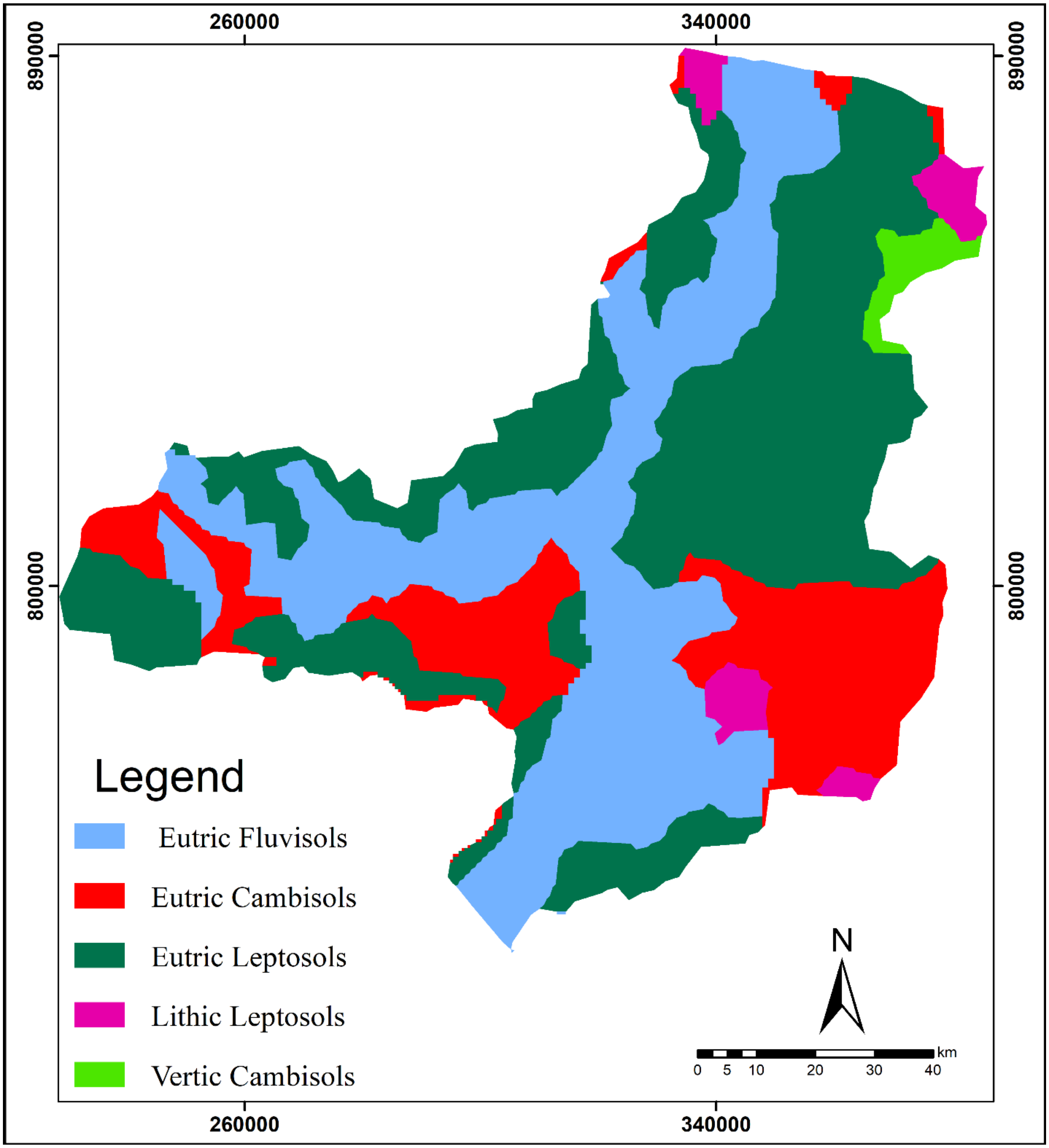

Figure 3. 12: Soil map

.

Table 3. 5: Area distribution of soil units

No.	Major_soilss	Area (ha)	Area (%)
1	Eutric cambisols	1.98E+5	18.5
2	Lithic leptosols	3.21E+4	3.0
3	Eutric leptosols	4.56E+5	42.7
4	Vertic cambisols	1.61E+4	1.5
5	Eutric fluvisols	3.66E+5	34.2

3.1.7 Population and socioeconomic environment

Administratively, the reservoir stretches over five zones and twelve weredas. According to (CSA, 2017), the total populations of the twelve Woredas which are found within the catchment area are about 1,832,959. The area is predominantly inhabited by SNNPR people of Dawuro, Wolaita, Hadiya, Kambata, Konta, Yem and some Wereda of Oromia people are also found. According to EEPow, (2009), the dominant economic bases of the people are subsistence farming and livestock production. The most cultivated cereal crops include Teff, Sorghum, and maize. Pulses, onions, cabbage, banana, Enset as well as coffee are grown in most highland parts of the study area. Due to primitive Farming techniques, the productivity of the Crops is low.

3.2 Materials and sources

3.2.1 Satellite image archives

Landsat imagery of 2000–2006, 2006–2010, 2010–2015, and 2015–2020 (OLI), (ETM+), and sentinel-2 (MSI) with Path 169 and row 055 acquired from free satellite imagery web: (https://earthexplorer.usgs.gov/) (Table 3.6). The landsat8, landsat7, and Sentinel-2 images are used to generate different thematic data layers such as the LULC map; water spread area extraction, and the reservoir storage capacity calculation. Sentinel -1A SAR image of 2016, 2017, 2018, 2019, and 2020, and 12.5m of Advanced Land Observation Satellite Phased Array type L-band Synthetic Aperture Radar Digital Elevation Model (ALOS PALSAR DEM) taken from the website of: (https://vertex.daac.asf.alaska.edu/). DEM is used to generate drainage networks, slope, flow accumulation, and elevation maps, while the Sentinel -1A SAR image is processed to extract the water spread area and used for the reservoir storage capacity calculation.

Table 3. 6: Satellite data description

Date of acquisition	Sensor	Spatial resolution	Used for	Path/Row (landsat & Sentinel 1) Tile (Sentinel-2)	Format	Source
2001, 2005, 2010	Landsat7 (ETM^+)	30m	LULC classification	169/055	Raster	USGS
2015, 2016 & 2017,	Landsat8 (OLI)	30m	LULC, NDWI and	169/055	Raster	USGS
2018,2019, &2020	Sentinel2 (MSI)	10m	LULC & NDWI calculation	T37NCH/T37NBH /T37NBJ/ T37NCJ / T37PCK	Raster	ESA (Copernicus)
2016,2017,2018, 2019 & 2020	Sentinel 1 (SAR)	10m	Waterbody mapping/Reservoir areal expansion mapping	152/566(Frame)	Raster	ASF and Copernicus

3.2.2 Ancillary data source

To accomplish the objective of the proposed study in addition to satellite image other secondary data sources are used. These data were collected from; Food and agricultural organization (FAO) portal, Geospatial Information Institute of Ethiopia (GIIE), Ethiopian Electrical Power (EEPOW), and Ethiopian Metrological Agency (EMA) (Table 3.7). The data collected from FAO was soil texture which was harmonized world soil database (HWDB) used for both study area description and as input for RUSLE, From GIIE topographic map, From EEPOW daily recorded reservoir height and the designed data of reservoir, and rainfall data from EMA.

Table 3. 7: Description of the ancillary data sets

No	Data types	Format	Source
1	Daily recorded reservoir data	Excel(text)	EEPOW
2	Metrological data	Excel(text)	Ethiopian meteorological agency
3	Topographic map	Raster	Geospatial Information Institute of Ethiopia
4	Soil map	Raster	FAO (HWSDB)
5	Geological map	JPg image	Geological Survey of Ethiopia
6	GPS field data	Excel(text)	Self
7	Stream flow	Excel(text)	EBDA
8	Sediment	Excel(text)	EBDA (Ethiopia basin dev.t authority)

All the data types collected are processed using different platforms starting from pre-processing to post-processing specifically ArcMap, ERDAS, ENVI, QGIS, and SNAP (Table 3.8).

Table 3. 8: Software's used to process the data

No	Software name	Version	Typically used for
1	ArcGIS	10.5	Data analysis and map preparation
2	ERDAS Imagine	2015	Image processing
3	ENVI	5.3	Image processing
4	QGIS	3.10	Data analysis and map preparation
5	SAGA GIS	2.3.2	Topographic map generation
6	ESA SNAP	7.0 & 8.0	Radar image processing
7	R	3.4.3 ®	Statically data analysis
8	MapInfo Professional	12.0	To sketch the reservoir level
9	Google Earth Pro	7.3.3	Visualize current reservoir level and Accuracy assessment for land-use/cover
10	Global Mapper	20.0.1	Map generation

3.3 Methods and data processing

Preparation of different thematic data layers was the main activity to build spatial modeling of soil erosion and land use land cover change on the earth's surface. The entire data layers created were retrieved for the model input.

Revised universal soil loss equation (RUSLE), which is an empirical model developed by (Renard, 1997) was framed with GIS and remote sensing techniques were employed to compute the mean annual soil loss of Gilgel Gibe III dam catchment. RUSLE was possibly applicable on every continent on earth where soil loss by water is a problem (Gelagya *et al*., 2016). The overall methodology flowchart (Fig. 3.13) was explained in detail for each model.

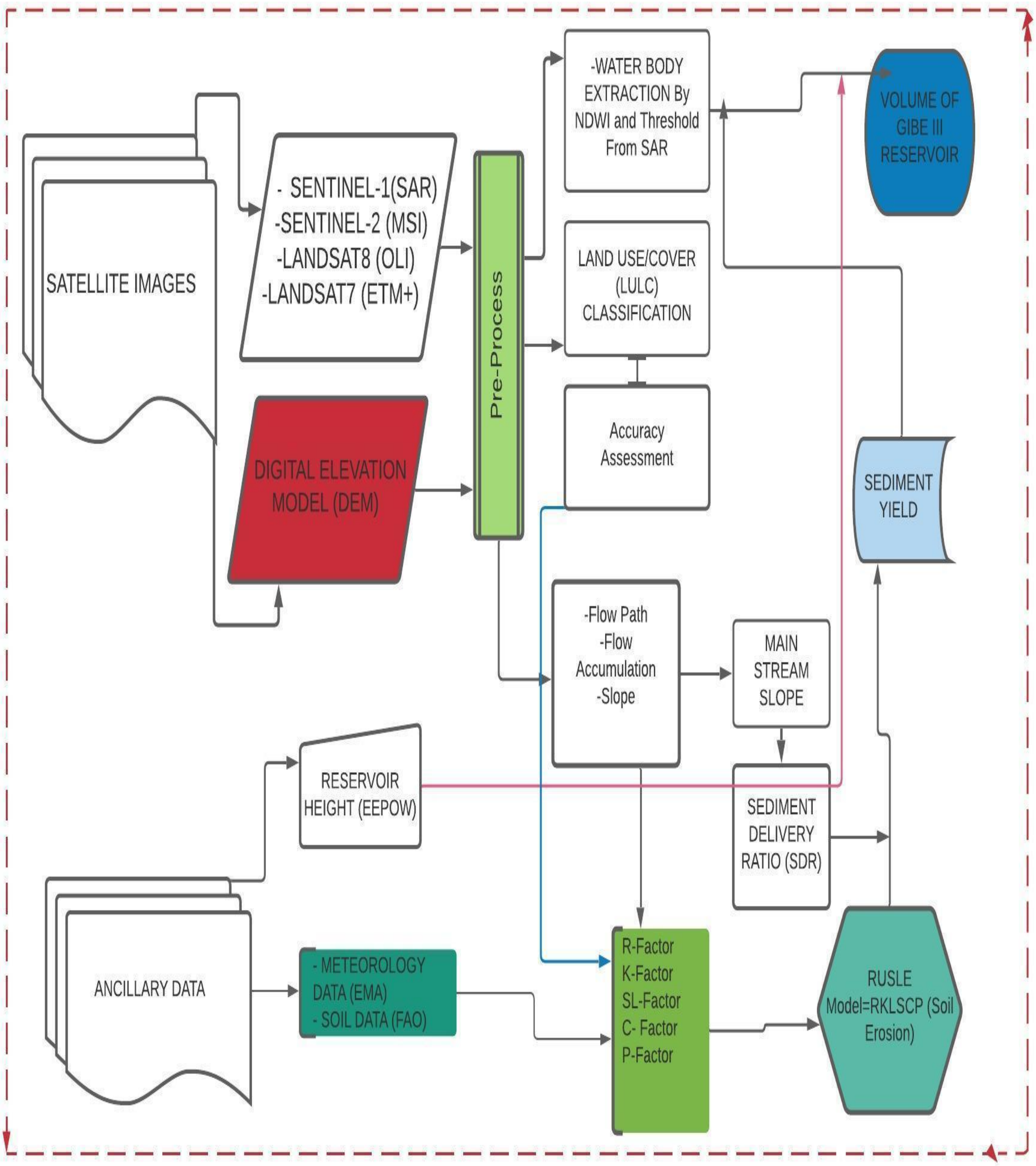

Figure 3. 13: Overall work flowchart

There are two typical conventional methods for reservoir sedimentation estimation, including direct quantification of sediment deposition by hydrographic surveys and indirect measurement employing the inflow outflow records of a reservoir. The two methods are non-cost-effective, cumbersome, and time-consuming (Jain and Goel, 2002). On the other hand, remote sensing technology also developed significantly with the number of reservoirs in the world. Remote sensing provides synoptic coverage of the earth's surface at a regular interval at reasonable resolution since the 1970s (Foteh *et al.*, 2018).

The basic principle of assessing sedimentation using a remote sensing approach is that the water spread at a particular elevation will increase due to the sediment deposition with time (Goel et al., 2002). Considering the volume stored between two dates or elevation as a trapezoid, the capacity between these two elevations can easily be calculated using the trapezoidal formula.

3.3.1 Satellite image utilization and processing

3.3.1.1 Pre- and post-processing of sentinel-1 image

The water spread area was monitored using microwave data of the sentinel 1 image. For this Sentinel-1A SAR having high resolution with 10m, operating at C-band data was used which was launched by European Space Agency (ESA) on April 03, 2014. It is having a repeat period of 12 days. Sentinel-1A ground range detected (GRD) data was obtained from Alaska Satellite Faculty (ASF) https://vertex.daac.asf.alaska.edu/) and European Space Agency (Copernicus hub) which is an open platform for all the sentinel data. So, SAR data is best suited to calculate the water spread area during the lowest and highest level of the reservoir, which is generally missed by optical data due to the presence of clouds (Prasad *et al*., 2018).

The value of Band Sigma0_VV_db ranges from -27.5-17.5 for a full scene image of the study area, but after mosaicking the two images the value ranged from -7-7. The threshold value used for this study was <-16.5 (Fig. 3.14) for the full scene image and <-1.75 for the mosaic image of Sentinel-1 (SAR). SAR data were pre-processed in Sentinel Application Platform (SNAP) to get area dynamics of Gilgel gibe III Reservoir (Fig. 3.15) and (Fig. 3.16). The water (reservoir) pixels were extracted using VV & VH polarization through the threshold approach.

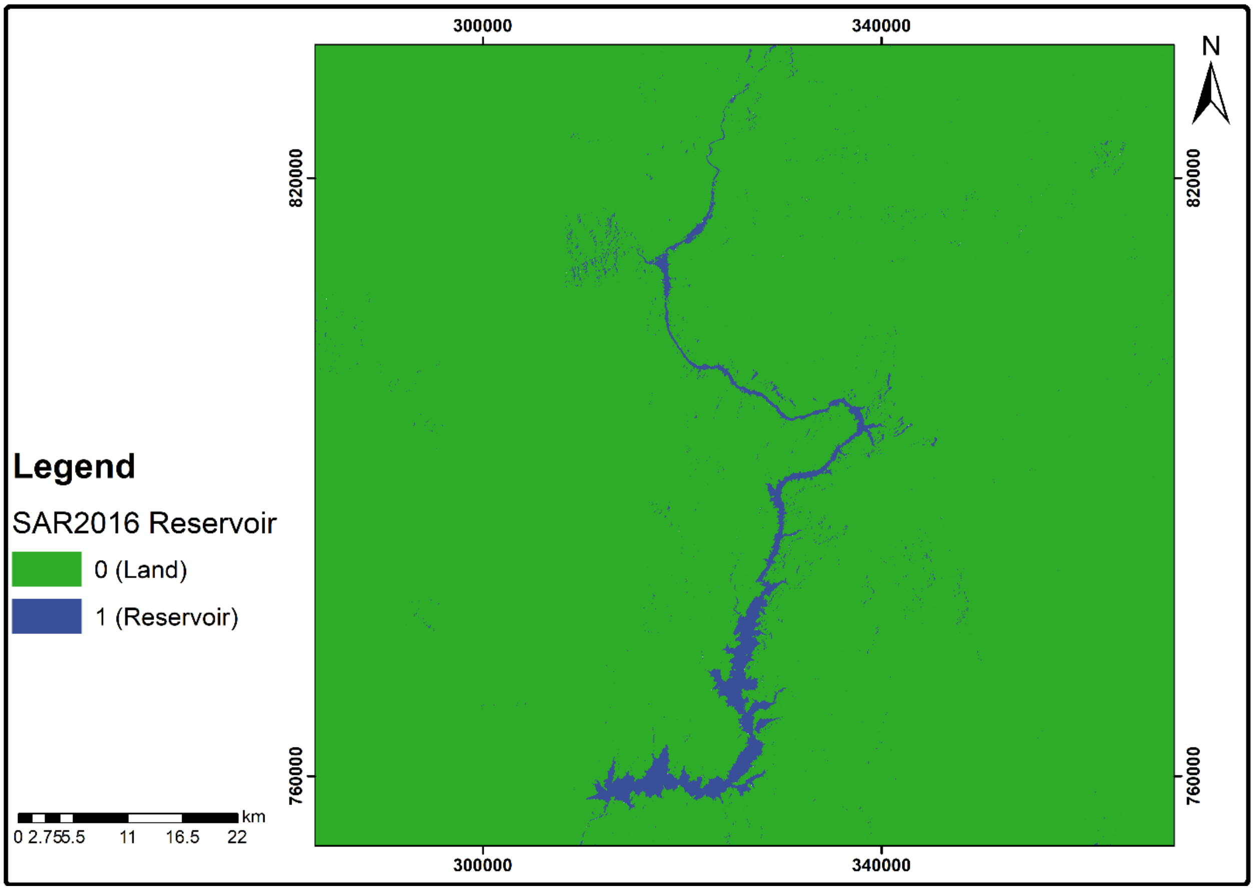

Figure 3. 14: Gilgel Gibe III reservoir after preprocessing Sentinel1 (SAR) image

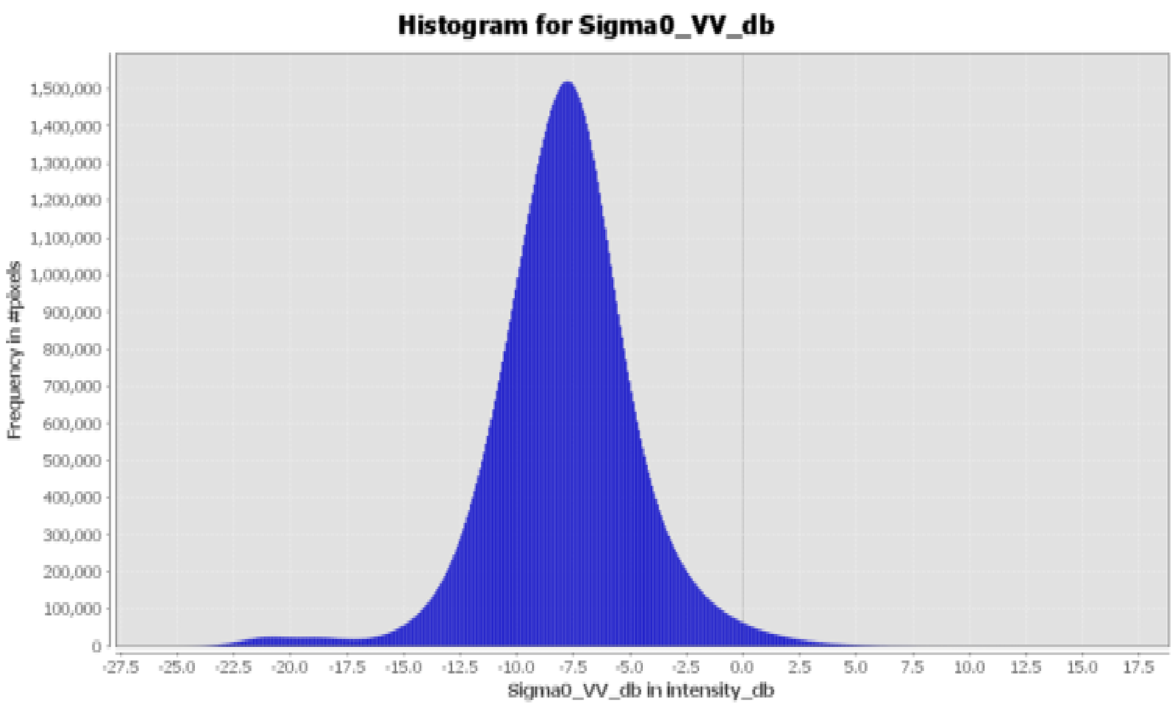

Figure 3. 15: Histogram for Sigma() _ vv band of sentinel1 image for threshold value

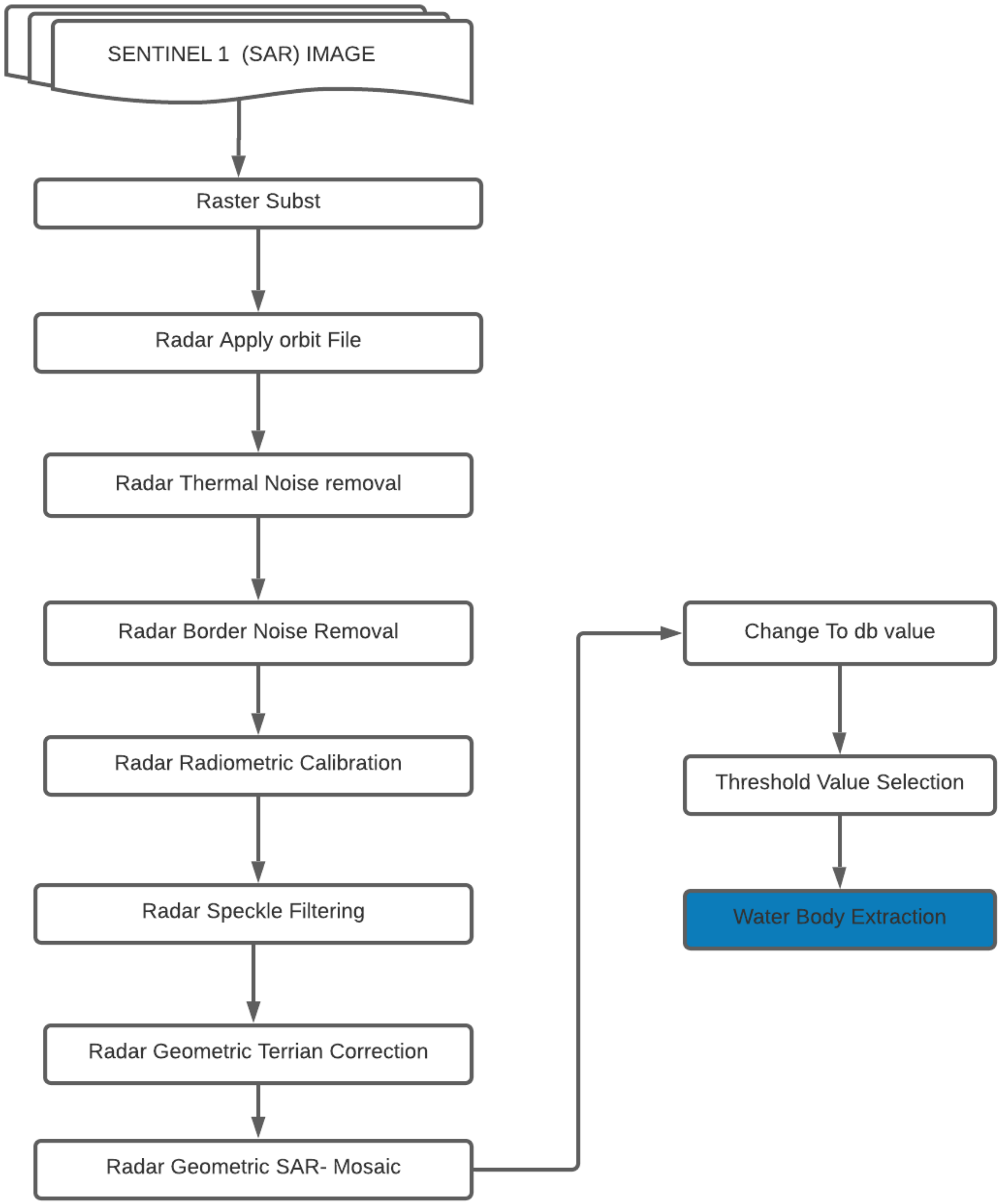

Figure 3. 16: Pre -and post-processing flow chart of sentinel-1 image

3.3.1.2 Pre- and post-processing of sentinel-2 Image

Land-use/cover of the Gilgel Gibe III dam catchment and water spread area of the reservoir by using Normalized difference water index (NDWI) generated after preprocessing of sentinel-2 images. Sentinel-2 gives global coverage every five days. It is equipped with a multispectral imager (MSI) with 13 bands (Cavur *et al*., 2019). Figure 3.18 shows the selected part from the study area, and band combinations for different land cover classification, which covers an area around the turbine of Gilgel Gibe Ill dam, downstream with newly settled settlements around the reservoir and some classes. Band composites of sentinel 2 images include natural color is Band4, Band3, Band2 is in the legend of the figure shown below, false-color infrared are: Band8, Band4, Band3, false color for urban are: Band12, Band11, Band4, band combination for agriculture are Band11, Band8, Band2, for land/water identification bands are" band8, Band11, Band4 and for vegetation analysis Band11, Band8, Band4 (Fig. 3.17) are the composites of bands for land use/cover classification and the preprocessing steps are applied in the QGIS platform those are resampling, layer stacking, mosaicking, and sub-setting.

Resampling is the function that changes the size of the image pixel to the demand size. It allows us to present and process the data with a different spatial resolution (e.g. from different sources) in a uniform way. For the case of sentinel family satellite data, it matters mainly for optical data which are provided with three different pixel sizes 10, 20, and 60m. Additionally, ESA SNAP software requires the same spatial resolution of every band in the source image in most of the functions.

3.3.1.3 Preprocessing of Landsat 7 (ETM+) and Landsat 8 (OLI)

The Landsat 7 was launched on April 15, 1999, which has an Earth-observing instrument of the Enhanced Thematic Mapper Plus (ETM+), replicating the capabilities of the highly successful Thematic Mapper instruments on Landsats4 and 5. It has eight spectral bands, including a pan and thermal band. The ETM+ also includes additional features that make it a more versatile and efficient instrument for global change studies, land cover monitoring and assessment, and large area mapping than its design forebears (USGS, 2018). These features are:

A panchromatic band with 15m spatial resolution on-board, full aperture, 5% absolute radiometric calibration a thermal IR channel with 60m spatial resolution an on-board data recorder, before using of landsat 7 image it needs preprocessing, those are Scan line error correction, layer stacking, mosaicking, and sub-setting.

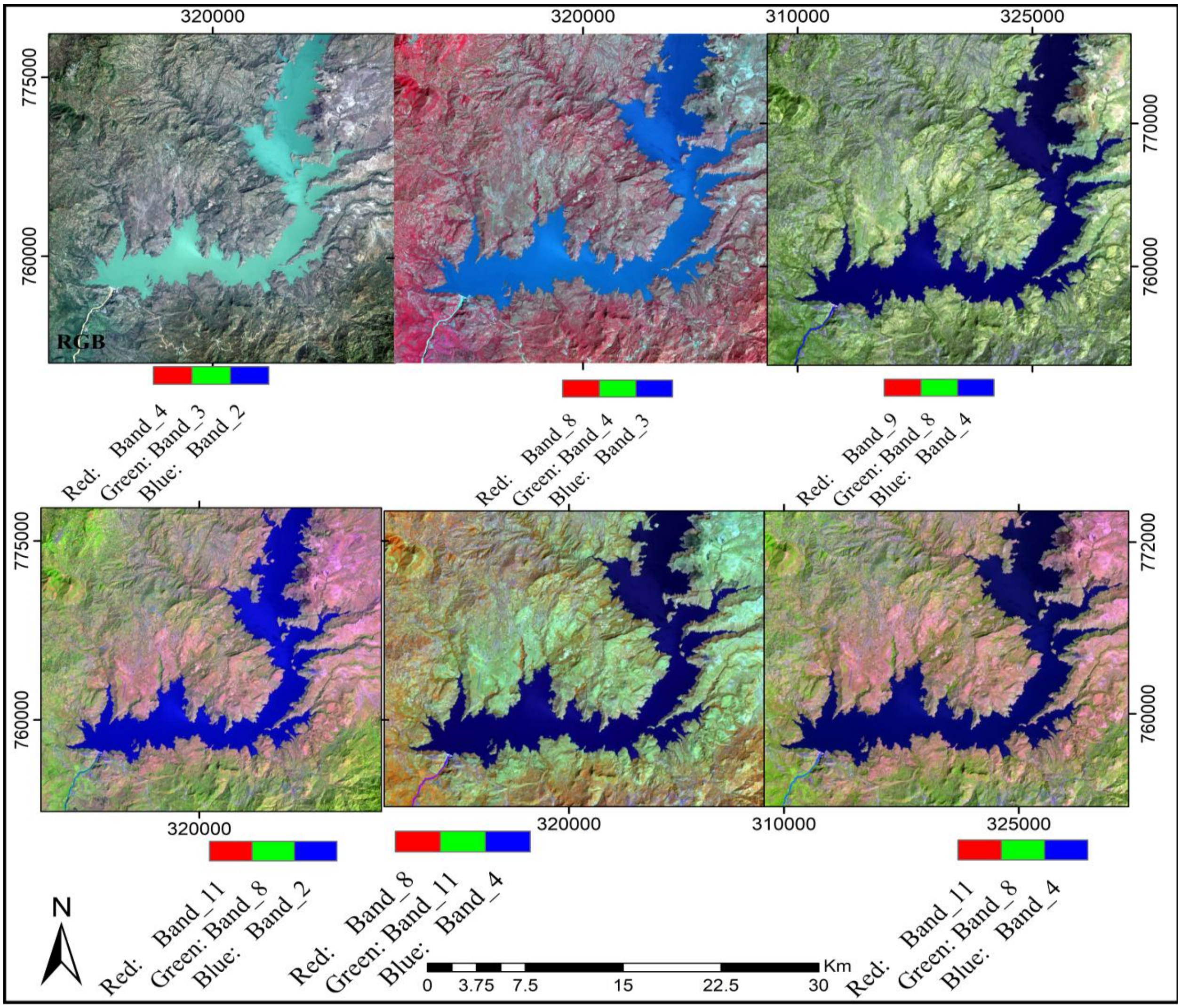

Figure 3. 17: Gilgel Gibe III reservoir turbine areas for sentinel-2 image (MSI) of 2020 band combinations

Landsat 7 is the most accurately calibrated Earth-observing satellite, i.e., its measurements are extremely accurate when compared to the same measurements made on the ground. Landsat 7's sensor has been called "the most stable, best characterized Earth observation instrument ever placed in orbit." Landsat 7's rigorous calibration standards have made it the validation choice for many coarse-resolution sensors. Landsat 8 was launched on February 11, 2013, and carries the Operational Land Imager (OLI) and the Thermal Infrared Sensor (TIRS) instruments. It has nine spectral bands, including a panchromatic band and two thermal infrared bands; all spectral have 30m spatial resolution except pan, which has 15m resolution, and for thermal 100m resolutions.

For landsat8 no need for radiometric and geometric correction, as it was already corrected before downloading and the remaining preprocess is TOA reflectance and brightness temperature are corrected with the use of Quantum GIS and besides these the preprocessing steps include: Converting TOA reflectance and brightness temperature, layer stacking, mosaicking, pan-sharpening, and sub-setting.

Pan-Sharpening is shorthand for "Panchromatic sharpening". It means using a panchromatic (single band) image to "sharpen" a multispectral image (an image that contains more than one spectral band). In this sense, to sharpen means to increase the spatial resolution of a multispectral image. A multispectral image contains a higher degree of spectral resolution than a panchromatic image, while often a panchromatic image will have a higher spatial resolution than a multispectral image. A pan-sharpened image represents a sensor fusion between the multispectral and panchromatic images which gives the best of both image types, high spectral resolution, and high spatial resolution (Lillesand *et al*., 2004).

In this work, 15m spatial resolution of the Landsat 8 (OLI) panchromatic band was used to sharpen the multispectral image for the land use/cover classification.

3.3.2 Land-use/cover classification and change detection

Pre-processing of satellite images before LULC classification and detection of changes is a very vital process with the exclusive aim of building a more direct association between the biophysical phenomena on the ground (Fig. 3.18) and the acquired data (Yogendra *et al*., 2019). In the watershed, land use/cover classification based upon (FAO, 2016) (Table 3.9)

Table 3. 9: Land-use/cover classes for the watershed (Source: FAO)

Class names	Description
Bare land	Rocks, open spaces, & others
Cropland	Standing crops, harvested crops, agricultural lands, farmed bare soil
Forest	Standing trees, harvested trees
Grassland	Grasses, scrubs (shrubs)
Settlement	Buildings, paved roads, residential, beaches around the river
Water	Wetlands, swamps, reservoirs (Gibe III), streams, rivers

After processing satellite images, land-use/cover classification was accomplished by using supervised classification methods and a maximum likelihood algorithm applied to detect the land cover types in the study.

Figure 3. 18: Partial view of land-use/cover in Gilgel gibe III reservoir catchment (Source: Field observation, 2021)

3.3.2.1 Accuracy assessment

The process of producing a land use land cover classification from remotely sensed data could take lengthily. After the classification method the accuracy assessment used for this work, and that has recorded the larger set of spectral classes into a reduced set of information classes, it is tempting to publish the resulting land cover map and then move on to other work. The following steps were applied to produce the accuracy of the Land use/cover classification in the Gilgel Gibe III dam catchment, data derived from Google Earth pro for Land use/cover of years 2001, 2005, 2010, and 2015 and handheld GPS for Land use/cover of the year 2020.

Accuracy assessment was critical for a map generated from any remote sensing data. Error matrix is the most common way to present the accuracy of the classification results (Reis, 2008). Overall accuracy, users and producers, and the Kappa statistic were then derived from the error matrices. Previously, accuracy assessment was not a priority in image classification studies. However, because of the accelerated chances for error presented by digital imagery, accuracy assessment has become a very vital process (Rwanga *et al*., 2017).

The overall accuracy was computed by dividing the total number of correctly classified pixels (Eqn1) (i.e., the sum of the elements along the major diagonal) by the total number of reference pixels.

$$Overall\ accuracy\ = \frac{Total\ Number\ of\ Correctly\ classified\ Pixels(Diagonal)}{Total\ Number\ of\ Reference\ Pixels} \times 100 \qquad (1)$$

The accuracies of individual classes can be calculated by dividing the number of correctly classified pixels in each category by either the total number of pixels in the corresponding row or column (Eqn 2 and 3). The producer's accuracies result from dividing the number of correctly classified pixels in each category (on the major diagonal) by the number of test set pixels used for that category (the column total). User accuracies are computed by dividing the number of correctly classified pixels in each category by the total number of pixels that were classified in that category (the row total).

$$User's\ Accuracer = \frac{Total\ Number\ of\ Correctly\ classified\ Pixels\ in\ each\ category}{Total\ Number\ of ClassifiedPixels\ in\ that\ category(RowTotal)} \times 100 \qquad (2)$$

$$Producer\ Accuracy = \frac{Total\ numberofCorrectly\ classifiedPixels\ in\ eachcategory}{Total\ numberofClassifiedPixels\ in\ that\ category(ColumnTotal)} \times 100 \qquad (3)$$

KAPPA analysis is a discrete multivariate technique used in accuracy assessments (Rwanga, 2017; Jensen, 1996). KAPPA analysis yields a Khat statistic (Eqn4) (an estimate of KAPPA) that is a measure of agreement or accuracy (Rwanga *et al*., 2017). The Khat statistic (K) is computed as;

$$Kappa\ Coefficient\ (\acute{K}) = \frac{N(\sum_i^r\ Xii) - \sum_{i=1}^r (Xi+*X+i)}{N^2 - \sum_i^r (Xi+*X+i)} \qquad (4)$$

Were,

r = number of rows and columns in error matrix, N = total number of observations (pixels)

Xii = observation in row i and column i

Xi+ = marginal total of row i, and X+i = marginal total of column i

A Kappa coefficient equal to 1 means perfect agreement whereas a value close to zero means that the agreement is no better than would be expected by chance. As per (Rwanga, 2017; Landis, 1977) categorization of Kappa statistics is widely referenced (Table 3.10).

Table 3. 10: Rating criteria of Kappa statistics

S.No	Kappa statistics	Strength of agreement
1	<0.00	poor
2	0.00 - 0.20	slight
3	0.21 - 0.40	Fair
4	0.41 - 0.60	Moderate
5	0.61 - 0.80	Substantial
6	0.81 - 1.00	Almost perfect

3.3.3 Soil erosion and model specification

The estimation of erosion rates is usually based on the empirical model that has been developed using data collected from specific geographical areas and hence, the application of those equations are generally limited to those areas represented in the base data (Laknath *et al*., 2017). An empirical relationship developed by Wischmeieir and Smith, namely Universal Soil-Loss/erosion equation (Eqn5) (USLE) (Wischmeier and Smith, 1965) is widely used to determine soil erosion in agricultural areas. USLE was modified in 1978, as developed for sheet and rill erosion (Fig. 3.19) on a large set of experimental data from agricultural plots. Modified Universal Soil Loss Equation (MUSLE) (Williams, 1977), and Revised Universal Soil Loss Equation (RUSLE) (Renard, 1997) are based on the extensive review of USLE and its database and are represented as an improvement of the former (Sirisena *et.al*., 2016).

Revised universal soil loss equation (RUSLE) is a well-known and universally accepted and implemented empirical soil erosion estimation model (Eqn5) (Kaushik *et al*., 2020).

RUSLE was employed at the intermediate watershed or catchment level by incorporating the advanced LS factor computation approach. RUSLE is empirically expressed as:

$$SE\ (metric\ t/ha/yr) = R * K * LS * C * P \qquad (5)$$

Where SE is the mean annual soil Erosion (metric tons ha-1year-1); R is the rainfall erosivity factor (MJ mm/h/ha/year); K is the soil erodibility factor (metric t/ha/MJ/mm); LS is the slope length-steepness factor (dimensionless); C is the cover and management factor (dimensionless, ranges from zero to one); and P is the erosion support practice or land management factor (dimensionless and ranges from zero to one) (Gelagya *et al*., 2016).

Figure 3. 19: Sheet erosion sourced from field observation

3.3.3.1 Rainfall erosivity (R) factor

The erosivity factor (R) in this study calculated based on the equation given by (Hurni, 1985) derived from spatial regression analysis (Eqn6)(Gelagya, 2016; Helden, 1987)for Ethiopian conditions due to the absence of rainfall kinetic energy and intensity data in the study area. The model adopted by (Hurni, 1985) for Ethiopian condition is based on the available mean annual rainfall data and the equation is expressed as;

$$R = -8.12 + (0.562 * P) \quad (6)$$

Where R is the rainfall erosivity factor and P is the available mean annual rainfall data. Inverse distance weighted (IDW) method of interpolation applied to produce uninterrupted rainfall data from point mean annual rainfall data and precipitation from center for hydrometeorology and remote sensing portal (CHRS). CHRS data used because of having high resolution which is 4 by 4km, as the study area has only two gauging stations and the rest was used by interpolation.

3.3.3.2 Soil erodibility (K) factor

Soil erodibility is the expression of the intrinsic resistance of soil particles for the removing and transporting power of rainfall (Wischmeier and Smith, 1978). The K-factor is empirically determined for a particular soil type and reflects the physical and chemical properties of the soil, which contribute to its erodibility potential. K-value will be assigned based on (Gelagya et al., 2016; Erdogan *et al*., 2006) recommendation.

- K is the susceptibility of soil to erosion (detachment and transport) and the rate of runoff (Eqn7)
- It is more sensitive for soil texture type and organic matter content because of its ability to govern the permeability; infiltration rate and structural stability of the soil (Suresh, 2012)
- Depending on soil texture and organic carbon (OC) content of the soil K factor will be estimated using the equation (William, 1995).

$$K_{usle} = K_W = f_{csand} * f_{ci-si} * f_{orgc} * f_{hisand} \quad (7)$$

- Where; - f_{csand} is a factor, that lowers the K indicator in soils with high coarse-sand content and higher for soils with little sand(Eqn8);
- f_{cl-si} gives low soil erodibility factors for soils with high clay-to-silt ratios (Eqn9)
- f_{orgc} reduces K values in soils with high organic carbon content (Eqn10),
- f_{hisand} lowers K values for soils with extremely high sand content (Eqn11):

$$f_{csand} = \left(0.2 + 0.3 * \exp\left[-0.256 * m_s * \left(1 - \frac{m_{sil}}{100}\right)\right]\right) \quad (8)$$

$$f_{cl-si} = \left(\frac{m_{sil}}{m_c + m_{silt}}\right)^{0.3} \quad (9)$$

$$f_{orgc} = \left(1 - \frac{0.25 * orgc}{orgc + expexp\,[3.72 - 2.95 * orgc]}\right) \quad (10)$$

$$f_{hisand} = \left(1 - \frac{0.7 * (1 - \frac{m_s}{100}}{\left(1 - \frac{m_s}{100}\right) + expexp\left[-5.51 + 22.9 * \left(1 - \frac{m_s}{100}\right)\right]}\right) \quad (11)$$

Where: ms – the sand fraction content (0.05-2.00 mm diameter) (%);

msilt – the silt fraction content (0.002-0.05 mm diameter) (%);

mc – the clay fraction content (<0.002 mm diameter) (%);

orgC – the organic carbon (SOC) content (%).

For this work soil data used from harmonized world soil database (HWSDB) of the food and agricultural organization (FAO) soil portal (Table 3.11).

Table 3. 11: Percentage of topsoil texture in soil group

Soil Groups	Tsand(%)	Tsilt(%)	Tclay(%)	Torg(%)
Eutric Fluvisols	43	29	28	0.39
Vertic Cambisols	51	22	27	0.63
Eutric Leptosols	38	26	36	1.79
Lithic Leptosols	37.5	24.5	38	1.54
Eutric Cambisols	22.5	26	51.5	1.76

3.3.3.3 Slope length-steepness (LS) factor

This relies on the slope percentage and length of the slope (Eqn12). The slope percentage layer is derived from the digital elevation model (DEM) of the study area which has a 12.5m resolution. The flow velocity influenced by slope steepness, and slope length describes the distance from where the origin of erosion to the point where deposition occurs (Bagegnehu and Yenealem, 2020). LS factor was calculated by;

$$LS = \left(\frac{As}{22.13}\right)0.6 \; * \; \left(\frac{sinB}{0.0896}\right)1.3 \qquad (12)$$

Where, AS = (flow accumulation × cell size) and B is the slope angle.

LS factor computation method based on upslope contributing area suggested by (Desmet and Govers, 1996; Mitasova and Mitas, 1999).

3.3.3.4 Cover and management (C) factor

It represents the ratio of soil loss from land with specific land cover to the corresponding soil loss from continuous fallow (Gelagya, 2016; Morgan, 2005). Different land use/cover classes and value of C-factor from different reference sources (Table 3.12).

Table 3. 12: Cover and management (C) factor value from different article source

Land-use/cover classes	**C-factor values**	**References**
Waterbody Cultivated land (Cropland) Forest land Shrub land Grazing land	0.00 0.15 0.01 0.014 0.05	Erdogan *et al*., (2006), Hurni, (1985a, 1985b), Wischmeir and Smith, (1978) Mengie *et al*., (2019)
Agriculture experimental stn Associated area Bare land Forest Grassland Market gardening Mine Mixed agriculture Orchard Residential area Scrub forest Shifting cultivation Sundry nontree cultivation Tea Urban Waterbody	0.60 0.35 1 0.01 0.015 0.35 1.0 0.35 0.25 0.003 0.01 0.25 0.25 0.35 0.50 0.00	Wischmeier, and Smith, (1965) Teh *et al*., (2014)
Built upland, Dense Forest Open forest Agricultural land Wasted land, Waterbody	0.004, 0.01 0.014 0.1 0.05, 0	Kayet *et al*., (2018)
Grassland Settlement Cereals or pulse Forest	0.01 0.14 0.17 0.02	Vente *et al*., (2009) and Habtamu *et al*., (2017)

Each land use classes and equivalent mean rate of soil erosion was assessed by using zonal statistical analysis and equivalent to logic of spatial analysis (Temesgen *et al*., 2019)

3.3.3.5 Support practice (P) factor

It is the ratio of soil loss with a specific support practice to the corresponding loss with up and downslope cultivation (Wischmeier and Smith, 1978). This factor will consider the erosion control practices such as contouring (Fig.3.20), strip cropping, and terracing (Table3.13), which reduces the eroding power of rainfall and runoff by their impact on drainage patterns, runoff concentration, and runoff velocity (Hyeon *et al*., 2006). The P-factor was assessed using major land cover and slope interaction adopted by (Wischmeier and Smith, 1978) for Ethiopia's condition. The corresponding P values were assigned to each land use land cover or farming practice and slope classes. Some researchers suggested the P-value is rather dependent on the slope inclination (Wischmeier and Smith, 1978; and Shin, 1999); while others use farming practices to calculate P value (Stone and Hilborn, 2012). P-Value ranges from 0 to 1 where the value 0 indicates very good man-made erosion resistance practices and the value 1 represents no man-made erosion resistance activities (El Jazouli *et al*., 2017).

Table 3. 13: Value of support practice (P) factor (Shin, 1999)

Slope%	Contouring	Strip cropping	Terracing
0−7	0.55	0.27	0.1
7−11.3	0.6	0.3	0.12
11.3−17.6	0.8	0.4	0.16
17.6−26.8	0.9	0.45	0.18
>26.8	1	0.5	0.2

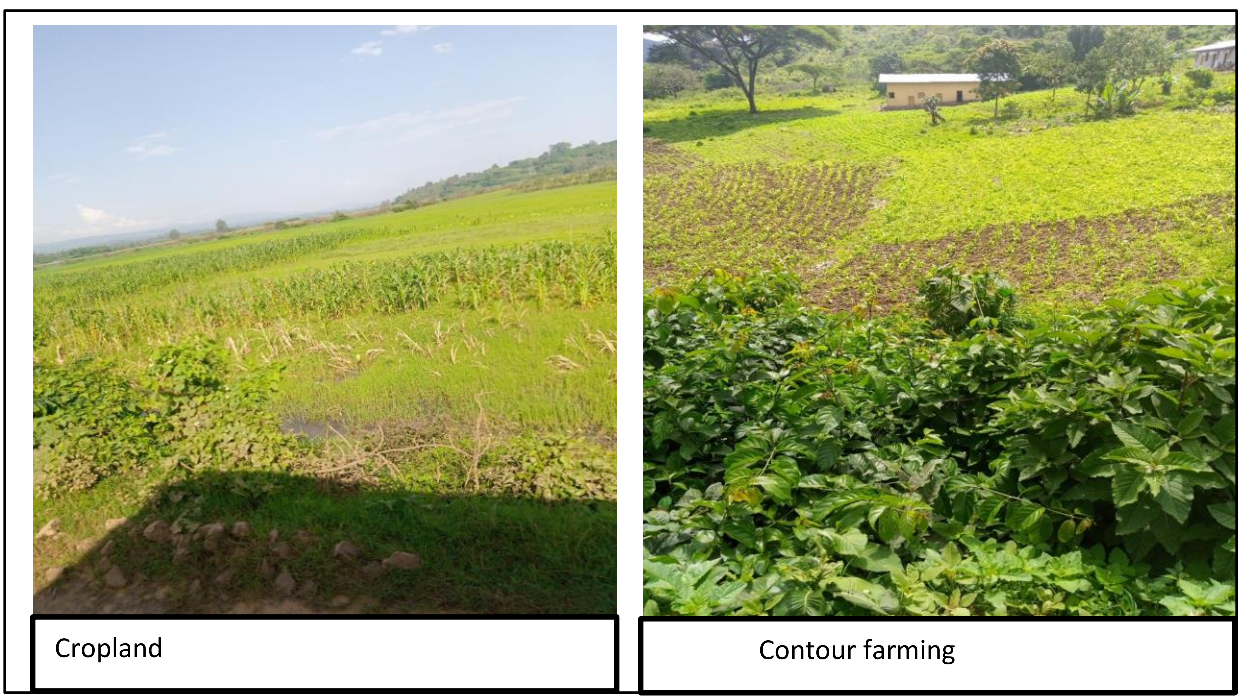

Figure 3. 20: Cropland a type of land-use and Contour farming practice in the study area

3.4 Sediment delivery ratio (SDR) estimation

SDR is a fraction of gross erosion that is transported from a given area in a given time interval. Sediment yield (SY) and siltation found in rivers and dams are not equivalent to the gross sediments that have dissociated from the slopes through land degradation processes. The sediment delivery ratio (SDR) was established as the relationship between the sediment yield (Sy) and the gross erosion (Thomas *et al*., 2020). It is a measure of sediment transport efficiency which accounts for the amount of sediment that is transported from the eroding sources to a catchment outlet compared to the total amount of soil that is detached over the same area above that point (Gelagya *et al*., 2016). The capability of a catchment for storing and transporting the eroded soil is the indication of SDR (Panditharathne *et al*., 2019). According to Williams and Berndt, (1972) the average slope of the stream channel is more significant than other parameters in estimating sediment delivery ratio, and it is a function of the slope of the mainstream channel (eqn13). SDR is expressed as a function of the percent slope of the mainstream channel. Empirically, the Sediment delivery ratio, in this case, is expressed as;

$$SDR = 0.627 * (SLP)^{0.403} \qquad (13)$$

Where, SLP is the percent slope of the mainstream channel. After determining the flow direction, –flow accumulation, and stream network using DEM, mainstream channel slope was computed using ArcGIS HEC-GeoHMS extension. Then using those SLP values, SDR for the main river of the OMO River Sub-basin was calculated in the raster calculator of ArcGIS toolbox.

3.5 Sediment yield (Sy) estimation

Sediment yield is the sediment load at the end of the slope length, at the outlet of the terrace diversion channels, or sediment basins that are considered by RUSLE (Gelagya et al., 2016). The (Eqn 14) used to estimate sediment yield in the study area.

$$Sy = n(SDR * SE) \qquad (14)$$

Where n is the total number of cells over the catchment, SE is the amount of soil erosion produced within the i th cell of the catchment estimated using (Eqn5) and SDR is the fraction of SE that ultimately reaches the nearest channel computed by (equation10).

3.6 Waterbody extraction from Landsat 8 (OLI), and sentinel-2 (MSI)

For surface water bodies' extraction, it is required to identify the number of water pixels. Though the spectral signature of water is quite distinct from other land uses like vegetation, built-up area, and soil surface, identification of water pixels at the water/soil interface is very difficult and depends on the interpretative ability of the analyst. To identify water pixels, the following steps are performed: Normalized difference water index (NDWI) is used to monitor changes related to water content in water bodies (Eqn15, 16, & 17), using green and NIR wavelengths, defined by (Foteh *et al*., 2018; McFeeters, 1996) the following formula:

$$NDWI = \frac{(Green - NIR)}{(Green - NIR)} \quad (15)$$

Where Green is a band that encompasses reflected green light and NIR represents near-infrared radiation. The NDWI image was produced in which generally the water features have positive values, whilst soil and other features have negative values (i, e, the value of NDWI ranges between -1 up to +1) (Yun Du et al., 2016). Normalized difference water index (NDWI) is used for the water bodies analysis. The index uses Green and near-infra-red bands of remote sensing images. The NDWI can enhance water information efficiently in most cases. It is sensitive to build-up land and results in over-estimated water bodies. The NDWI products can be used in conjunction with NDVI change products to assess the context of apparent change areas (Bahadur, 2018).

$$\text{NDWI(Landsat 8)} = \frac{(\text{Green} - \text{NIR})}{(\text{Green} + \text{NIR})} = \frac{(\text{B3} - \text{B5})}{(\text{B3} + \text{B5})} \quad (16)$$

$$\text{NDWI (Sentinel 2)} = \frac{(\text{B3} - \text{B8})}{(\text{B3} + \text{B8})} \quad (17)$$

The extracted water information in those regions was often mixed with built-up land noise. To remove the built-up land noise, its signature features need to be examined and modified normalized difference water index (MNDWI) (Eqn18) was used (Xu, 2006).

$$MNDWI = \frac{Green - MIR}{Green + MIR} \quad (18)$$

MIR is a Middle Infrared band such as Band 6 for (OLI) and Band 5 for TM. Therefore, if a MIR band is used instead of the NIR band in the NDWI, the built-up land should have negative values. According to (Sekertekin *et al*., 2018), the threshold value of Sentinel 2 (MSI) for NDWI and MNDWI (Fig.3.21) were 0.2627 and 0.3647 respectively. For the case of landsat8 (OLI) the threshold value greater than zero (Mcfeeters, 1996; Xu, 2006).

During field observation, the reservoir area dynamic for different months of the year 2021 (Fig.3.22), for the months February and May the reservoir level varied and the cloud coverage was rising from May.

3.7 Estimation of dynamic storage capacity of the reservoir

The remote sensing technique helps to calculate the dynamic storage capacity of the reservoir, which is compared with the original capacity, and reduction in capacity over a while is attributed to sediment deposition. The remote sensing technique for estimating sedimentation is useful only for lakes and reservoirs where rise and fall in water level is a regular phenomenon (Naima *et al*., 2014).

Calculation of live storage capacity of a reservoir involves creation of database, calculation of water spread area from the SAR, Sentinel2 (MSI), and landsat8 (OLI) data, daily observed data for reservoir height for the satellite pass dates (Chowdary *et al*., 2017). The basic principle of assessing sedimentation using a remote sensing approach is that the water spread at a particular elevation will increase due to the sediment deposition with time (Goel *et al*., 2002). Considering the volume stored between two dates or elevation as a trapezoid, the capacity between these two elevations can easily be calculated using the trapezoidal formula. **Trapezoidal** or Mid Area methods were used to estimate the volume of the reservoir (Prasad *et al*.,2018) in this study as given in (Eqn 19 and20).

$$V = \frac{H}{3} * ((A1 + A2 + \sqrt{A1 * A2}) \qquad (19)$$

Where V is the capacity of the reservoir between two elevations, A1 and A2 are the water spread area at these two elevations or two dates of the satellite pass. H is the elevation difference between two elevations of the respective dates.

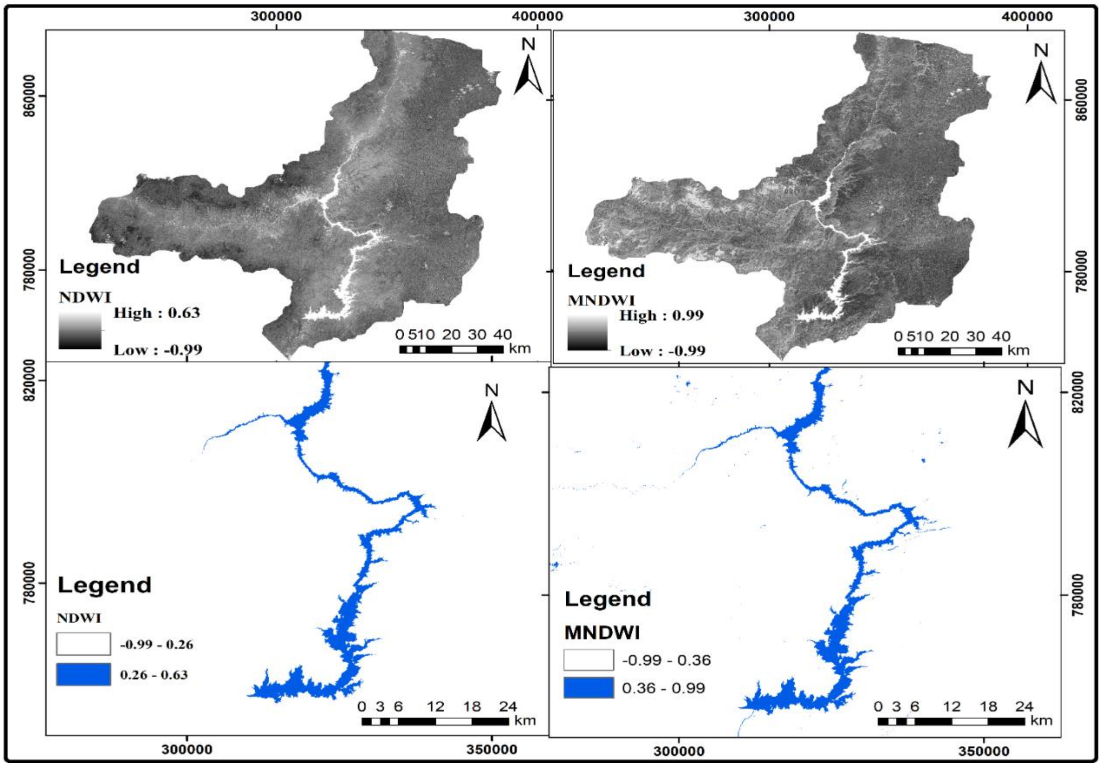

Figure 3. 21: Value of NDWI and MNDWI of Gilgel gibe III reservoirs from Sentinel-2 image.

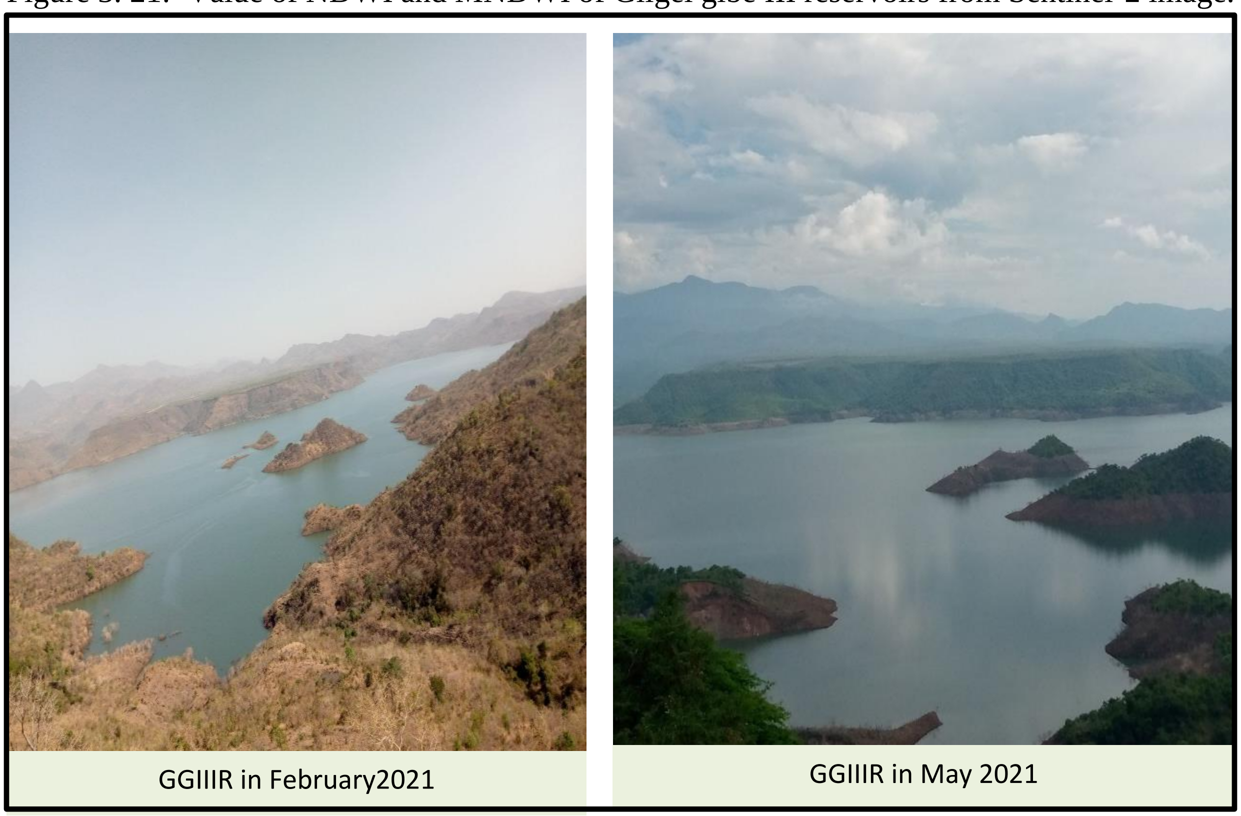

Figure 3. 22: Gilgel Gibe III reservoir in February and May

The corresponding reservoir heights for dates of satellite data pass obtained from Ethiopia Electric power (EEPow). Cumulative revised live storage capacity was calculated by adding all the capacity at each elevation under consideration. The difference between the original and revised capacity will give total sediment deposition between the lowest and highest observed elevations. The live storage capacity or sedimentation is assessed between either below the full reservoir level (FRL) or above the maximum drawdown level (MDDL) of the reservoir. And

Mid Area Method

$$V(Reservoir\ Capacity) = \sum_{i=1}^{n} dh\left(\frac{A_i + A_{i+1}}{2}\right) \tag{20}$$

Where, V = Reservoir capacity, Ai = Area at elevation interval i, Ai+1 = area at the next elevation above the elevation level i. This method is more suitable where the elevation interval dh, is small (Tendai, 2005).

CHAPTER-4 RESULTS

4.1 Land-use and land cover

The land-use/cover pattern of the study area was the result of natural and socio-economic factors and their utilization by man in time and space. Applying the pixel-based image classification method; the land use/cover map values were computed by using the Supervised and unsupervised classification technique and likelihood algorithm in ENVI 5.3 and ArcGIS10.5 from 2001−2020. These land use/cover values were divided into six classes based on the different researchers on the watershed land use classification. Land use/cover classification by using satellite images is the process of sorting pixels into a finite number of individual classes, or categories of data based on their data file values. In the study, the land use/cover classes are divided into six classes. Those are bare land, cropland, forest, grassland, settlement, and water body (which include rivers, swamps, and reservoir of gibe III dam).

The area of each class was calculated taking into account the pixel count and total area (study area). Thus, coverage of each classified area, (percentage) is tabulated in (Table 4.1). The percentage of areas in 2001 and 2005 (free dam construction) as classified are; bare land (5.1 and 11.22), cropland (23.6 and 31.26), forest (6.35 and 8.95), grassland (58.81 and 43.02), settlement (5.97 and 5.23), and water (0.2 and 0.32). Grassland dominates in the time of free dam construction which covers about 58.81 and 43.02 of the total study area that considered the type of land classes like shrubs and grasses based on the FAO classification in the watershed. The dominance of grassland followed by croplands, while the least classified as waterbody, were rivers (sand river and swamps), which accounts for (0.2 and 0.32) for respective years. Land use/cover maps of the Gilgel Gibe III Dam catchment from the years 2001 up to 2020 are classified as free dam construction (Fig. 4.1) (2001−2005), during dam construction (Fig. 4.2) (2010−2015), and after dam construction (Fig. 4.3) (2016−2020). In the free dam, the dominating classes were grassland which accounts for 58.81 and 43.02 percent in the years 2001 and 2005 (Table 4.2) respectively, and cropland that has 23.6 and 31.26 percent in 2001 and 2005 in the order.

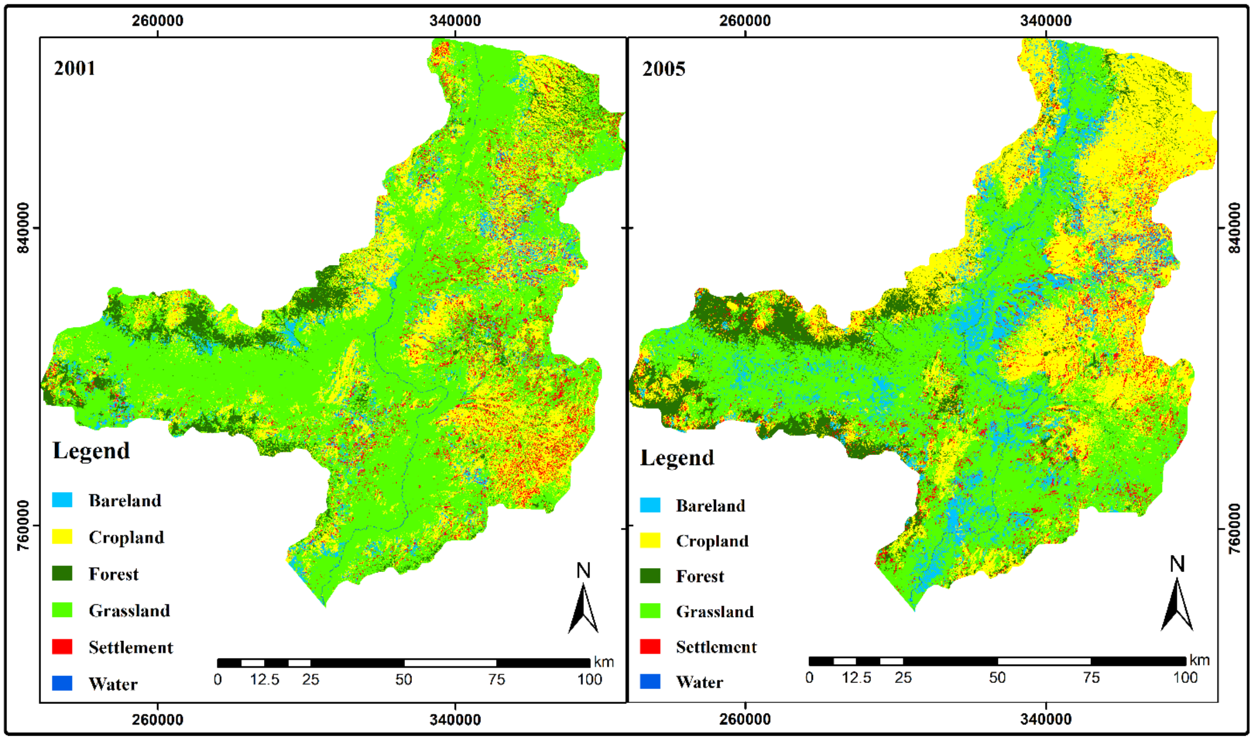

Figure 4. 1: Land-use/cover of free dam construction (2001 − 2005)

The percentage cover of land-use/cover in the year 2010 and 2015 (during dam construction) as classified are bare land (23 and 15.1), cropland (32.2and 32.7), forest (5.5 and 9.3), grassland (34.8 and 29.7), settlement (4.3 and 11.6), and water (0.3 and 1.51). Grassland dominates in the time of dam construction which covers about 34.8 of the total study area followed by cropland in 2010 and cropland dominates in 2015, followed by grassland with respective percent of (32.72 and 29.7). The least classified as waterbody, were rivers (sand river and swamps), which accounts for (0.3 and 1.5) for the respective year.

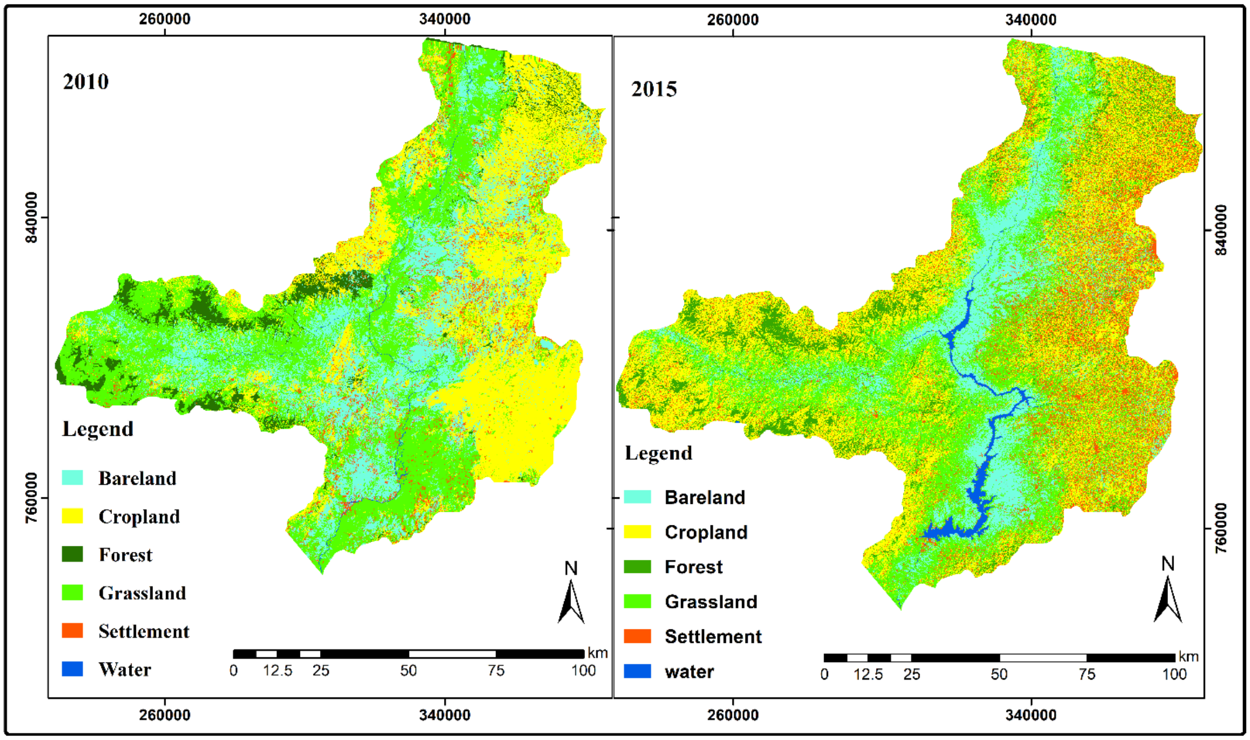

Figure 4. 2: Land-use/cover during dam construction (2010 – 2015)

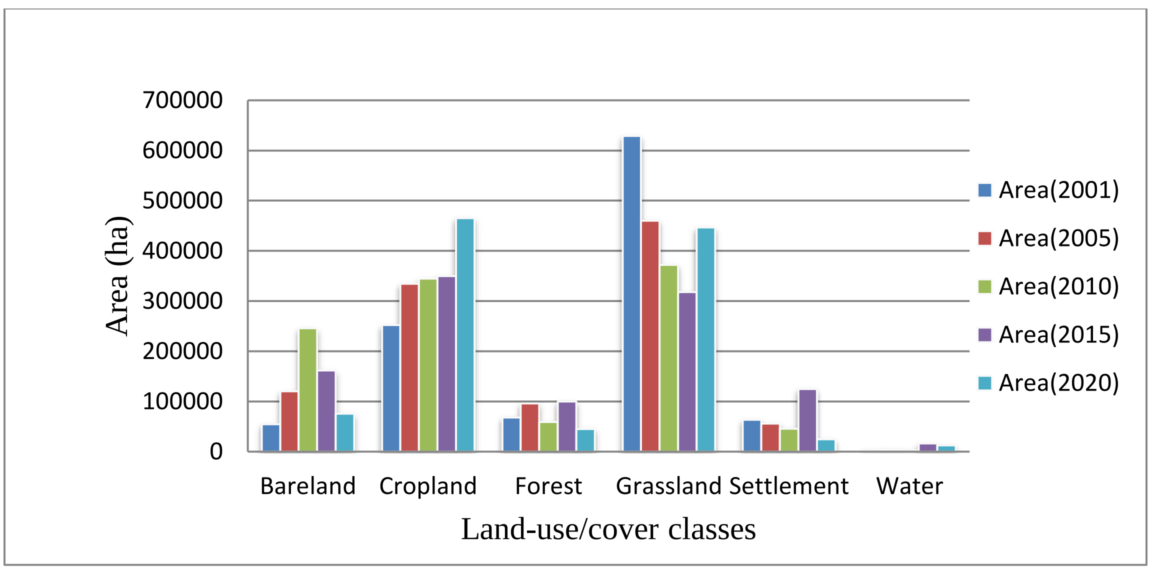

Figure 4. 3: Land-use/cover class *vs* area coverage from 2001 – 2020

Land-use/cover during dam construction practices is grassland, cropland, and bare land having 35, 32.3, and 23 percent respectively in the year of 2010, which showed the loss and gain of the classes in the time of dam construction.

Table 4. 1: Land use/covers change percentage and area in hectare

	2001		2005		2010		2015		2020	
LULC classes	Area(ha)	Area (%)	Area(ha)	Area (%)	Area(ha)	Area (%)	Area(ha)	Area (%)	Area(ha)	Area (%)
Bare land	5.4E+4	5.1	1.2E+5	11.2	2.45E+5	23	1.62E+5	15	7.59E+4	7.10
Cropland	2.5E+5	24	334514.5	31.3	344424.5	32.2	350066	32.7	465015.5	43.5
Forest	6.8E+4	6.3	95801.8	9	58892.3	5.5	99661.9	9.3	44963.0	4.2
Grassland	6.3E+5	58.8	460270.7	43	372160.3	34.8	317742.2	29.7	446739.3	42
Settlement	6.4E+4	6	55961.1	5.2	45441.4	4.2	124448	11.6	24435.76	2.3
Water	2113.1	0.2	3391.11	0.3	3180.7	0.3	16118	1.5	12778.80	1.2
Total	1.07E+6	100	1.07E+6	100	1.07E+6	100	1.07E+6	100	1.07E+6	100

Land-use/cover of post-dam area percent coverage are bare land (7.10), cropland (43.5), forest (4.2), grassland (41.74), settlement (2.28), and water (1.2). This period dominated with the land cover of cropland which accounts for 43.5, followed by grassland having 41.74 and the last class was waterbody (1.2). Land-use and land cover dominance based on area coverage was grassland, cropland, bare land, and settlement through the years 2001−2020 (Fig. 4.4). During the dam construction (i.e., 2006-2015) the land-use/cover is progressively changed and modified, especially settlement and bare land coverage area and the percentage increased that is 5.2 and 11.2 and 15.1 and 11.6 percent in the year 2005 and 2015 respectively.

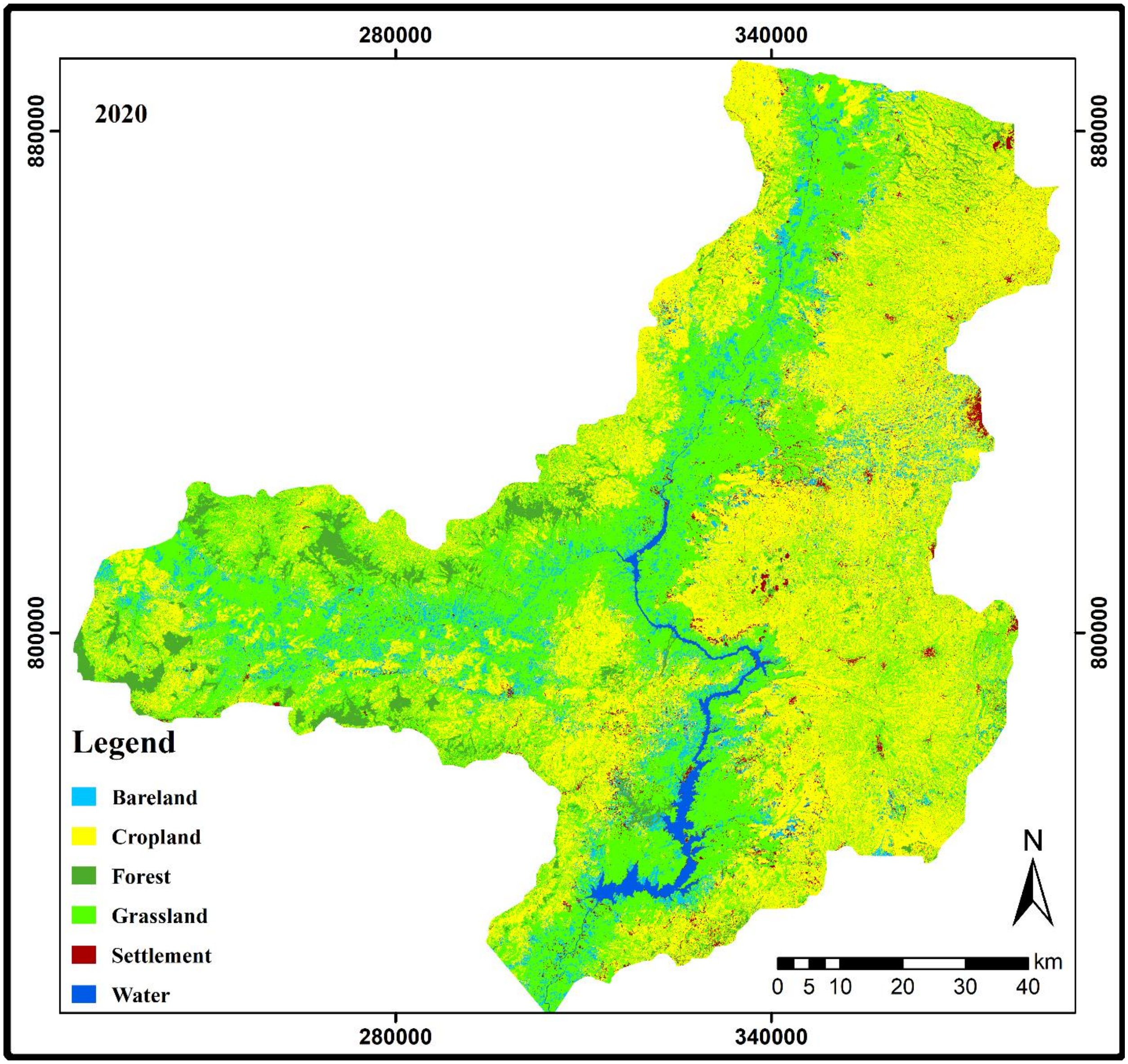

Figure 4. 4: Land-use/cover after dam construction (2020)

The study area covers 1,068,925 hectares among those 465,016ha was cropland in 2020 and 252347.5ha in 2001. After the construction of the dam (i.e., open for service that provides electricity from (2015−2020) and the percentage coverage of all land-use/cover classes is changed. A waterbody or river becomes a reservoir and the area changes from 3,181 hectares during dam construction to 16,118 hectares after the construction of the reservoir in the year 2010 and 2015 respectively.

4.1.1 Accuracy assessment

For supervised classification training points were used (Fig. 4.5), with validation points. Accuracy assessment was taken for all five-year intervals of 2001, 2005, 2010, 2015, and 2020. The overall accuracy, users, producers, and kappa coefficient accuracy were assessed for all years of land-use/cover.

User's accuracy in percent varies from 77 (grassland) to 100 (water) in 2001 and 88 (bare land) to 100 (water) in 2020. Producer's accuracies in percent range from just 75 (Bare land) to 100 (water) in 2001 and 89 (grassland) to 100 (water). For user's accuracy assessment of land use/cover for 2001 30 points for each class, and (180 total points) were generated from classified images, and the same points are checked for validation (producer's accuracy) with the same year on Google Earth pro. The correctly classified classes of land-use/cover are bare land (24/30), cropland (26/30), forest (28/30), grassland (23/30), settlement (28/30), and Water (30/30) (Fig. 4.5). Similar steps are applied to validate the classified land-use/cover with ground truth (Appendix I and Appendix IV).

The kappa coefficient for all classes was above 80 percent and that shows the classification was almost perfect based upon the rating criteria of kappa statistics.

4.1.2 Land-use and land cover change (LULCC) assessment

Land-use and land cover change detection was an advantage of remote sensing images in their ability to capture and preserve a record of conditions at different points in time, to enable the identification and characterization of changes over time. Change detection is among the most common uses of digital image analysis. The types of changes that might be of interest can range from nearly instantaneous to long-term phenomena such as increment of settlement or deforestation. Change detection matrix had been generated by using ArcGIS of overlay analysis to investigate the trends and patterns of land cover change. In this study, six classes of Land use/cover used for change detection by the post-classification technique of five dates of satellite images (i.e., 2001−2005, 2005−2010, 2010−2015, 2015−2020) (Appendix II) were used to detect changes. The results are analyzed as free dam construction changes, during dam construction, and after dam construction changes. Before the Gilgel Gibe III dam construction, the highest percentage change took place between grassland and cropland, which accounts for 15 percent change. Among the classes, bare land, cropland, grassland, settlement, forest, and water remained 1.1, 11, 31, 1, 5, and 0.2 percent respectively.

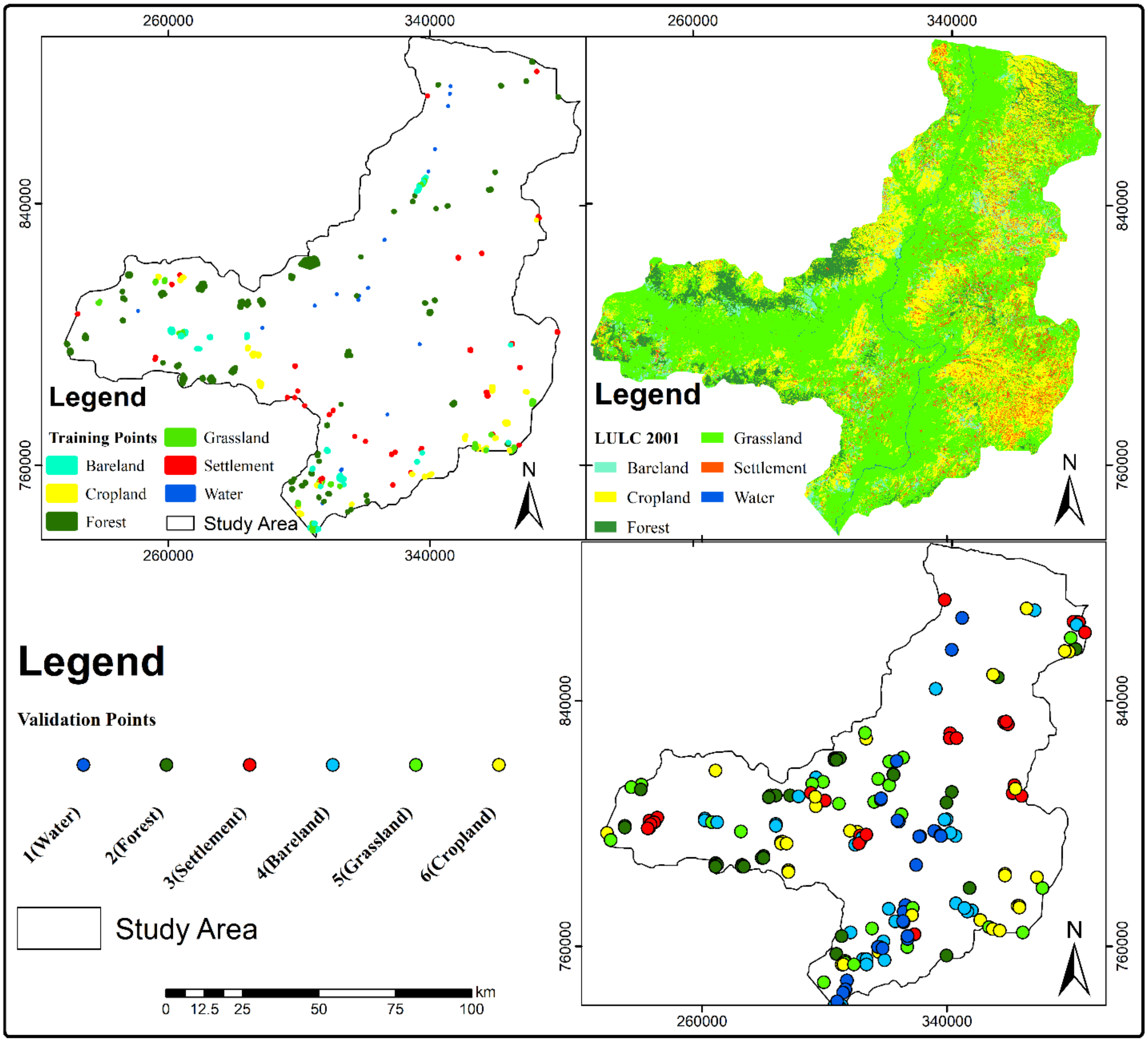

Figure 4. 5: Training samples, land-use/cover of 2001, and validation sample points

The change between 2005−2010 and 2010−2015 took place during GGIIID construction, those shows the dominating change of grassland to cropland and grassland to bare land, and succeeding change occurred from cropland to grassland and cropland to settlement with percentage cover orderly, 9.8, 7.3, 6.5, and 6.3. The unchanged land covers in this period are cropland to water and forest to water, those having zero percentage cover during the construction of GGIIID, but a little change took place from cropland to water in the year of 2010, that account percentage of 0.01. In addition, this period was known by deforestation because the change from forest to cropland and forest to settlement was increased from free dam construction of respective percentages.

The change detection within 2015−2020, specifically after Gilgel Gibe III dam (GGIIID) construction indicates that the most prominent alteration between cropland to grassland and vice versa. Throughout this time deforestation and agricultural activities increased from the previous period of land cover change, peculiarly exchanged amongst cropland, forest, and bare land.

4.2 Soil erosion

The RUSLE model was used to generate the rate of soil erosion in the reservoir catchment. The erosion of the study area simulated for five-year interval starting from 2001 up to 2020 (Fig. 4.9) that ranges from 0 −5, 5−10, 10−30, 30−50, and greater than 50 t/ha/yr. (i.e., very slight to very severe) estimated by using the integration of GIS and remote sensing approach. The percentage of severity cover was not more than 1.98 which was the only severe percent in the year 2010 of the study. Five factors are used to produce soil erosion by using the RUSLE model computed through (Eqn2). The elements are:

4.2.1 Rainfall erosivity (R) factor

The erosivity factor (R) in this study calculated based on the (equation2) and inverse distance weighted (IDW) method of interpolation applied to produce uninterrupted rainfall data from point mean annual rainfall data and precipitation from the Center for hydrometeorology and remote sensing portal (CHRS) (Fig. 4.6). The value of the R factor range within 472 - 713.5 was the average of the r-factor from metrology (gauging station) and R factor from CHRS of portal source throughout the study, and the western and southern part of the study area get a higher range of the factor. The value of the R factor used through all years assessed in the study (2001, 2005, 2010, 2015and 2020) was different.

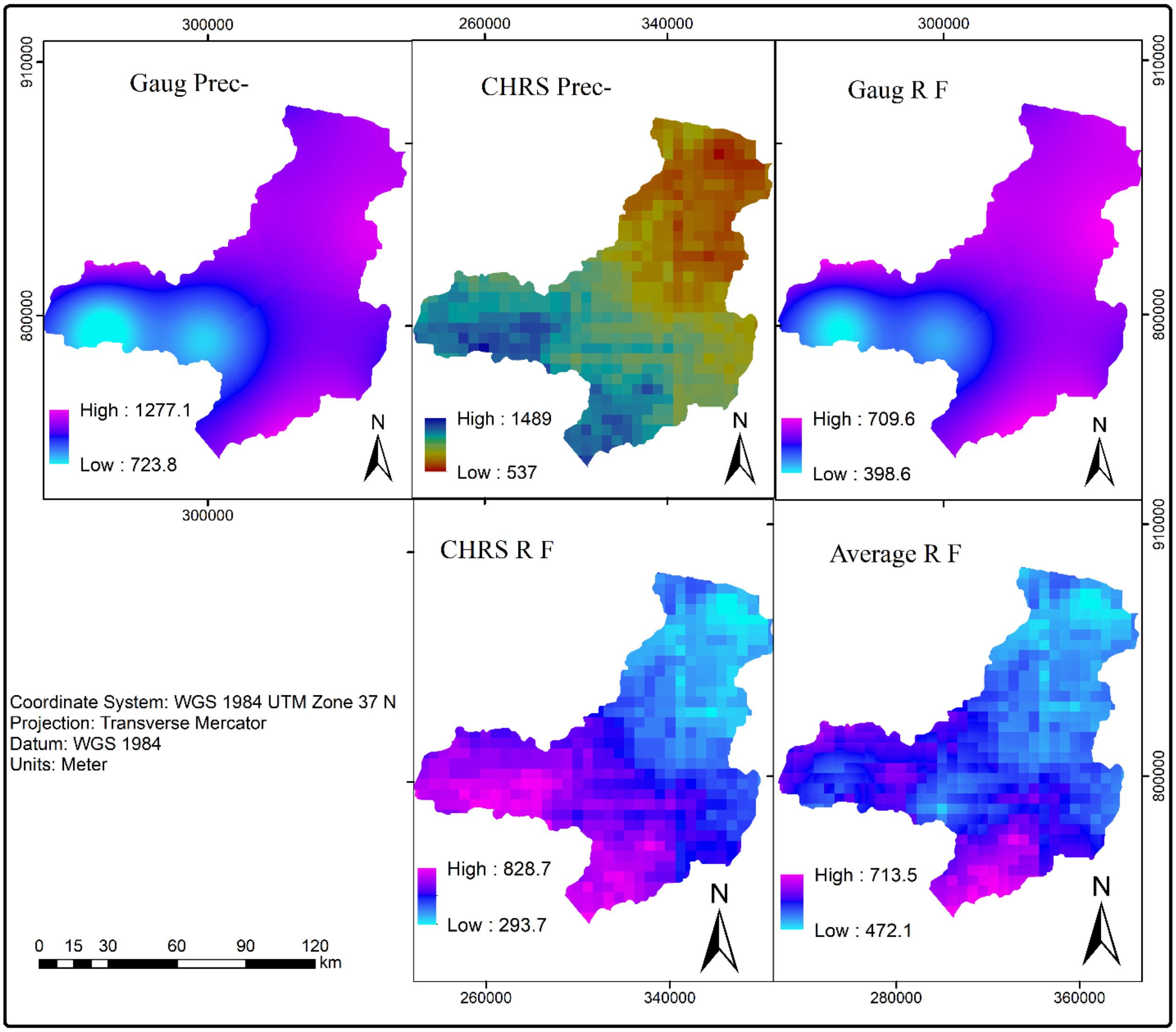

Figure 4. 6: Precipitation and R factor (erosivity) of rainfall in 2001

4.2.2 Soil erodibility (K) factor

The erodibility is the soil-born property affecting the soil detachment by splash during rainfall or by surface flow during sheet erosion or both. The equations 4-8 of the last chapter, were used to derive the value of K-factor (soil erodability), for which the respective soil classes and percentage of soil textures were applied from harmonized world soil data of FAO. The value of the K factor ranges between (0.09- 0.11) and the percentage of soil textures was used from Table 3.10 of this study. This value of the K factor was used through all years assessed in the study. The area shelters a higher portion along the main river line of the catchment in the Gilgel gibe III dam (Fig. 4.8).

4.2.3 Slope length-steepness (LS) factor

Another name for slope length and steepness factor is the topographic factor was generated from slope percentage and length of the slope. LS factor value ranges from 0 to 6776.4 (Fig. 4.7) and most of the ranges fold in the (0-2.2) which was around 98.2percent of LS-factor.

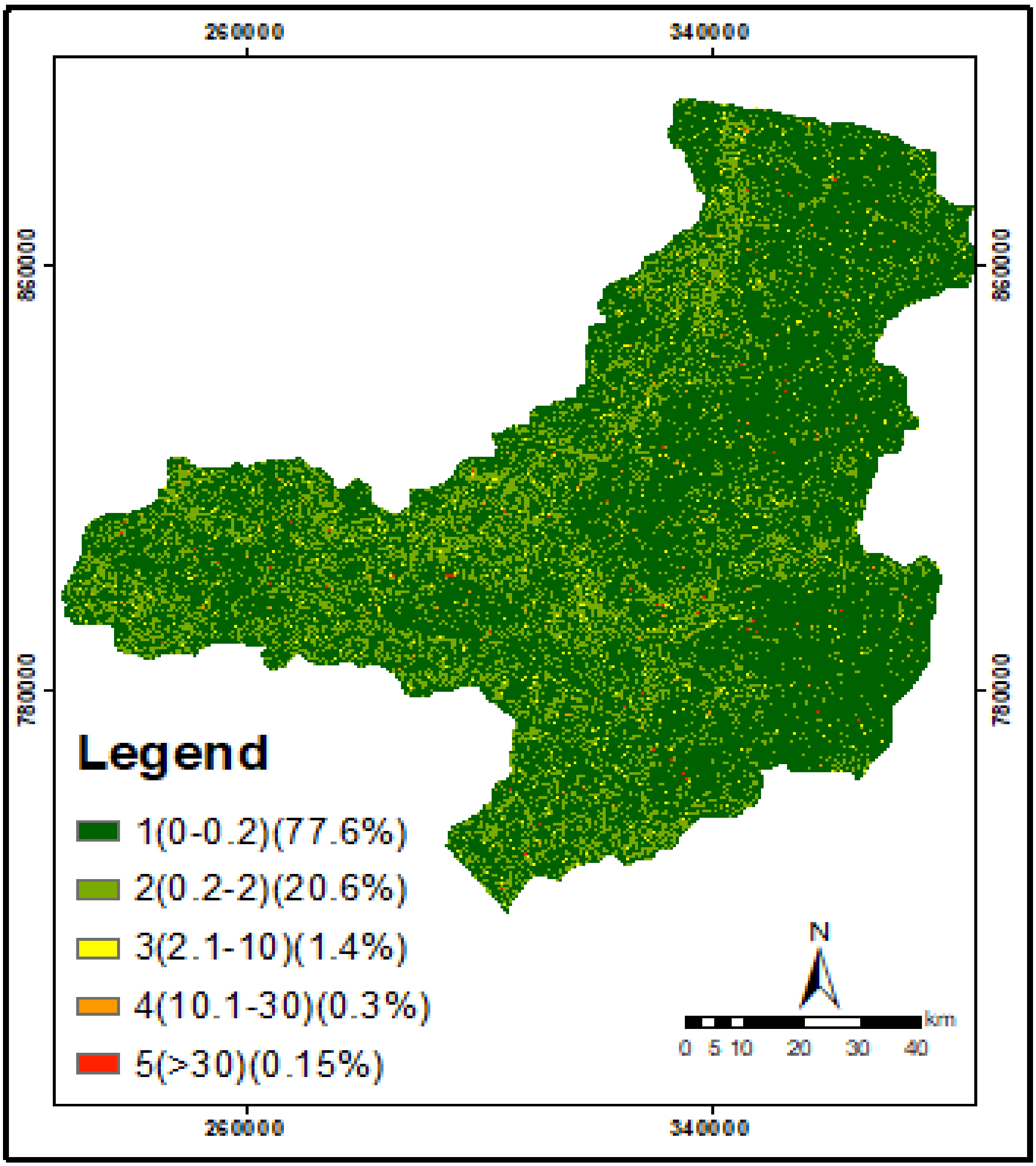

Figure 4. 7: LS factor map

The slope percentage layer is derived from the digital elevation model (DEM) of the study area which has a 12.5m resolution. LS factor was calculated by applying (Eqn9) of this research and is one of the components in the RUSLE model.

4.2.4 Cover and management (C) factor

It measures the combined effect of all the interrelated cover and management variables on soil erosion. The value of management factors generated using land use land cover practices based on different previous researchers. The value varies from 0 to 1 (i.e. water body to Bare land) (Table 3.11) was used as input for the RUSLE model (Fig. 4.8). C-factor value of thematic map used through this work was generated based upon land use/cover assessment year (i.e. for years 2001, 2005, 2010, 2015, and 2020). The remaining part of RUSLE factors of the years is included in (Appendix V).

4.2.5 Support practice (P) factor

It is the specific soil and water conservation practices to reduce run-off speed and increase infiltration. In this study P factors were determined by applying the types of conservation measures implemented and the class of slope percent in the watershed of Gilgel Gibe III Dam. As different researchers used, the most common types of conservation in the catchment were contouring or contour farming. Therefore, the value of the p-factor ranges from 0.55 to 1 (Fig. 4.8). The P-factor value of the thematic map used through this work was the same for the years 2001, 2005, 2010, 2015, and 2020.

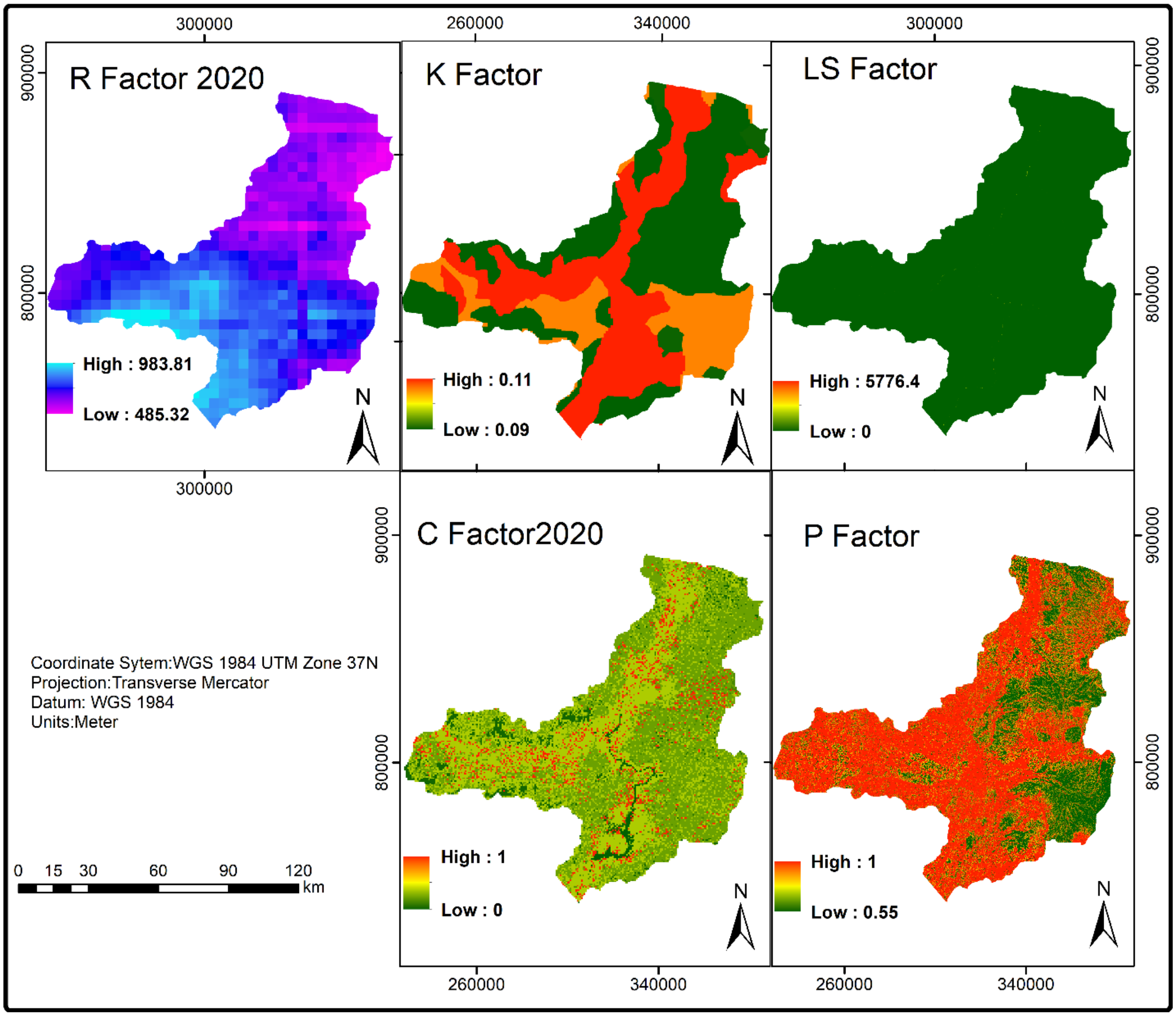

Figure 4. 8: RUSLE factors map of rainfall erosivity and cover and management of 2020, soil erodibility, slope length-steepness, and support practice factors.

It was observed from the results that the area under study is subject to different intensities of soil erosion ranging from none (0–5) to very severe (>50 t /ha/yr.) erosion.

In 2010 very severe erosion took place with a percentage of 2.0 and it was observed at the central part of the study area (Table 4.2). Very slight and slight to moderate levels of erosion dominated across the entire study area for the year 2001–2005 and 2015–2020. For example, the results show that approximately 97.3 percent of the area was covered by very slight to moderate erosion levels in 2020, with the lowest percentage area (i.e. 2.8 percent) covered by very severe to severe erosion in the same year.

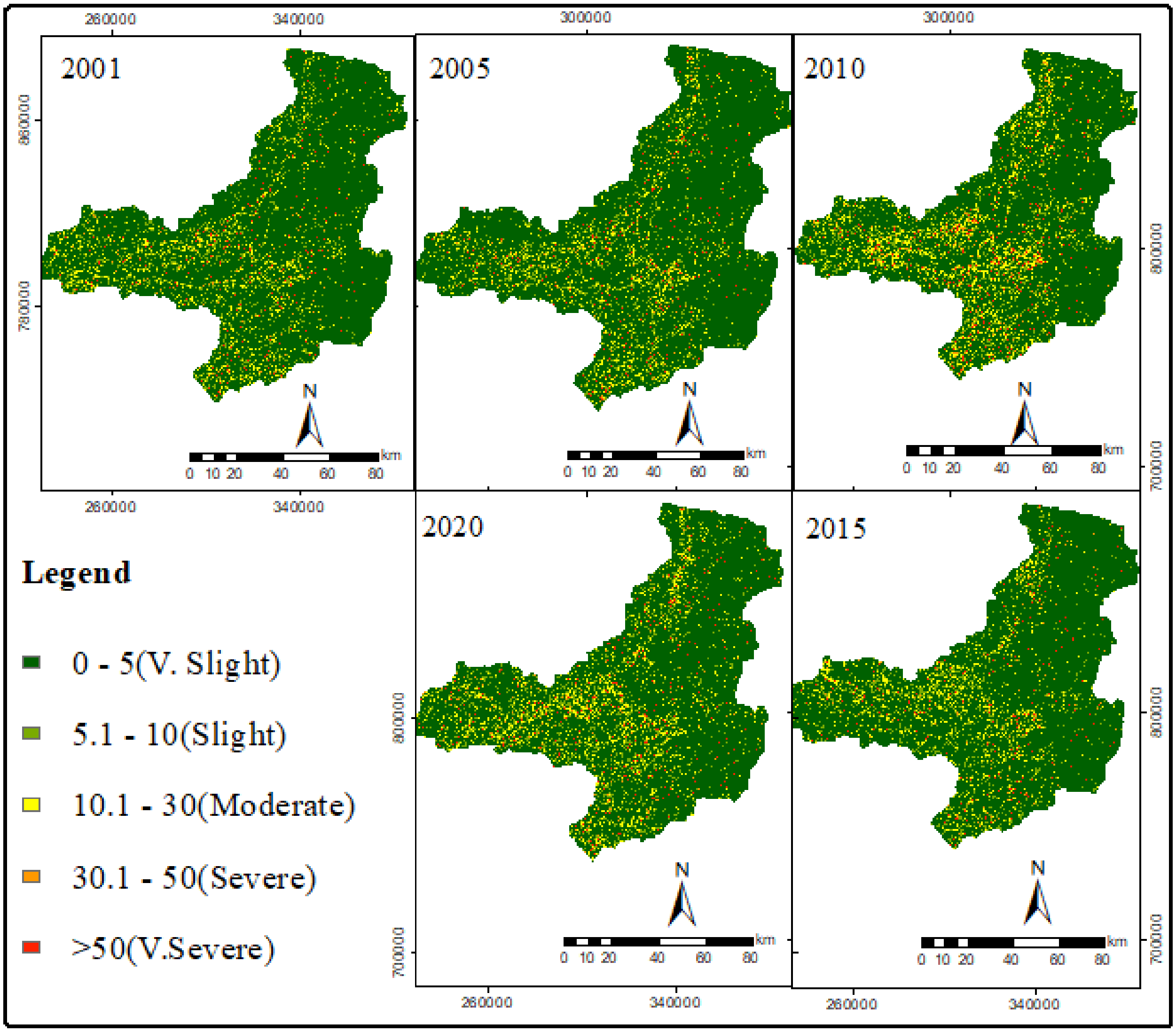

Figure 4. 9: Soil erosion severity map of 2001, 2005, 2010, 2015, & 2020 from RUSLE model

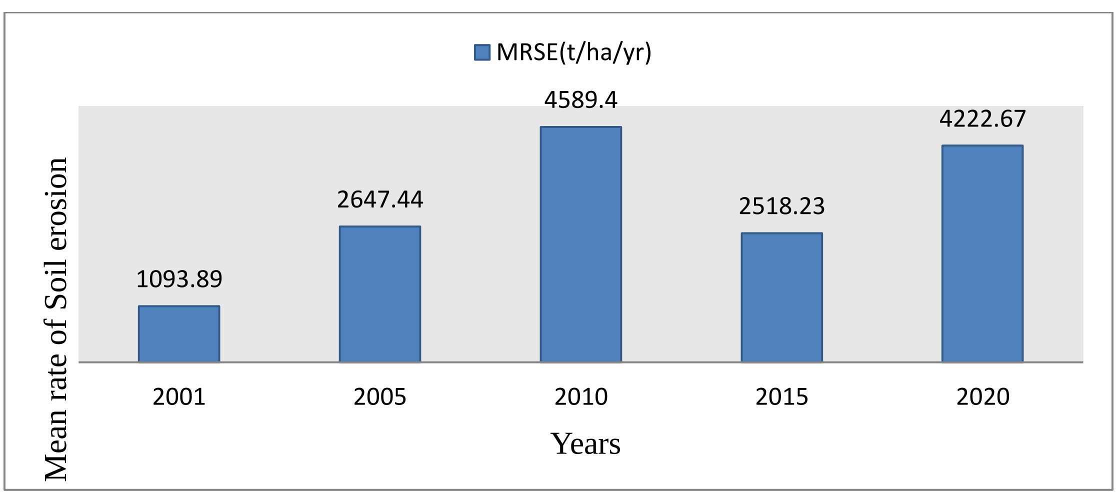

Figure 4. 10: Mean rate of soil erosion from years 2001−2020 in the GGIIID catchment

Table 4. 2: Erosion severity classes area and percent of 2001, 2005, 2010, 2015, & 2020

	2001		**2005**		**2010**		**2015**		**2020**		
Erosion Classes (t/ ha/yr)	Area(ha)	Area (%)	Area(ha)	Area (%)	Area(ha)	Area (%)	Area(ha)	Area (%)	Area(ha)	Area (%)	Severity Classes
0−5	902,016	85	909,059	86	840,700	79	904,966	85	864,396	82	Very Slight
5.1−15	83,628.6	8	77,552	7.3	97,454	9.2	80,078	7.5	96,103	9.1	Slight
15.1−30	54,574.1	5.1	53,663	5.1	86,199.4	8.1	55,010	5.2	71,169	6.7	Moderate
30.1−50	9,091.5	0.9	9,139	0.9	16,856.8	1.6	9,231.6	0.9	12,483	1.2	Severe
>50	12,891.2	1.2	12,787	1.2	20,990.4	2.0	12,767.0	1.2	16,865	1.6	Very severe

The mean rate of soil loss in the study area is 1093.9, 2647.4, 4589.4, 2518.2, and 4222.7t/ha/yr. in the years 2001, 2005, 2010, 2015, and 2020 in the order given. The highest mean rate of soil erosion was observed in the year 2010 which was 4589.4t/ha/yr. (Fig.4.10). The result shows the mean rate of soil loss increased from the beginning (2001) to 2010 and then decrease in 2015 and then also increased in 2020.

4.3 Land-use/cover change caused soil erosion

The land-use/cover changes assessed through the 2001–2020 periods have also increased the mean rate of soil erosion (t/ha/yr.) from about 1093.9 in 2001 to (2647.4) in 2005 to (4589.4) in 2010 to (2518.23) in 2015, and to (4,222.7) in 2020 (Fig. 4.11). Mean rates of soil erosion from individual land-use/cover types were made, and (Table 4.3) indicates that the highest mean rate of soil erosion (t/ha/yr.) was obtained in grassland (1085) in 2001, (794) in 2005, (548) in 2015, (770.5) in 2020), and bare land accounts (816) in 2010.

Table 4. 3: Mean rate of soil erosion (MRSE) in (t/ha/yr.) and area distribution in (ha) across land-use/cover classes

LULC classes	2001		2005		2010		2015		2020	
	Area(ha)	MRSE	Area(ha)	MRSE	Area(ha)	MRSE	Area(ha)	MRSE	Area(ha)	MRSE
Bare land	54456.1	182.5	120046.5	399	245886.6	816	161949.8	537.5	75948.4	292
Cropland	252347.5	368.7	334514.5	479.8	344424.5	512.8	350066.1	501.5	465015.5	666.2
Forest	67940.5	343.6	95801.8	484.5	58892.3	298	99661.9	504	44963.0	227
Grassland	629289.7	1085	460270.7	794	372160.3	642	317742.2	548	446739.3	770.5
Settlement	63838.9	263	55961.2	230.7	45441.4	187	124447.9	513	24435.8	101
Water	2113.1	0	3391.1	0	3180.7	0	16118.0	0	12778.8	0

4.4 Sediment delivery ratio (SDR) and sediment yield estimation

Sedimentary delivery ratio (SDR) is a fraction of gross erosion that is transported from a given area at a given time interval. It indicates the capability of a catchment for storing and transporting the eroded soil. Sediment yield (Fig. 4.12) of the Gilgel Gibe III dam catchment was determined by the sediment delivery ratio (Fig. 4.10) of the mainstream channel. Mainstream channel slope and sediment delivery ratio in the study area divided into three (A western part, B northeastern part, and AB southeastern) sub-basins having different densities. SDR was computed using (Eqn 10) of this study. The sediment delivery ratio results ranged from 0 to 0.24 for the mainstream sub-basin of Omo river. The dominating range switched under 0.05 which has 78.4 percent of the total SDR (Table4.4).

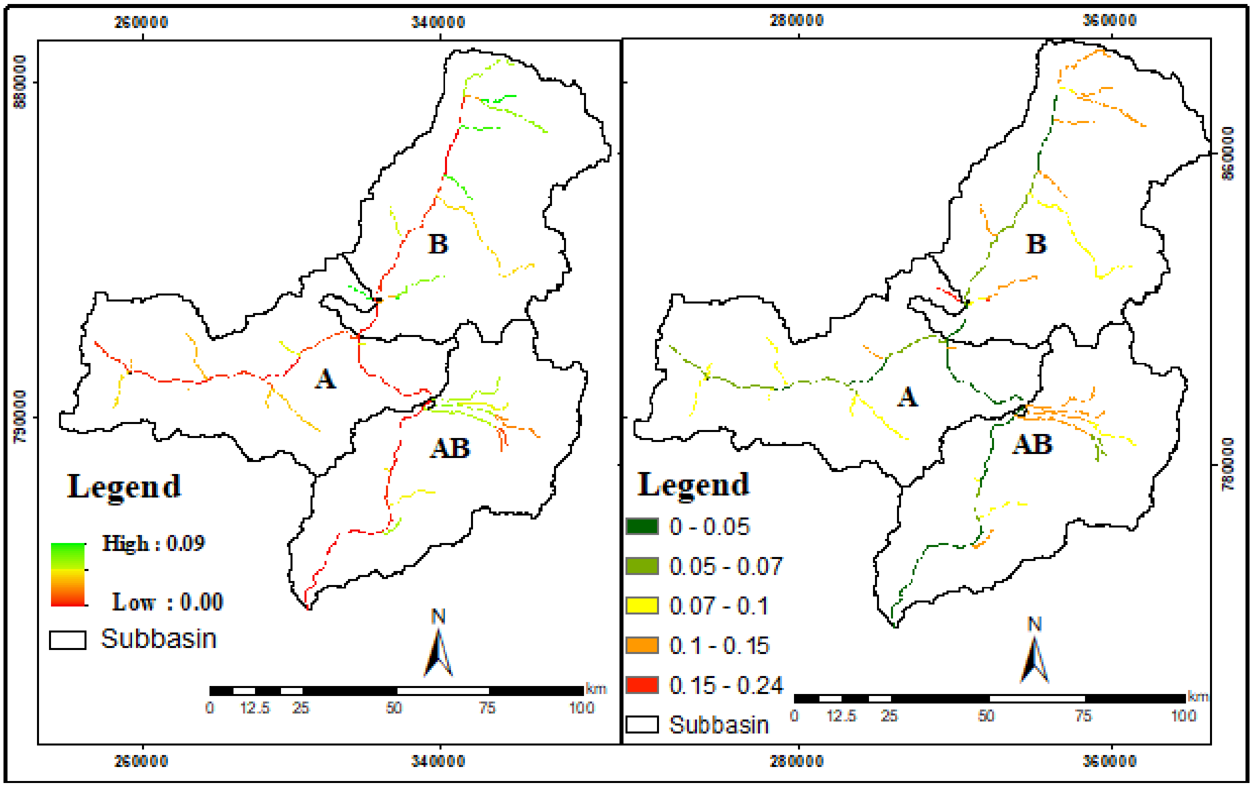

Figure 4. 11: Stream channels slope (left) and sediment delivery ratio (right) map

Table 4. 4: Area distribution and percentage of sediment delivery ratio(SDR)

Value	SDR	Area(ha)	Area (%)
1	0–0.05	960.9	78.4
2	0.05–0.07	93.8	7.6
3	0.07–0.1	56.3	4.6
4	0.10–0.15	36.2	2.9
5	0.15–0.24	78.2	6.4

4.4.1 Sediment yield

The sediment yield of the basin was estimated over the mainstream by using the (Eqn11) of this study. The mean sediment yield for the mainstream of the Gilgel Gibe III dam catchment was estimated for five-year intervals, starting from 2001-2020. The mean rate of sediment yield in the Omo sub-basin is 573.27, 639.19, 827.63, 263.49, and 609.02t/ha/yr. (Fig. 4.12) in 2001, 2005, 2010, 2015, and 2020 respectively.

Sediment yield in t/ha/yr. ranged from 0 to 9952.47 in 2001, 0 to 11717.1 in 2005, 0 to 12249.9 in 2010, 0 to 8820.86 in 2015, and 0 to 8560.1 in 2020 and classified into five sediment load classes based on Soil erosion classes used in this study illustrated in (Table 4.5) below.

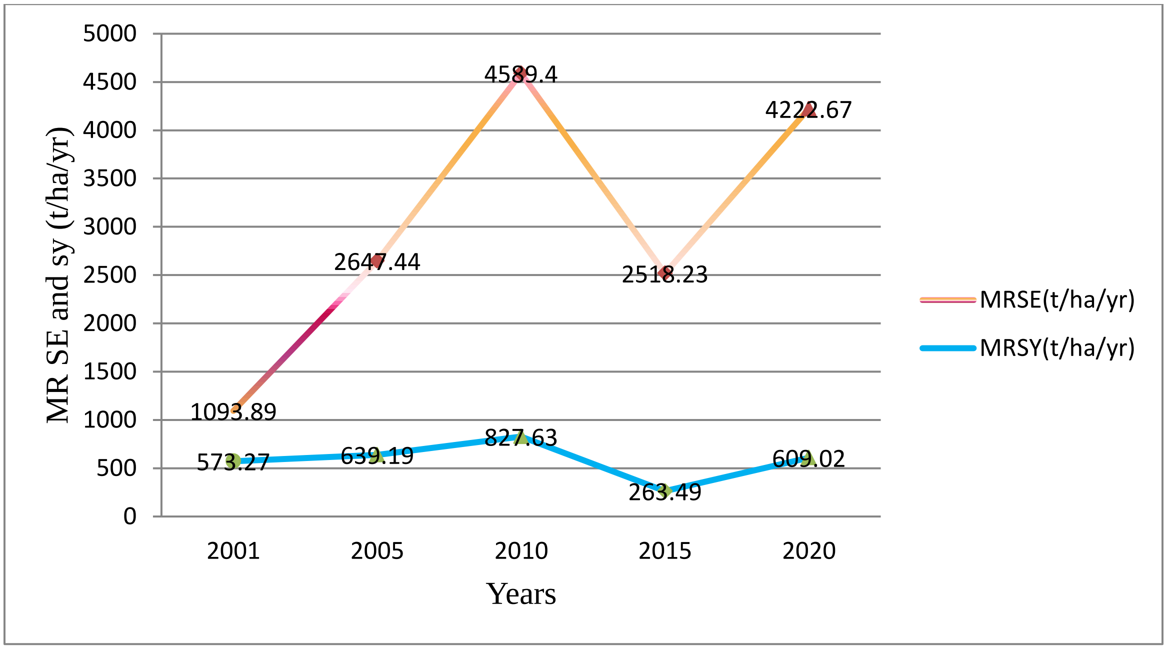

Figure 4. 12: Mean rate of soil erosion *vs* sediment yield

Table 4. 5 Percentage and area coverage of sediment yield(t/ha/yr.) from 2001−2020

	2001		2005		2010		2015		2020	
Sediment yield(t/ha/yr)	Area (ha)	Area (%)	Area (ha)	Area (%)	Area (ha)	Area (%)	Area (ha)	Area (%)	Area (ha)	Area (%)
0−100	674.7	54.5	661.6	53.5	1371	49.3	1019	83.2	675.7	54.6
100−150	113.0	9.1	105.7	8.5	226.5	8.1	41.8	3.4	103.2	8.3
150−300	164.7	13.3	162.4	13.1	369.4	13.3	58.9	4.8	168.0	13.6
3001000	193.9	15.7	202.2	16.3	486.4	17.5	66.9	5.5	190.8	15.4
>1000	91	7.3	105.3	8.5	330.1	11.8	38.3	3.1	99.5	8.0

The highest percent of sediment yield class (0−100) t/ha/yr. was recorded in 2015 and accounts for 83.2 percent. The highest class of sediment yield along streamlines (> 1000) t/ha/yr. with having 11.8 percent in 2010.

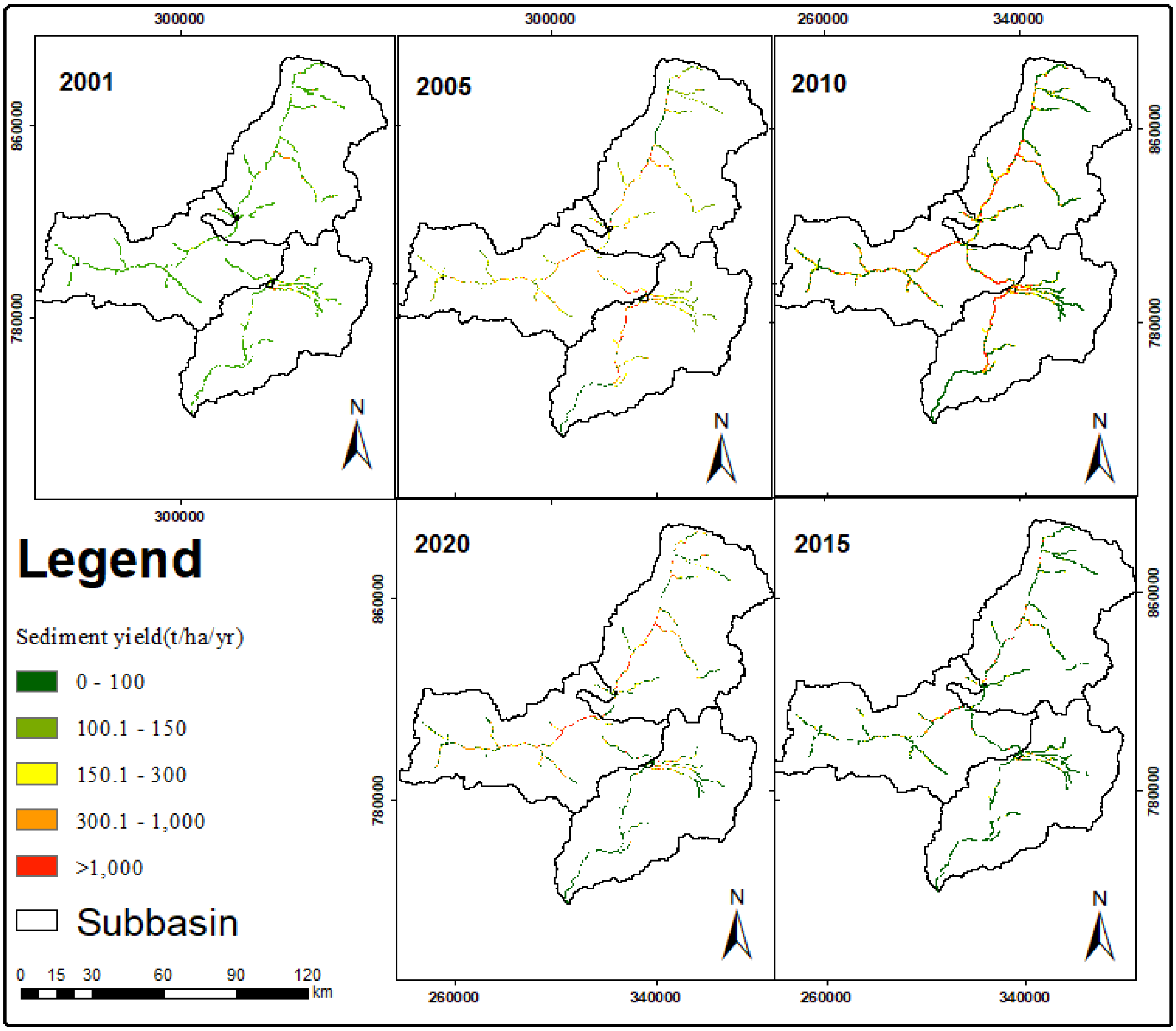

Figure 4. 13: Sediment yield along streamline of the Gilgel gibe III dam catchment 2001−2020.

4.5 Reservoir area dynamics

The reservoir area change was derived by using the remote sensing technique of satellite images specifically sentinel-1 (SAR), Sentinel 2(MSI), and Landsat8 (OLI). For the sentinel1 (SAR) image using the threshold value, the water body was extracted. Area dynamics of reservoir vary from season to season, which shows an increment in months from September to February and shows a decrease from April to August (Table 4.6, and Fig. 4.12).

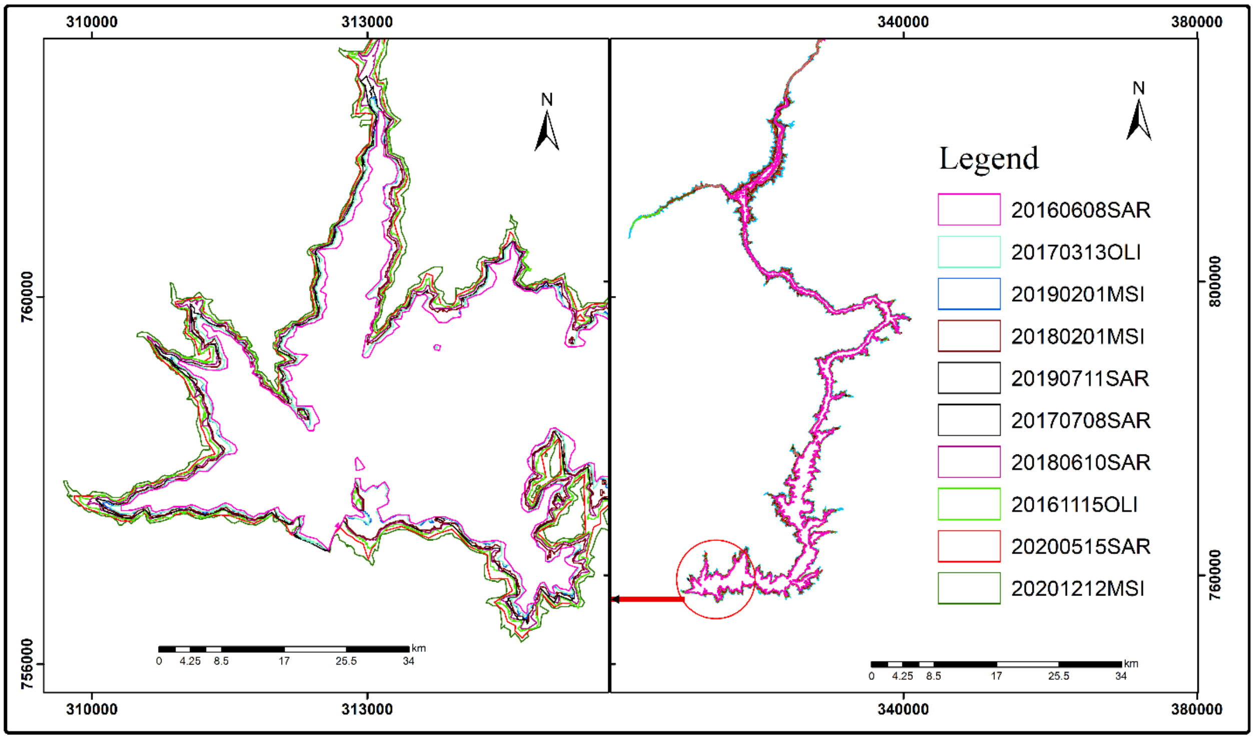

Figure 4. 14: The change in water spread area of the reservoir during the year 2016-2020 extracted from sentinel-1(SAR), sentinel-2(MSI), and Landsat 8(OLI)

For sentinel-2 (MSI) and Landsat 8 (OLI), the normalized difference water index and Modified water index were applied to segregate water from non-water objects. Equations 12 and 13 of this research were applied to generate the water spread area of the reservoir. Bands used for landsat8 and sentinel-2 are (Band3 and Band5 for NDWI and Band6 for MNDWI instead of Band5) and (Band3 and Band8 for NDWI and Band12 for MNDWI).

4.6 Estimation of dynamic storage capacity of the Gilgel Gibe III reservoir

Calculation of live storage capacity of the reservoir involved the water spread area calculation from satellite images and using respective satellite pass time elevation of the reservoir from hydrology survey of a reservoir (Appendix-VIII). Considering the volume stored between two dates or elevation as a trapezoid, the capacity between these two elevations can easily be calculated using the trapezoidal formula. Trapezoidal or Mid Area methods were used to estimate the volume of the reservoir in this study as given in (Eqn 19 and 20) of this study. (Table 4.6) gives the results of dates of satellite pass; water spread area of the reservoir, reservoir elevation, and capacity of the Gilgel Gibe III dam reservoir. Progressive volumes were computed and compared with the design volumes for the same levels. The reduction in volume was attributed to the estimation of present storage capacity and capacity loss due to sedimentation.

Table 4. 6: The results of reservoir capacity assessment of Gilgel Gibe III reservoir using remote sensing approach

Date	Area (km^2)	Reservoir height (m)	Capacity (Mm^3) (Trapezoidal)	Capacity (Mm^3) Mid area	Cumulative capacity (Mm^3)
11_July_2019SAR	127.01	831.50			
08_June_2016SAR	121.5	839.53	1969.22	997.78	997.78
13_March_2017OLI	136.21	839.72	126.1	27.72	1025.50
10_April_2018SAR	161.65	842.50	2024.27	414.03	1439.52
08_July_2017_SAR	143.55	842.66	113.62	24.42	1463.94
01_Feb_2019(MSI)	139.54	844.10	938.38	203.82	1667.76
15_Nov_2016(OLI)	163.74	846.07	1469.29	298.73	1966.50
01_Feb_2018_MSI	141.78	859.34	2035.16	2027.13	3993.62
15_May_2020_SAR	178.77	862.68	2611.80	535.32	4528.94
12_Dec_2020(MSI)	195.76	889.94	3408.72	5104.84	9633.78

From the above result at the elevation of 889.9 m a.s.l, the reservoir revised (live storage) capacity is 9511.4Mm^3 (9.5Km^3) which shows the current live storage capacity of the reservoir. Figure 4.16 shows the designed elevation volume curve of the reservoir and (Fig. 4.15) shows the relationship (Correlation) of the designed and calculated elevation-Volume graph of a reservoir.

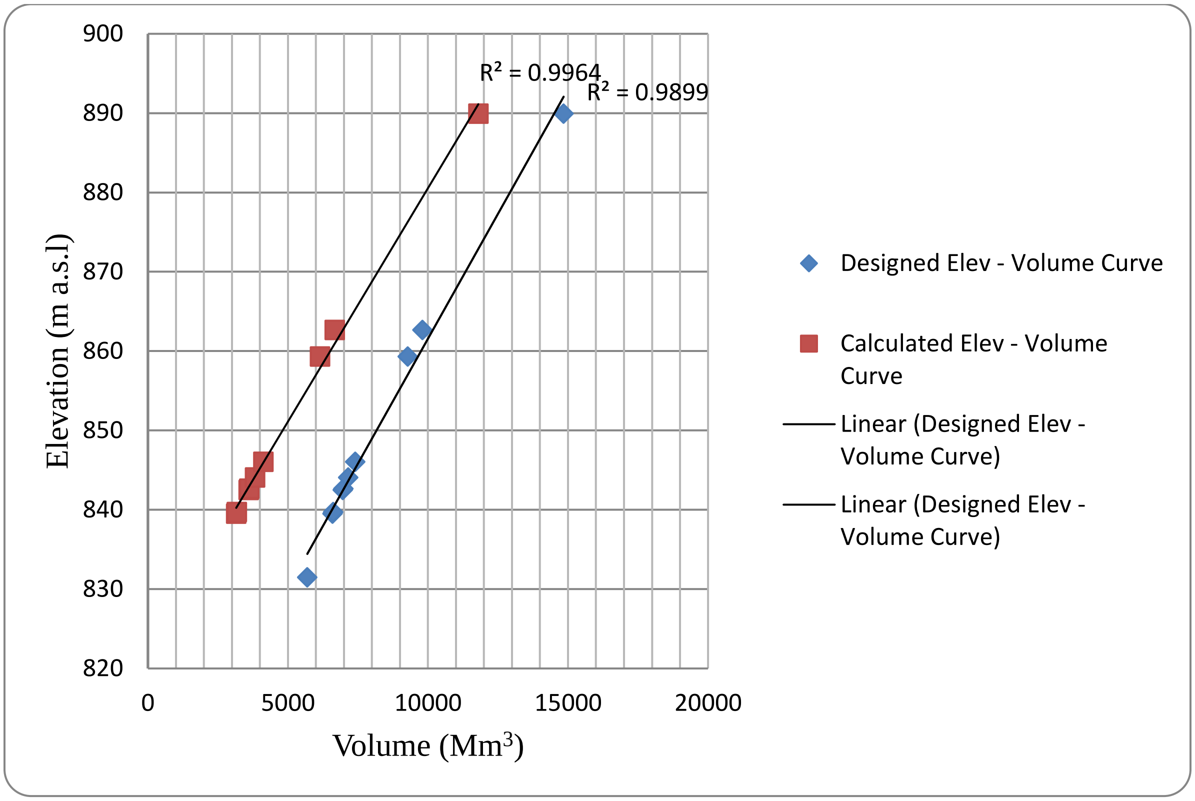

Figure 4. 15: Reservoir: elevation-volume curve generated from remote sensing and hydrographic survey data comparison

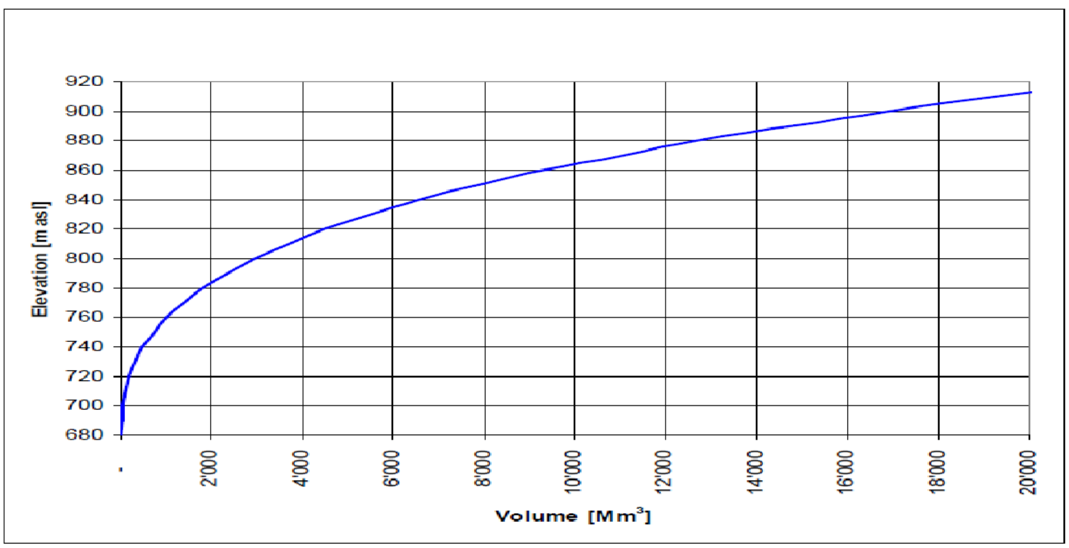

Figure 4. 16: Designed curve of elevation *vs* volume of reservoir

4.7 Comparison of RUSLE model result with other previous studies

Using the different results of previous studies in Ethiopia which were undertaken to estimate the impacts of LULC change on the mean rate of soil loss and sediment yield in different watersheds were applied to compare with estimated soil erosion, sediment yield, and land-use/cover change (Appendix III). In this study land use/cover change from forest to cropland and grassland to cropland lead to severe erosion rate in the catchment after construction of the dam. Erosion increases from forest to bare land in the study area of all years from before dam to after dam construction.

4.8 Runoff around Gilgel gibe III dam and comparison with erosion

There are seven streamflow (discharge) gauging stations in the sub-Omo basin near Gilgel Gibe III dam, which is found upstream of the dam. The annual streamflow recorded in each station has a different value and used to generate runoff near to the study area, even if the recording years were different the mean annual rate of erosion in the study area through 2001-2020 was 3014.326 ton per hectares and the mean annual runoff in the Gilgel Gibe near Asendabo the recording years of 2000-2017 was 16878.8 mm (Appendix VII). This gauging station has a higher recording period compared with another gauging station and has data uniformity relative to other gauging stations; the remaining have a gap of data and low recording periods.

CHAPTER-5 DISCUSSION

5.1 Land-use and land cover change

Land-use/cover of the Gilgel gibe III Dam catchment is frequently changing through the year 2001 to 2020. Grassland and cropland cover larger areas of the Sub-basin of the Omo river basin and they account for 41.76 and 43.46 percent in the year 2020. The change of forest and settlement in the study period is increasing at the beginning and decreases at the end of 2020. Forest to cropland change is progressively rising and that covers 2.5 percent at the end of the assessment (table4.2). Gilgel Gibe III Dam catchment is dominated by the semi-arid ecosystem that is vulnerable to human interventions and activities (International Rivers, 2011). Land-use conversion due to increasing human and livestock population is a common experience in eastern African countries like Ethiopia through appropriate agricultural practices and high settlement pressure that led to severe soil erosion (Bekele, 2019).

Bare land in the study rose from the beginning (2001-2010) with 11.76 percent and decreased by 8 percent from (2010-2020), this shows free dam construction and during dam construction the catchment around the dam and the place where reservoir fill, freed from other land use, because the project took place and landowner farmers leave their farmland and rural settlements near to the project area. The decrease of bare land from the year's 2010 to 2020 shows part of the dam construction period and after the construction of a dam, and this result much with (EEPOW,2014) report of environmental (ecological) protection plan report.

Cropland practice shows incremental by 10.26 percent from the start of the assessment to the end of the appraisal (i.e. 2001-2020) in this study. This result the same as the study taken in this catchment (Assefa, 2014) assessed increased coverage of cropland areas over 26 years (1987–2013).

Forest area coverage portrays rippling that becomes raised from the beginning, then fall and grow then finally shows a reduced result from the previous outcome by 5 percent in 2020. This outcome related to (Assefa, 2014) confirmed the decrease in forest land use and land cover in the Gilgel gibe III dam catchment.

The decrease in the grassland of land use/cover by 17 percent over 20 years (2001–2020) was confirmed in the Gilgel gibe III dam catchment. This was similar to the study by Gemechu Shale,

(2021) in the Huluk watershed in the Oromia region western Welega. The decrease of grassland cover in the study area indicates overgrazing before dam construction, the interaction between settlement and the environment during the dam construction, and the replacement of water bodies after the fill of Gilgel gibe III reservoir.

Settlement falls at the beginning by 1.72 percent from (2001-2010) and increased by 7.38 percent in 2015, and finally decreased by 9.35 percent was assessed in the study area. This result was the same with (EEPOW, 2009; International River, 2011), as the report says the project site was a rural area and the campsite has an effect during and after the project time. As paved roads, beaches around riversides, and weathered roads, and asphalt road construction projects affected the incremental of settlement in 2015 by 7.3 percent. Some of the rural settlements are displaced from their farmland and residential or built-up for the replacement of reservoirs in the sub-basin. Some of the peoples settled during the dam construction and later at the cease period they moved to the new site where Gibe IV (Koysha) project site.

The increase in area coverage of water body land covers by 1 percent over 20 years was affirmed in the Gilgel gibe III dam. This result confirmed in the Gibe III reservoir area, as mentioned by (EEPOW, 2014) of the first impounding plan report of Gilgel gibe III dams.

5.2 Soil erosion, sediment yield, and LULC change

Based on soil erosion classification used by (Zhou and Wu, 2008) the estimated soil erosion was classified into five classes, namely, very slight (<5), slight (5.1-15), moderate (15.1-30), Severe (30.1–50), and very severe (>50) t/ha/yr. According to (Rediet and Eshetu, 2020) annual soil loss in the Omo basin was conducted for the year 2018 and that ranged greater than 60 t/ha/yr. or (very severe) accounts for 7.01 percent, this was comparable with this study of erosion in the year 2020.

This study evaluated the temporal-spatial interaction of land-use/cover status with soil erosion and sediment yield characteristics in the Gilgel Gibe III Dam Catchment, using the revised universal soil loss equation model and Sediment delivery ratio. As the result showed the rate of soil erosion increased, then the rate of sediment yield increased along the main streamlines in the watershed of the sub-basin. Soil erosion irreversibly deteriorates on-site soil quality and is quantified by the average amount of soil removed from a study area over the year 2001-2020. Sediment yield is the amount of soil removed to rivers and reservoirs in a given period, which is an important process in catchment soil erosion. According to (Rediet and Eshetu, 2020) sediment yield result in this study area (Omo basin) was the same with area coverage and applied the RUSLE model for soil erosion and environmental water management. According to (Mehari et al., 2020), the increment of the human settlement area of a watershed and cultivated land show that various human needs affect the Land covers and increase surface erosion in the watershed. The same study showed that four-fifths of the reservoir sedimentation was caused by erosion of soil from an upstream watershed and cultivated lands.

There are seven gauging stations around Gilgel Gibe III Dam that record river flow within the Omo river basin, for each tributary of the basin. Annual average runoff generated from river flow data (Sourced: Ethiopia basin authority development (EBAD)) of the station and applying baseflow separation and all necessary unit conversion. Near the study area, the higher runoff observed in the station of Gojeb near Shabe (24878.9mm), result correlated with the bare land of land-use/cover map of this study and runoff value of (EEPOW, 2009). The river flow of this station was recorded for seventeen years (2000-2016) and shows higher results relative to other gauging stations. Gilgel gibe III reservoir was filled on 15 March 2014 and opened for service in October 2015 (EEPOW, 2014).

A comparative study between sediment yield and soil erosion also showed a direct relationship between the two results. This implies that the sediment yield at the river mouth increase due to the direct and indirect consequence of Land use/cover changes. The same work conducted by (Moges et al., 2019) on the Guder sub watershed and shows the increment of soil erosion and sediment yield caused by the conversion of land use/cover from one class to another upstream of the watershed. The mean rate of soil erosion (t/ha/yr.) 1085, and 770.5, and area coverage of grassland were 58.8 and 41.8 percent in 2001 and 2020 in order and the equivalent rates of soil erosion in the catchment increased from 1093.9 and 4222.7 t/ha/yr. These results are similar to the work taken in Three Gorges Reservoir in China by (Bao *et al*., 2012).

Sediment yield was assessed using integrates of RUSLE and SDR models. The mean rate of soil erosion (t/ha/yr.) decreased from 4589.4 in 2010 to 2518.2 in 2015 and similar manner means a rate of sediment yield (t/ha/yr.) along the streamline declined from 827.6 to 263.5 with corresponding years of soil erosion. According to (Temesgen *et al*., 2019) the pattern of sediment yield follows the outline of soil erosion in the specific area of survey, where there is a similar increase of sediment delivery ratio.

5.3 Area dynamics and capacity of reservoir

Based upon results from the satellite image and water index method used, the area of Gilgel Gibe III reservoir increased starting from (121.5 sq. km) in 2016 to (195.76 sq. km) in 2020 and likewise the mean rate of soil erosion, and sediment yield. The same work conducted for sediment yield in the Gilgel Gibe I Dam shows the increment of soil erosion and sediment yield (Devi *et al*., 2008). The revised storage capacity of Gilgel Gibe III Reservoir is 9.51cu.Km. This result is close to the designed and original storage capacity of 11.75 cu. km with the Ethiopia Electrical Power report of (2015). The same work was conducted in the Ghataprabha reservoir of Karnataka state in Krishna basin, India (Prasad *et al.*, 2018), the result shows closer to designed reservoir capacity and revised storage capacity before that work.

CHAPTER-6 CONCLUSION AND RECOMMENDATIONS

6.1 Conclusion

This study demonstrates the use of remote sensing and Geographic Information System (GIS) to assess the impact of land use/cover practices on reservoir capacity, erosion, and sediment yield. An effort was made to map six classes of land use/cover using supervised and unsupervised methods and likelihood algorism. Data from the satellite are found to be useful in mapping and quantitatively analyze land use/cover and change of it using different available software. Overall accuracy and Kappa coefficient were above eighty percent agreed with classified land cover. In this study, six classes of land-use/cover used for change detection by the post-classification technique of five-year dates of satellite images from 2001 − 2020 were used to detect changes. Land cover change assessment resulted that 15 percent change took place between grassland and cropland which is the highest conversion. Therefore, the changes that took place were in free, during, and post-dam construction of the Gilgel Gibe III Dam catchment. Area percentage coverage of dominant land cover class for years of 2001, 2005, 2010, 2015, and 2020 classified are: grassland (58.81), grassland(43.02), grassland(34.8), cropland(32.72), and cropland(43.5) orderly.

Land-use and land cover change is a major cause of soil loss at dam catchment, regional and global scales. The mean annual soil loss in the study area was estimated using the RUSLE model. The result showed that the mean annual soil loss for 2001, 2005, 2010, 2015, and 2020 were 1093.89, 2647.44, 4589.4, 2518.23, and 4222.67 t/ha/yr. respectively.

Land-use/cover change is a critical factor for enhancing the soil erosion risk and storage capacity of reservoir decline in the sub- Omo basin. The soil erosion severity within the study area was classified into five categories, and the estimated mean soil loss rates (t/ha/yr): very slight (< 5), slight (5–10), moderate (15–30), Severe (30 - 50), and Very Severe (>50).

Due to the construction of the dam, the transported sediments get deposited into the reservoir and along the streamline, causing a reduction of the storage capacity. Analysis of sediment distribution is important to tackle the problems such as rising reservoir levels, increasing flood levels, and entry of sediments into the reservoir. Sediment yield along streamlines of the Gilgel gibe III dam catchment is accelerating year by year; the frequent floods, soil erosion, deforestation for farmland,

and change in land use/cover practices all have aggravated the problem at a higher rate. Conventional surveys are not possible to be carried out frequently for large reservoirs in estimating sedimentation because of their cost and time-consuming nature.

The estimation of sediment yield by integrating SDR and annual soil loss (sheet erosion) computed from RUSLE could be replicated in another part of the upper Omo basin where sheet and rill erosion is dominant. The mean annual sediment yield in the study area was estimated using the soil erosion generated from the RUSLE model and SDR from the slope of the main streamlines. The result showed that the mean annual sediment yield of the study area for 2001, 2005, 2010, 2015, and 2020 were 573.2, 639.19, 827.63, 263.49, and 609.02 t/ha/yr in the order given. Sediment yield estimation in this study, therefore, plays a vital role for Gilgel gibe III hydroelectric power reservoir in particular and for the watershed as a whole in identifying non-point source pollution, critical sediment source areas, and to take site-specific measures such as different drainage and water harvesting structures.

The water spread area was delineated from sentinel-1A, sentinel-2A, and landsat8 for different dates of the water year 2016-20, and the corresponding reservoir water level was obtained from Ethiopia Electrical Power (EEPOW) was used to calculate the revised live storage capacity of the reservoir. The area (sq. km) of Gilgel Gibe III reservoir augmented starting from 121.5 in 2016 to 195.8 in 2020. The revised live storage capacity between elevations from 839.53to 889.94 m was assessed by using the Trapezoidal and Mid area method was 9,511.40Mm3. It was compared with the designed capacity of the reservoir estimated in the year 11/November 2015 through geometrical modeling of reservoir formulated by (EEPOW) survey method as 11750 Mm3. Reservoir live capacity loss was found out to be 2238.6 Mm3 and the sedimentation has occurred from 2015 to 2020 at the rate of 263.49 to 609.02 t/ha/1yr in these 5 years along the streamlines of Gilgel gibe III dam watershed. The rate of sediment yield increased by345.5t/ha/yr. along streamline of the sub-basin with the age of five years. The approach of remote sensing also provides a capacity of a reservoir at different reservoir levels; it was used to draw the revised elevation-capacity curve of the reservoir, which is an important input for dam authorities.

Therefore, the conversion of grassland area percentage from the steep slope of the watershed to extensive cropland caused a high rate of soil loss. Due to this change in land use, a high amount of sediment yield can be easily transported to the reservoir and downstream regions along streams.

In general, the model revealed that erosion-prone areas were increasing during the past two decades (2001–2020).

In general, accelerated usage of remote sensing data and techniques has made the geospatial process faster and powerful, although the increased complexity also creates increased possibilities for error.

6.2 Recommendations

There is a need to plan for studying possible land use land cover change caused erosion and sediment yield that could reduce and affect reservoir capacity, environment, natural resource, and agriculture lands, which found in the erosion-prone area. Therefore, it is important to prioritize erosion-prone areas around Gibe III dam and reclaim using physical and biological soil and water conservation (SWC) structures to alleviate land degradation. This includes institutionalizing sustainable biological and physical soil conservation measures to mitigate land degradation and improve the livelihood of the local community in the watershed. Some of the recommendations forwarded to EEPOW and for all stakeholders in the catchment of the Gilgel Gibe III dam, that have to be supervised and addressed well while analyzing such kinds of research in the future and to manage the reservoir from unadvisable Land use/cover practices, erosions, and sedimentations:-

- Appropriate land use planning and management in the watershed should be practiced to reduce the negative local effects of land use and land cover change in the Gilgel gibe III dam catchment; Appropriate tree species should be planted and managed on the upstreams of the dam and water conservation structures, and the activities like overgrazing and charcoal productions should be controlled.
- The result of this study could help different stakeholders to plan and implement appropriate soil and water conservation strategies in the dam catchment. As a mitigation measure for the prevention of severe erosion and conservation mechanism, it is recommended to cover the mountainous and hilly areas with plantations and control further degradation by erosion. An accurate prediction of sediment delivery ratio (SDR) is also important in controlling sediments for sustainable natural resource development and environmental protection.
- To sustain the design life of the Reservoir of Gilgel Gibe III and to achieve the objective of the construction of the Dam, the watershed shall be prevented from erosion or sediment

it is recommended to have a continuous assessment of reservoir capacity and sediment load by using remote sensing and hydrological survey of the reservoir.

- Modeling erosion and sediment of the watershed depends on the quality of input data. One of the constraints in conducting this research work was the lack of continuously measured sediment data. Therefore, the absence of actual sediment and simulated sediment data validation and calibration struck. However, consistent results can be obtained if detail suspended sediment data are used at the outlet of the reservoir. Hence, responsible bodies should give due attention to the time and frequency of sampling, method of sampling, and recording of reliable sediment data together with flow measurement.
- It is recommended that all the Zone and Woreda Offices of Agriculture (the Development Agents and the Development Committee), and Environment, Forest and Climate Change (EFCC) that fall and be affected directly or indirectly by the project will be involved in the intervention proposed and establish at each Woreda a management unit as a focal responsible body for coordinating the activities.
- Deposition of sediment in reservoirs reduces the storage capacity of the reservoir and can cause serious problems concerning the operation and stability of the dam. Therefore, a strong recommendation is to apply a variety of tools (like the HEC-RAS model, a two-dimensional hydrodynamic model, and the hydrodynamic, sediment transport, and physical habitat model) those available for hydro-morphological simulation to optimize reservoir management.
- Finally, I recommend that the study should further extend to evaluate the reduction of reservoir capacity for the next remaining years of designed life spans, and further researchers involve using this research as input, high-resolution satellite image, and data having the capability to penetrate cloud effect in particular wet and summer period.

7 References

Abileah R and Vignudelli S A 2011 Completely Remote Sensing Approach To Monitoring Reservoirs Water Volume International Water Technology Journal Alexandria **1(1)** 63-77

Abreham Berta Aneseyee, Eyasu Elias, Teshome Soromessa, and Gudina Legese Feyisa (2020). Land use/land cover change effect on soil erosion and sediment delivery in the Winike watershed, Omo Gibe Basin, Ethiopia. Science of the Total Environment

Aiello A, Adamo M, Canora F (2015). Remote sensing and GIS to assess soil erosion with RUSLE3D and USPED at River Basin Scale in Southern Italy CATENA **131:**174–185. https ://doi.org/10.1016/j.caten 04.00

Ajanaw Negese (2021), Impacts of Land Use and Land Cover Change on Soil Erosion and Hydrological Responses in Ethiopia, Applied and Environmental Soil Science https://doi.org/10.1155/2021/6669438.

Amiya Gayen, Sunil Saha & Hamid Reza Pourghasemi (2019): Soil erosion Assessment using RUSLE model and its Validation by FR probability model, Geocarto International, DOI: 10.1080/10106049.2019.1581272

Arvidson, T., Goward, S., Gasch, J., & Williams, D. (2006). Landsat-7 long-term acquisition plan. Photogrammetric Engineering & Remote Sensing, **72(10**), 1137-1146.

Ashish Pandey, U.C. Chaube, S.K. Mishra & Dheeraj Kumar (2016): Assessment of reservoir sedimentation using remote sensing and recommendations for desilting Patratu Reservoir, India, Hydrological Sciences Journal, 61:4, 711-718, DOI: 10.1080/02626667.2014.993988

Assefa Nigussie, (2017). Impact of Land uses Land cover change on Streamflow (CASE STUDY GILGEL GIBE III). Unpublished MSc Thesis, Addis Ababa University, Addis Ababa, Ethiopia, 89 pp.

Bagegnehu Bekele and Yenealem Gemi (2020) Soil erosion risk and sediment yield assessment with universal soil loss equation and GIS: in Dijo watershed, Rift valley Basin of Ethiopia. Modeling Earth Systems and Environment. https://doi.org/10.1007/s40808-020-01017-z

Bao Y. He X. Wei J. Tang Q. & Guo F. (2012) "Soil erosion under different land uses in the riparian zone of the Three Gorges Reservoir, China". Erosion and Sediment Yields in the

Changing Environment (Proceedings of a symposium held at the Institute of Mountain Hazards and Environment).

Beasley D.B., L. F. Huggins, E. J. Monke (1980). ANSWERS: A Model for Watershed Planning. Trans. ASAE **23**, 938–944.

Bedilu Betela, (2015). "Swat-based runoff - sediment yield modeling and development of management options": (a case study of gibe iii watersheds, upper Omo-Gibe, Ethiopia) Unpublished MSc Thesis. Arbaminch University Arbaminch, Ethiopia.

Bekele T. (2019) Effect of Land Use and Land Cover Changes on Soil Erosion in Ethiopia. Int J Agric Sci Food Technol 5(1): 026-034. https://doi.org/10.17352/2455-815X.000038.

Bloschl, G., & Sivapalan, M. (1995). Scale issues in hydrological modeling: a review. , Modeling, J. D., Kalma, & Sivapalan, M. (Eds.). (1995). Scale issues in hydrological DOI: 10Ð1016/0022-1694(82)90117-2. New York, New York: Wiley and Sons, 9–49.

Bo Huang and Jionghua Wang (2020) "Big spatial data for urban and environmental sustainability" Geospatial information science, **32(2)** 125-140.DOI: 10.1080/10095020.2020.1754138.

Borghero, C. (2018): Feasibility study of dam deformation monitoring in northern Sweden using Sentinel1 SAR interferometry. The University of GAVLE, Faculty of engineering and sustainable development

Boroujeni, H.S. (2012). Sediment management in hydropower Dam (Case study: Dez Dam project). In Hydropower Practice and Application. In Tech New York

Bosch, J. M., & Hewlett, J. D. (1982). A review of catchment experiments to determine the effect of vegetation changes on water yield and evapotranspiration. Journal of Hydrology, **55**, 3–23 DOI: 10Ð1016/0022-1694(82)90117-2.

Chhabra, A., Geist, H., Houghton, R. A., Haberl, H., Braimoh, A. K., Vlek, P. Lambin, E. F. (2006). Lambin, E. F., & Geist, H. J. (Eds.). (2006). Multiple impacts of land use/ cover change. In Land-use and Land-cover Change: Local Processes and Global Impacts 2002. Berlin: Springer, 71–116.

CSA (2017). Population Projection of Ethiopia for All Regions at Wereda Level from 2014 – 2017. Addis Ababa, Ethiopia

Clubb, F. J., S. M. Mudd, M. Attal, D. T. Milodowski, and S. W. D. Grieve (2016), The relationship between drainage density, erosion rate, and hilltop curvature: Implications for sediment transport processes, J. Geophys. Res. Earth Surf., **121**, 1724–1745, doi:10.1002/2015JF003747.

Delmeire S 1997 Use of ERS-1 data for the extraction of flooded areas Hydrological Processes **11(10)** 1393-1396

Desmet PJJ, Govers G (1996) AGIS procedure for automatically calculating the USLE LS factor on topographically complex landscape units. Journal of Soil and Water Conservation **51**: 427-433.

Devaraja Pathirage Chanaka laknath, & Thotapitiya arachchillage Jeewanthi Gangani sirisena (2017). Sediment yield estimation on a reservoir in a severely eroding river basin. Proceedings of the 37th IAHR World Congress August 13 – 18, 2017, Kuala Lumpur, Malaysia

Djebou, D.C.S., (2018). Assessment of sediment inflow to a reservoir using the SWAT model under undammed conditions: A case study for the Somerville reservoir, Texas, USA. *International Soil and Water Conservation Research*, *6*(3), pp.222-229

Du, Y., Zhang, Y., Ling, F., Wang, Q., Li, W., & Li, X. (2016). Water bodies' mapping from Sentinel-2 imagery with modified normalized difference water index at 10-m spatial resolution produced by sharpening the SWIR band. Remote Sensing, 8(4), 354.

Dutta, S., (2016). Soil erosion, sediment yield and sedimentation of reservoir: a review. Modeling Earth Systems and Environment, 2(3), p.123.

El Jazouli, A., Barakat, A., Ghafiri, A., El Moutaki, S., Ettaqy, A., & Khellouk, R. (2017). Soil erosion modeled with USLE, GIS, and remote sensing: a case study of Ikkour watershed in the Middle Atlas (Morocco). Geoscience Letters, 4(1), 1-12.

Environmental System Research Institute (ESRI), (2020). What is GIS? https://www.esri.com/en-us/what-is-gis/overview. Accessed on 14/01/2021

Erdogan HE, Erpul G, Bayramin I (2006) Use of USLE/GIS Methodology for Predicting Soil Loss in a Semi-arid Agricultural Watershed, Department of Soil Science, University of Ankara, Turkey.

E.S.A. (2020). User Handbook of Sentinel-2. *ESA Standard Document*, *64*.

Ethiopian Electrical Power (EEPOW) (2014) "First impounding plane report" Gibe III Hydroelectric project.

Ethiopian Electric Power (EEPOW) (2009). Gibe III Hydroelectric project executive summary, environmental and social impact assessment Report 45p.

Ethiopian Electrical power (EEPOW) (2021). Koysha Hydropower (Ethiopia). https://www.pietrangeli.com/koysha-hydropower-plant-ethiopia-africa.Studio Pietrangeli Consulting Engineers

European Environment Agency. (1995), CORINE Soil erosion risk and important land resources - in the southern regions of the European Community, Commission of the European Communities.

Filipponi, F. (2019). Sentinel-1 GRD Preprocessing Workflow. In Multidisciplinary Digital Publishing Institute Proceedings (Vol. 18, No. 1, p. 11).

Food and agricultural organization (FAO)(2021). land and water. http://www.fao.org/3/x0596e/x0596e00.htm accessed on 29/01/2021

Gelagay H. S. and Minale A. S.,(2016) "Soil loss estimation using GIS and remote sensing techniques: a case of Koga watershed, Northwestern Ethiopia," International Soil and Water Conservation Research, vol. 4, no. 2, pp. 126–136, 2016.

Gelagay HS (2016) RUSLE and SDR Model-Based Sediment Yield Assessment in a GIS and Remote Sensing Environment; A Case Study of Koga Watershed, Upper Blue Nile Basin, Ethiopia. Hydrol Current Res 7: 239. doi:10.4172/2157-7587.1000239

Geological Survey of Ethiopia (GSE, 1983). Omo River Project. Reconnaissance Geology and Geochemistry of parts of Illubabor, Kefa, Gamo Gofa, and Sidamo, Ethiopia

Geospatial Awareness Hub, (2020). Geospatial Technology. [Online available at https://geospatialawarenesshub.com/our-services/geospatial-technology]/ Accessed on 23/10/2020 09:05 PM.

GezahegnWeldu Woldemariam, and Arus Edo Harka, (2020). "Effect of land use and land cover change on soil erosion in erer sub-basin, Northeast Wabi Shebelle Basin, Ethiopia," Land, vol. 9(4).111

Girma Redeit and Gebre Eshetu., (2020). Spatial modeling of erosion hotspots using GIS-RUSLE interface in Omo-Gibe river basin, Southern Ethiopia: implication for soil and water conservation planning. Environmental Systems Research, 9(1), pp.1-14.

Goel, M.K., Jain, S.K., Agarwal, P.K., 2002. Assessment of sediment deposition rate in Bargi Reservoir using digital image processing. Hydrological Sciences Journal. Special Issue: Towards Integrated Water Resources Management for Sustainable Development. https://doi.org/10.1080/02626660209493024

Hanqiu Xu (2006): Modification of normalised difference water index (NDWI) to enhance open water features in remotely sensed imagery, International Journal of Remote Sensing, 27:14, 3025-3033

Hanqiu Xu (2006): Modification of normalised difference water index (NDWI) to enhance open water features in remotely sensed imagery, International Journal of Remote Sensing, **27**:14, 3025-3033 http://dx.doi.org/10.1080/01431160600589179

Helden U (1987) An Assessment of Woody Biomass, Community Forests, Land Use and Soil Erosion in Ethiopia. Lund University Press

Helena Mitasova , Jaroslav Hofierka , Maros Zlocha & Louis R. Iverson (1996) “Modelling topographic potential for erosion and deposition using GIS”, International Journal of Geographical Information Systems, 10:5, 629-641, DOI: 10.1080/02693799608902101 https://doi.org/10.1080/02693799608902101.

https://earthexplorer.usgs.gov/ Accessed on 05/10/2020 09:05 am.

https://vertex.daac.asf.alaska.edu/ Accessed on 25/9/2020 10:05 am

Hurni, H. (1985). Erosion-productivity-conservation systems in Ethiopia

Hussen Muhammed, (2020). Sedimentation modeling (case study, gololcha dam reservoir, upper wabe shebelle river basin, Ethiopia). Unpublished MSc Thesis, Addis Ababa University, Addis Ababa, Ethiopia, 105PP.

Hyeon SK, Pierre YJ (2006) Soil erosion modeling using RUSLE and GIS on the IMHA watershed. Water Engineering Research 7

Ijam, A. Z., Al-Mahamid, M. H. (2012): Predicting Sedimentation at Mujib Dam Reservoir in Jordan. - Jordan Journal of Civil Engineering 6(4): 448-463.

Imre V.Nagy, Kofi Asante-Duah, Istvan Zsuffa, (2002). Determination of the Optimal Reservoir Storage Capacity and Operational Parameters for a River Dam. In: Hydrological

Dimensioning and Operation of Reservoirs. Water Science and Technology Library, vol **39**. Springer, Dordrecht. https://doi.org/10.1007/978-94-015-9894-1_8

International Rivers, (2011) “Ethiopia’s Gibe 3 Dam: Indigenous Peoples of Ethiopia’s Lower Omo Valley,” Available at: http://internationalrivers.org/en/ node/2794

J. De Vente, J. Poesen, G. Govers, and C.Boix-Fayos, “The implications of data selection for regional erosion and sediment yield modelling,” Earth Surface Processes and Landforms, vol. 34, no. 15, pp. 1994-2007, Dic. 2009. Doi: https://doi.org/10.1002/esp.1884

J. O. Onyando, P. Kisoyan, and M. C. Chemelil, (2005) “Estimation of potential soil erosion for river perkerra catchment in Kenya,” Water Resources Management, vol. 19, no. 2, pp. 133–143

J. R. Williams and H. D. Berndt, (1972) “Sediment yield computed with universal equation,” Journal of the Hydraulics Division, vol. 98, no. 12, pp. 2087–2098, 1972.

Jain Satish Kumar, (2018) Sedimentation Study on Ranapratap Sagar Reservoir Using Remote sensing Data – A case study, International Journal of Scientific research: Volume-7/Issue – 8/ August-2018. DOI:10.36106/ijsr

Jensen, J.R. (1996) Introductory Digital Image Processing: A Remote Sensing Pers-pective. 2nd Edition, Prentice Hall, Inc., Upper Saddle River, NJ.

Jillo, A. Y., Demissie, S. S.,Viglione, A., Asfaw, D. H., & Sivapalan, M. (2017). Characterization of regional variability of seasonal water balance within Omo-Ghibe River Basin, Ethiopia. Hydrological Sciences Journal, 62(8), 1200-1215

Jørgenson, S.E., Loffler, H., Rast, W., Straskraba, M. (2005): Lake and reservoir management (1sted.). - Boston, MA: Elsevier Science.

Juval Cohen, Henri Riihimäki, Jouni Pulliainen, Juha Lemmetyinen and Jyri Heilimo (2016). Implications of boreal forest stand characteristics for X-band SAR flood mapping accuracy Remote Sensing of Environment **186(1)** 47–63

K. Naschen, B. Diekkr¨uger, M. Evers, B. H¨ollermann, S. Steinbach, and F. Thonfeld, (2019) Impact of land use/land cover change (LULCC) on water resources in a tropical catchment in Tanzania under different climate change scenarios,” Sustainability, vol. 11, no. 24

Kaushik Ghosal, and Santasmita Das Bhattacharya (2020). A Review of RUSLE Model. Journal of the Indian Society of Remote Sensing 48(4):689–707

Kayet, N., Pathak, K., Chakrabarty, A., & Sahoo, S. (2018). Evaluation of soil loss estimation using the RUSLE model and SCS-CN method in hillslope mining areas. International Soil and Water Conservation Research, 6(1), 31-42.

Kent Thomas, Walter Chen, Bor-Shiun Lin, and Uma Seeboonruang (2020) "Evaluation of the sediment delivery distributed (SEDD) Model in the Shihmen Reservoir Watershed. Sustainability, 12, 6221; doi: 10.3390 /su12156221

Kidane M., Bezie A., Kesete N., and Endrias M.,(2019) "comprehensive assessment of land use land cover (LU/LC) dynamics on soil erosion and sediment yield in the central highland of Blue Nile basin, Ethiopia," pp. 1–23

Lambin, E. F.,Samuel, B. and Geist, H. J. (2003). Global Land-Use and Land-Cover Change: What Have We Learned So Far? Global Change Newsletter, Land-Use/Cover Change.

Landis, J.R. and Koch, G.G. (1977) A One-Way Components of Variance Model for Categorical Data. Biometrics, 33, 671-679. https://doi.org/10.2307/2529465

Legleiter, C. J., Pavelsky, T., Durand, M., Allen, G. H., Tarpanelli, A., Frasson, R., & Woodget, A. (2020). Editorial for the Special Issue "Remote Sensing of Flow Velocity, Channel Bathymetry, and River Discharge".

Lemlem T., K. V. Suryabhagavan, G. Sridhar, and G. Legesse, (2017)"Land use and land cover changes and soil erosion in Yezat watershed, North Western Ethiopia," International Soil and Water Conservation Research, vol. 5, no. 2, pp. 85–94.

Liao J J, Shao Y and Wang S X (2004). Monitoring for 2003 Huai River flood in China using multisource SAR dat International Geoscience and Remote Sensing Symposium 4 2260-2263

Lillesand, T.M., Keifer, R.W. and Chipman J.W.(2004, 2015). ―Remote Sensing and Image Interpretation‖, 5th Edition

Lv X L, Liu R G and Liu J Y (2005). Monitoring flood using multi-temporal ENVISAT ASAR data International Geoscience and Remote Sensing Symposium 5 3627-3629

M. Mariye, M. Mariyo, Y. Changming, Z. L. Teffera, and B. Weldegebrial, (2020). "Effects of land use and land cover change on soil erosion potential in Berhe district: a case study of Legedadi watershed, Ethiopia," *International Journal of River Basin Management*, vol. 18, pp. 1–13.IEEE.

Marcelo.H,Garcia,ph.D.,P.Eng,(2008):SedimentationEngineeringProcess,Measuremen,Modeling and Practice,(110),p.1132.

Mc Feeters, S. K. (1996). The use of the Normalized Difference Water Index (NDWI) in the delineation of open water features. International Journal of Remote Sensing, 17(7), 1425–1432.

McConnell WJ (2015) Land Change: The Merger of Land Cover and Land use Dynamics. International Encyclopedia of the Social & Behavioral Sciences (Second Edition), pp. 220-223.

Mengie B., Teshome Y. and Dereje T. (2019). Potential soil erosion estimation and area prioritization for better conservation planning in Gumara watershed using RUSLE and GIS techniques'. Environmental Systems Research, 8(1), 1-17.

Mengie Belayneh, Teshome Yirgu and Dereje Tsegaye.(2019). Potential soil erosion estimation and area prioritization for better conservation planning in Gumara watershed using RUSLE and GIS techniques'. Environ Syst Res 8, 20 (2019). https://doi.org/10.1186/s40068-019-0149-x

Merina, R. N., Sashikkumar, M. C., Rizvana, N., & Adlin, R. (2016). Sedimentation study in a reservoir using remote sensing technique. Applied ecology and environmental research, 14(4), 296-304.

Mitas, L., Mitasova, H., (1998). Distributed soil erosion simulation for effective erosion prevention. Water Resour. Res. **34**, 505–516.

Mitasova H, Mitas Z (1999) Modeling soil detachment with RUSLE 3D using GIS. champaign: University of Illinois at Urbana-champaign.

Mitasova, H., Mitas, L., (1999a, 1999b). Erosion/deposition modeling with USPED using GIS.

Moges K., Alemu B., Nega K., Terefe T. (2019) “The impact of land use and land cover (LULC) dynamics on soil erosion and sediment yield in Ethiopia”. Heliyon 5 (2019) e02981

Morgan RPC (2005) Soil Erosion and Conservation. 3rd edn. Blackwell Publishing, Oxford, p: 304.

Morgan, R. P. C. and Quinton, J. N. and Smith, R. E. and Govers, G. and Poesen, J. W. A. and Auerswald, K. and Chisci, G. and Torri, D. and Styczen, M. E. (1998). The European Soil Erosion Model (EUROSEM): a dynamic approach for predicting sediment transport from fields and small catchments. Earth Surface Processes and Landforms **23**, 527–544

Morris, G. L., & Fan, Jiahua (2009). Reservoir Sedimentation Handbook, Design, and management of dams, reservoirs, and watersheds for sustainable use, McGraw-Hill, New York.

Muke, M. (2019) Driving Factors of Land-Use/Cover Changes and Its Mounting Consequences in Ethiopia: A Review Afr. J. Environ. Sci. Technol., 13, 273–280

Murty, P.S. and Tiwari, H. (2015). Accuracy Assessment of Land Use Classification —A Case Study of Ken Basin. Journal of Civil Engineering and Architecture Research, 2, 1199-1206.

Naima Alahiane, Ahmed El Mouden, Abderrahmane Ait Lhaj, &Said Boutaleb (2014). Practical Method Proposed to Estimate Silting’s Rate in Small and Hillside Dams. Journal of Water Resource and Protection. DOI: 10.4236/jwarp.2014.610088

National Institute of Hydrology, Regional Centre, Bhopal (M. P.) (NIHRCB) and Water Resources Department, Govt. of Chhattisgarh, Raipur (WRDGCR), (2013). Study of reservoir sedimentation, impact assessment and development of catchment area treatment plan for kodar reservoir in chhattisgarh state, India. 155 PP.

Nearing,M.A (1989). A process-based soil erosion model for USDA-Water Erosion Prediction Project technology. Trans. ASAE **32**, 1587–1593.

Nill,D(1996)"soil erision by water in Africa,"p.292.Available at:http://www.theeuropeanlibrary.

Nina Siu-Ngan Lam, (2008). Methodologies for mapping land cover/land use and it’s Change. Advances in Land Remote Sensing, ISBN: 978-1-4020-6449-4

Omo-Gibe River basin development Master plan study, (1995) Survey and analysis Report. Volume IV, Land resource surveys

Panditharathne, D. L. D., Abeysingha, N. S., Nirmanee, K. G. S., & Mallawatantri, A. (2019). Application of revised universal soil loss equation (Rusle) model to assess soil erosion in "kalu Ganga" River Basin in Sri Lanka. Applied and Environmental Soil Science, 2019.

Panditharathne, D. L. D., Abeysingha, N. S., Nirmanee, K. G. S., & Mallawatantri, A. (2019). Application of revised universal soil loss equation (Rusle) model to assess soil erosion in "kalu Ganga" River Basin in Sri Lanka. *Applied and Environmental Soil Science*, *2019*

Park, E., Merino, E., W Lewis, Q., O Lindsey, E., & Yang, X. (2020). A pathway to the automated global assessment of water level in reservoirs with synthetic aperture radar (SAR). Remote Sensing, **12**(8), 1353.

Prasad N.R., Vaibhav Garg and Praveen K. Thakur (2018): role of sar data in water body mapping and reservoir sedimentation assessment. ISPRS Annals of the Photogrammetry, Remote Sensing and Spatial Information Sciences, Volume IV-5, 2018 ISPRS TC V Mid-term Symposium "Geospatial Technology – Pixel to People", 20–23 November 2018, Dehradun, India

Prasad, S., (2015). Remotely sensed data characterization, classification, and accuracies (Vol. **1**, pp. 277-293).

Profeti G and Macintosh H (1997). Flood management through Landsat TM and ERS SAR data: a case study Hydrological Processes **11(**1) 397-1408

Rahimov Foteh, Vaibhav Garg, Bhaskar Ramchandra Nikam, Madhusudan Y. Khadatare, Shiv Prasad Aggarwal, & A. Senthil Kumar, (2018) - Reservoir Sedimentation Assessment Through Remote Sensing and Hydrological Modeling: Journal of the Indian Society of Remote Sensing.

Rani Devi, Esubalew Tesfahune, Worku Legesse, Bishaw Deboch, & Abebe Beyene, (2008). Assessment of siltation and nutrient enrichment of Gilgel Gibe II dam, Southwest Ethiopia. Article in Bioresource Technology • April 2008, DOI: 10.1016/j.biortech.2007.03.013

Rawat JS, Kumar M (2015) Monitoring land use/cover change using remote sensing and GIS techniques: A case study of Hawalbagh block, district Almora, Uttarakhand, India. The Egyptian Journal of Remote Sensing and Space Science 18(1): 77-84.

Rediet Girma and Eshetu Gebre (2020). “Spatial modeling of erosion hotspots using GIS-RUSLE interface in Omo-Gibe river basin, Southern Ethiopia”: implication for soil and water conservation planning. Environ Syst Res 9:19 https://doi.org/10.1186/s40068-020-00180-7

Reis, S. (2008). Analyzing land use/land cover changes using remote sensing and GIS in Rize, North-East Turkey. Sensors, 8(10), 6188-6202.

Roy, D. P., Wulder, M. A., Loveland, T. R., Woodcock, C. E., Allen, R. G., Anderson, M. C., ... & Zhu, Z. (2014). Landsat-8: Science and product vision for terrestrial global change research. Remote sensing of Environment, **145**, 154-172.

Rwanga, S. S., & Ndambuki, J. M. (2017). Accuracy assessment of land use/ cover classification using remote sensing and GIS. International Journal of Geosciences, **8**(04), 611.

Rwanga, S.S. and Ndambuki, J.M. (2017) Accuracy Assessment of Land Use/Land Cover Classification Using Remote Sensing and GIS. Inter-national Journal of Geosciences, 8, 611-622. https://doi.org/10.4236/ijg.2017.84033

Rwanga, S.S. and Ndambuki, J.M. (2017) Accuracy Assessment of Land Use/Land Cover Classification Using Remote Sensing and GIS. Inter-national Journal of Geosciences, 8, 611-622. https://doi.org/10.4236/ijg.2017.84033

S. K. McFEETERS (1996) The use of the Normalized Difference Water Index (NDWI) in the delineation of open water features, International Journal of Remote Sensing, 17:7, 1425-1432, DOI: 10.1080/01431169608948714

Schneider, L.C.; Pontius, G.R (2001). Modeling land-use changes in the Ipswich watershed, Massachusetts USA. Agric. Ecosystems & Environment, 85, 83–94. https://doi.org/10.1016/S0167-8809 (01)00189-X

Sekertekin A., Yasemin S. C., and Arslan N., (2018). “Index-Based Identification of Surface WaterResources Using Sentinel-2 Satellite Imagery” 2018 2nd international symposium on multidisciplinary studies and innovative Technology (ISMSIT), pp. 1-5, https://doi.org/10.1109/ISMSIT.2018.8567062

Seleshi Bekele.; Aster Denekew.; Makonnen Loulseged.; Loiskandl, W., Mekonnen Ayana.; Tena Alamirew. (2007). Water Resources and Irrigation Development in Ethiopia. Colombo, Sri Lanka: International Water Management Institute. 78p. (Working Paper 123)

Sheffield, J., Wood, E.F., Pan, M., Beck, H., Coccia, G., Serrat-Capdevila, A. and Verbist, K., (2018). Satellite remote sensing for water resources management: Potential for supporting sustainable development in data-poor regions. Water Resources Research, **54**(12), pp.9724-9758.

Shin, G. J. (1999). The analysis of soil erosion analysis in watershed using GIS. Department of Civil Engineering, Gang-won National University, Gangwon-do, South Korea, Ph. D. dissertation

Tadele, H., Mekuriaw, A., Selassie, Y. G., & Tsegaye, L. (2017). Land use/land cover factor values and accuracy assessment using a GIS and Remote Sensing in the case of the Quashay watershed in Northwestern Ethiopia. Journal of Natural Resources and Development, 7, 38-44.

Taye Adugna, (2009). The impact of land use/ land covers change on catchment hydrology and water quality of legedad-dire catchments, Ethiopia. Unpublished MSc Thesis, Addis Ababa University, Addis Ababa, Ethiopia, 94PP.

Teh, S. H., Sidek, L. M., Julien, P. Y., & Luis, J. (2014). GIS-Based Upland Erosion Mapping. In Handbook of Engineering Hydrology: Modeling, Climate Change, and Variability (pp. 313-330). CRC Press.

Temesgen G., Taffa T., Mekuria A., & Abeyou W. W (2019) “Modeling the impacts of land use–land cover changes on soil erosion and sediment yield in the Andassa watershed, upper Blue Nile basin, Ethiopia” Environmental Earth Sciences **78**:679 https://doi.org/10.1007/s12665-019-8726-x.

Tendai Sawunyama, (2005). Estimation of small reservoir storage capacities in Limpopo River Basin using Geographic information System (GIS) and Remotely Sensed surface Areas. A case of Mzingwane Catchment. Unpublished MSc thesis, University of Zimbabwe, 78pp

Tholey N, Clandillon S and Fraipont P D (1997). The contribution of spaceborne SAR and optical data in monitoring food events: examples in northern and southern France Hydrological Processes **11** 1409-1413

Thomas, K., Chen, W., Lin, B. S., & Seeboonruang, U. (2020). Evaluation of the Sediment Delivery Distributed (SEDD) Model in the Shihmen Reservoir Watershed. Sustainability, **12**(15), 6221

Tibebu K., Eckert S., Hurnic K., Gete Z., & Hurni, H. (2016). Reducing landscape heterogeneity for improved land use and land cover (LULC) classification across the large and complex Ethiopian highlands, Geocarto international, **33**(1), 53-69

Turner, B.L.; Meyer, W.B.; Skole, D.L (1994) Global land-use/land-cover change: Towards an integrated study. Ambio. Stockholm 1994, 23, 91–95. 13.

UCGIS (University Consortium for Geographic Information Science) (2003) The Strawman Report: Development of Model Undergraduate Curricula for Geographic Information Science & Technology. Task Force on the Development of Model Undergraduate Curricula, University Consortium for Geographic Information Science

United States Geological survey, (2018) Landsat missions, Science for a changing world. Online available at [https://www.usgs.gov/core-science-systems/nli/landsat/landsat-7] accessed on 09/04/2021

Upadhya, R., Pandey, K., Upadhyay, S. K., & Bajpai, A. (2012) Annual Sedimentation Yield and Sediment Characteristics of Upper Lake,Bhopal, India. Journal of Chemical Sciences, Vol. 2(2), 65–74.

Vanoni, Vito A., (2006): Sedimentation Engineering. American Society of Civil Engineers, Virginia.

W.S. Merritt, R.A. Letcher, & A. J. Jakeman, (2003). A review of erosion and sediment transport models. Environ. Model Softw. **18,** 761–799. https://doi.org/10.1016/S1364-8152(03)00078-1

Wakjira Takala Dibaba, Tamene Adugna Demissie and Konrad Miegel, (2020) Drivers and Implications of Land Use/Land Cover Dynamics in Finchaa Catchment, Northwestern Ethiopia

Wang, G. X., Liu, J. Q., Kubota, J., & Chen, L. (2007) Effect of land-use changes on hydrological processes in the middle basin of the Heihe River, northwest China. Hydrological Processes, 21, 1370–1382 DOI: 10Ð1002/hyp.6308.

Wikipedia, the Free Encyclopedia, (2020). Gilgel Gibe III Dam [Online available at https://en.wikipedia.org/wiki/Gilgel_Gibe_III_Dam] / Accessed on 03/11/2020 09:30 am

Wikipedia, the Free Encyclopedia, (2020). Omo Rive. [Online available at https://en.wikipedia.org/w/index.Omo_River&oldid=977339209] / (Accessed on 30/10/2020 12:05 am).

Wischmeier WH, Smith DD (1978) Predicting rainfall erosion losses- A guide to conservation planning. Series: Agriculture Handbook No.537.USDA, Washington DC, pp: 3-4.

Xing, M. M., Jianchu, X. U., Shive, P., Aggarwal, & Jiatong, L. (2009). Response of hydrological processes to land-cover and climate changes in Kejie catchment southwest China. Journal of hydrological process.

Yogendra Y., Bir Bahadur K. C., Santosh R., Krishna R. and Bishal K. S. (2019), Dynamics of Land use Land Cover Change and Mapping of Tree outside Forest (TOF) in Terai, Nepal. International journal of environmental sciences and natural resource DOI: 10.19080/IJESNR.2019.18.556002

Zhang,Y.,Degroote,J.,Wolter,C.,&Sugumaran,R.(2009).Integration of modified universalsoillossequation(MUSLE)intoaGISframeworktoassesssoilerosion risk. Land Degradation & Development, 20(1), 84–91.

Zheng, W., & Shao, J. (2018). Water Body Change Detection Based on Sentinel-1 and HJ-1AB Satellites Data. In Proceedings of the International Workshop on Environment and Geoscience (pp. 484-488).

Zhou Q, Yang S, Zhao C, Cai M, Ya L (2014) A soil erosion assessment of the upper mekong river in Yunnan Province, China. Mt Res Dev 34:36–47

Zhou W, Wu B (2008) Assessment of soil erosion and sediment delivery ratio using remote sensing and GIS: a case study of upstream Chaobaihe River catchment, north China. Int J Sedim Res 23:167–173

8 Appendices

Appendix- I: Error matrix resulting from classifying test pixels (2001, 2005, 2010, 2015, and *2020*

Class 2001		B	C	F	G	S	W	Rtot	User's Accuracy	Producers Accuracy
	B	24	2	0	2	2	0	30	Bare land =80%,	Bare land =75%,
	C	1	26	2	1	0	0	30	$Cropland = 87\%$,	Cropland=84%,
	F	0	1	28	1	0	0	30	Forest=93%,	$Forest = 88\%$,
	G	3	2	2	23	0	0	30	Grassland =77%	$Grassland = 85\%$,
	S	4	0	0	0	26	0	30	Settlement =93%,	$Settlement = 87\%$,
	W	0	0	0	0	0	30	30	Water=100%	$Water = 100\%$
	Ctot	32	31	32	27	28	30	180	Overall A = 87%	Kappa = 0.85=85%
Class 2005		B	C	F	G	S	W	Rtot		
	B	56	4	0	2	5	0	67	Bare land=84%	Bare land=81%
	C	6	72	2	4	0	0	84	Cropland=86%,	Cropland=91%,
	F	0	1	64	6	0	0	71	Forest=90%,	Forest=93%,
	G	2	2	3	55	0	0	62	Grassland =89%	Grassland =82%
	S	5	0	0	0	72	0	77	Settlement =93%,	Settlement =93%,
	W	0	0	0	0	0	45	45	Water=100%	Water=100%
	Ctot	69	79	69	67	77	45	406	Overall A =89.7%	Kappa = 0.875=87%
Class 2010		B	C	F	G	S	W	Rtot		
	B	60	3	0	0	2	0	65	Bare land=92%	Bare land=79%
	C	2	52	0	3	0	0	57	Cropland=91%	Cropland=91%
	F	0	1	64	5	0	0	70	Forest=91%	Forest=95%
	G	6	2	3	81	0	0	92	Grassland =88%	Grassland =91%
	S	8	0	0	0	78	0	86	Settlement =90%	Settlement =97
	W	0	0	0	0	0	42	42	Water=100%	Water=100%
	Ctot	76	57	67	89	80	42	412	Overall A =91%	Kappa =0.897=89.7
Class 2015		B	C	F	G	S	W	Rtot		
	B	61	6	0	2	4	0	73	Bare land=83%	Bare land=82%
	C	2	58	0	3	0	0	63	Cropland=92%	Cropland=84%
	F	0	2	48	4	0	0	54	Forest=88.9%	Forest= 96%
	G	1	3	2	57	0	0	63	Grassland = 90%	Grassland =86%
	S	10	0	0	0	61	0	71	Settlement = 86%	Settlement = 94%
	W	0	0	0	0	0	50	50	Water=100%	Water=100%
	Ctot	74	69	50	66	65	50	374	Overall A =89%	Kappa =0.87=87%
Class 2020		B	C	F	G	S	W	Rtot		
	B	81	2	0	5	4	0	92	Bare land= 88%	Bare land=90%
	C	2	64	2	1	0	0	69	Cropland= 93%	Cropland= 91%
	F	0	3	49	2	0	0	54	Forest= 90%	Forest= 90%
	G	2	1	3	65	0	0	71	Grassland =91%	Grassland = 89%
	S	5	0	0	0	56	0	61	Settlement = 92%	Settlement = 93%
	W	0	0	0	0	0	40	40	Water=100%	Water=100%
	Ctot	90	70	54	73	60	40	387	Overall A =92%	Kappa =0.899=90%

Where, B=Bare land, C= Cropland, F= Forest, G= Grassland, S= Settlement, W=Water, Ctot=Column Total, Rtot= Row Total

Appendix -I I:Land-use and land cover change Area(ha)distribution and percentage of 2001−2020

LULC Change	2001-2005 (ha)	area (%)	2005-2010 (ha)	area(%)	2010-2015 (ha)	area (%)	2015-2020(ha)	area (%)
B- B	12053.6	1.13	43840.5	4.10	55026.1	5.14	24362	2.3
B - C	15889.15	1.48	30025.2	2.81	50477.9	4.72	32930.9	3.08
B - F	838.49	0.08	778.0	0.07	12108.9	1.13	667.4	0.06
B - G	21295.92	1.99	37169.8	3.47	101231.2	9.46	99504.6	9.30
B - S	4255.91	0.40	8097.6	0.76	23354.1	2.18	4222.0	0.39
B - w	123.03	0.01	135.5	0.01	3688.3	0.34	261.3	0.02
C - B	21037.05	1.97	66626.4	6.23	22026.8	2.06	16300.4	1.52
C - C	116447.82	10.88	178109.8	16.65	162059.9	15.15	193496.0	18.09
C - F	4532.81	0.42	9711.6	0.91	23689.5	2.21	11048.1	1.03
C - G	91759.41	8.58	62309.7	5.82	69013.9	6.45	124017.7	11.59
C - S	18552.59	1.73	17677.3	1.65	67617.9	6.32	5144.8	0.48
C - w	17.82	0.00	79.7	0.01	16.6	0	23.4	0.00
F - B	249.09	0.02	4272.6	0.40	650.8	0.06	1191.5	0.11
F - C	14595.75	1.36	10767.6	1.01	16562	1.55	28369.0	2.65
F - F	50946.63	4.76	45621.7	4.26	36007.8	3.37	27739.7	2.59
F - G	1559.85	0.15	34734.7	3.25	3752.6	0.35	41430.2	3.87
F - S	581.19	0.05	393.0	0.04	1909.9	0.18	916.3	0.09
F - w	8.01	0.00	12.2	0.00	9.2	0	6.8	0.00
G - B	79750.83	7.45	119929.1	11.21	78482.1	7.33	27999.7	2.62
G - C	157933.31	14.76	101799.1	9.51	104702.8	9.79	129573.4	12.11
G - F	38859.55	3.63	2511.2	0.23	26166.5	2.45	3752.6	0.35
G - G	329320.46	30.78	223543.7	20.89	130534.4	12.2	147929.7	13.83
G - S	21942.74	2.05	11380.4	1.06	22540	2.11	8003.2	0.75
G - w	1482.81	0.14	1107.2	0.10	9734.5	0.91	418.0	0.04
S - B	6918.12	0.65	10232.2	0.96	5478.2	0.51	5630.0	0.53
S - C	29624.49	2.77	23673.7	2.21	16208	1.51	80601.3	7.53
S - F	617.85	0.06	236.1	0.02	1622.9	0.15	1695.7	0.16
S - G	16052.49	1.50	13959.6	1.30	12424.4	1.16	30532.6	2.85
S - S	10621.53	0.99	7854.0	0.73	8925.4	0.83	5771.9	0.54
S - w	4.41	0.00	5.6	0.00	782.5	0.07	201.0	0.02
W - B	37.80	0.00	985.9	0.09	285.7	0.03	463.8	0.04
W - C	24.03	0.00	49.1	0.00	55.5	0.01	34.7	0.00
W - F	6.48	0.00	33.7	0.00	66.2	0.01	57.3	0.01
W - G	282.53	0.03	442.8	0.04	785.8	0.07	3317.4	0.31
W - S	7.20	0.00	39.1	0.00	100.7	0.01	376.4	0.04
W - W	1755.03	0.16	1840.5	0.17	1886.9	0.18	11868.4	1.11
B= Bare land, C= cropland, F= Forest, G= Grass land, S= Settlement, W= water								

Appendix -III: Different studies on LULC change impact on soil erosion and sediment yield in Ethiopia.

Study catchments	Basin	Area (km2)	Study period	Model used	Major LULC change between study period	LULCchange impact indicators	Change Between study period	References
Omo-Gibe	OMO River	57,464.1	1999–2018	RUSLE	-	Mean rate (SL) (t/ha/yr)	+ 69	Rediet and Eshetu, 2020
Gelda	Blue Nile	262.64	2004–2014	RUSLE	Farmlands increased by 1.44% and forestland decreased by 1.1%	Mean rate (SL) (t/ha/yr) Mean sediment yield	+16.3 +16	(Ebrahim, et al., 2018)
Guder	Blue Nile	466.54	1973–2015	RUSLE	Forest loss by 5.43%; and cropland increased by 4.42%	Mean rate of (SL) (t/ha/yr) Total (SL)(million t/yr) Mean Sediment yield (t/ha/yr)	+4.5 +41 +2.65	Moges, *et al* 2019
Andassa	Blue Nile	587.60	1985–2015	RUSLE	Forest area decreased by 1.59%, and cropland increased by 14.11%	Mean rate of soil loss (t/ha/yr) Mean sediment yield (t/ha/yr)	+19.5 +7.3	Gashaw *et al.*2019
Winike	Omo Gibe	1091.8	1988–2018	InVEST SDR	Forest area decreased by 3.4%, and cropland increased by 13.59%	Total soil loss (thousand tons) Sediment yield (thousand tons)	+176.4 +3.85	Aneseyee *et al.* 2020
Yezat	Blue Nile	150.85	2001–2015	RUSLE	Shrubland decreased by 3.95%, and cropland increased by 2.6%	Mean rate of (SL) (t/ha/yr) (2001–2010) Mean rate of (SL) (t/ha/yr) (2010–2015)	+0.5 −2.9	Lemlem T. et al. 2017
Legedadi	Awash	203.18	1985–2013	RUSLE	Cropland increased by 18.3% and grazing land decreased by 25.74%	Mean rate of (SL) $(t/ha/yr)$ Maximum annual (SL) $(t/ha/yr)$	+12.02 +72.9	(Mariye, et al., 2020)
Rib	Blue Nile	1975.00	1986–2016	RUSLE	Cropland increased by 13.38%, and shrubland and grassland decreased by 5.92% and 6.28%, respectively	Mean rate of (SL) (t/ha/yr) Maximum annual soil loss (t/ha/yr)	+28 +570.5	(Moges and Bhat, 2017)
Erer	Wabi Shebelle	3860.0	2000–2018	RUSLE	Cropland increased by16.44%, and forest area and shrubland decreased by 1.57% and 16.8%, respectively	Mean rate of (SL) $(t/ha/yr)$	+31.22	Gezahegn and Arus, (2020)

Appendix - IV: Training samples, LULC of 2020, and validation sample points

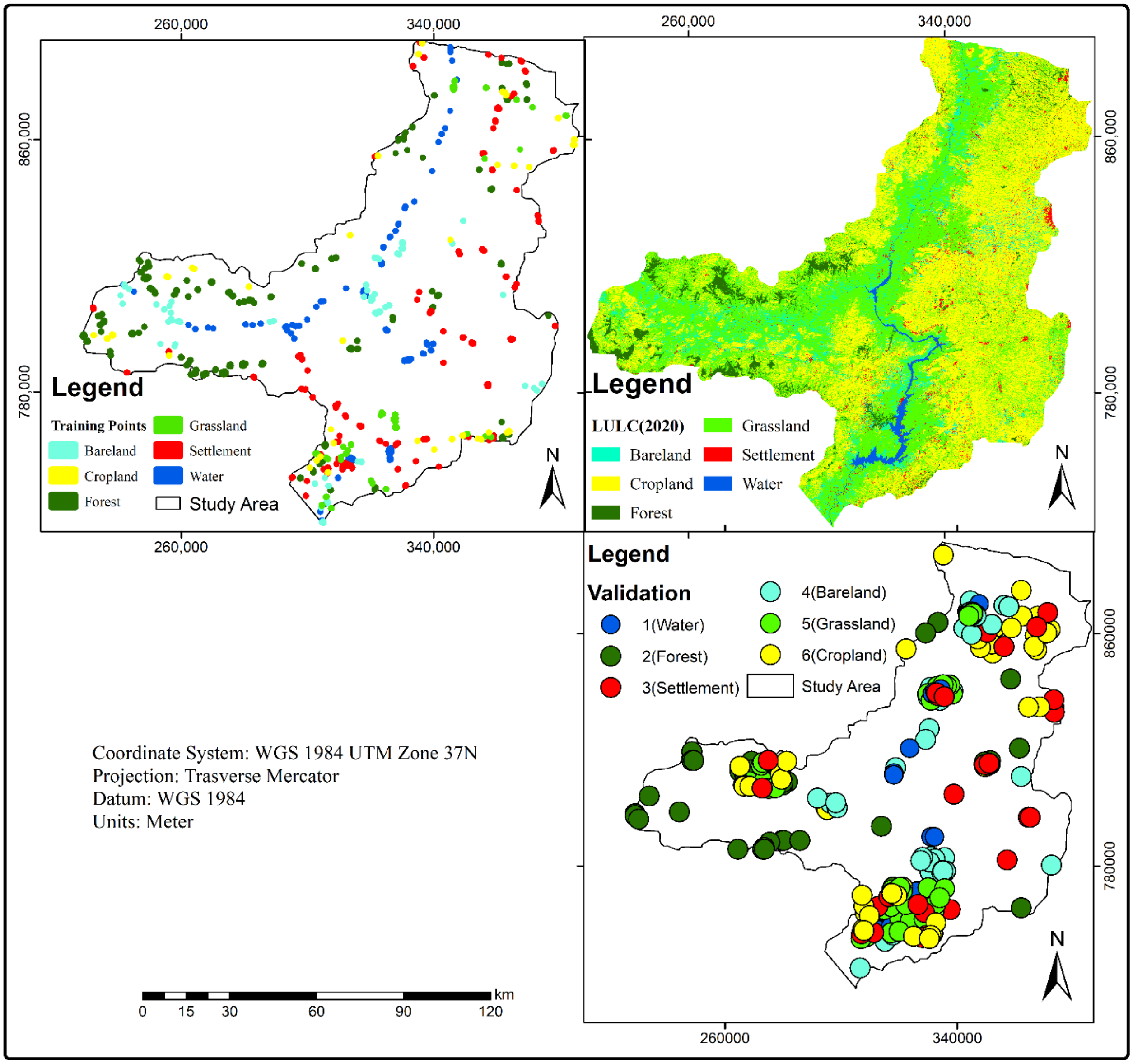

Appendix - V: Rainfall (erosivity) (RF) and cover and management (CF) factors of 2005, 2010, and 2015

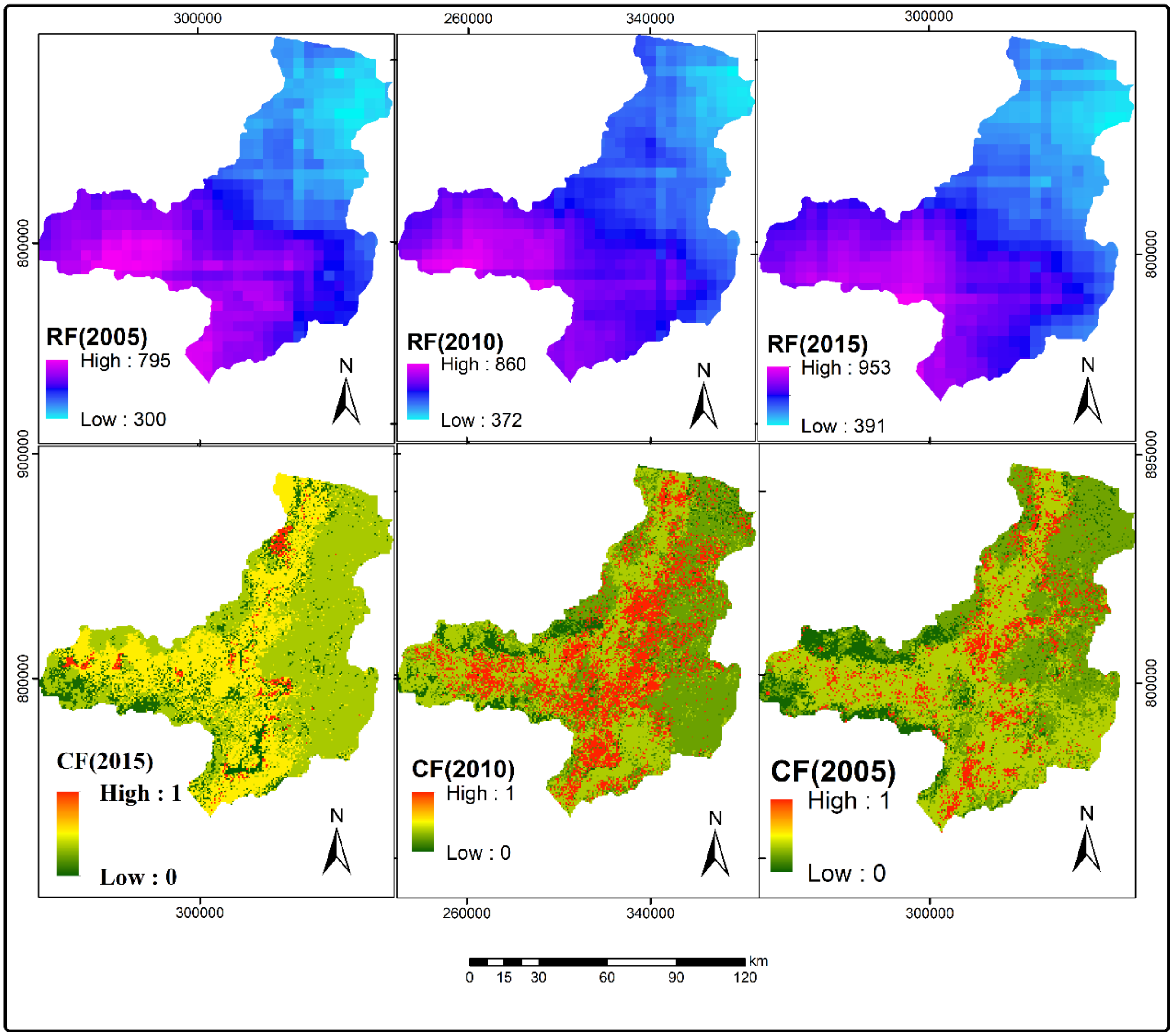

Appendix -VI: Mean annual rainfall at gauging stations around Gilgel Gibe III dam (2000-2018)

Gauging Stations		Arba Minch	Jimma	Hosana	Woliso Giyon	Billate	Wolaita	Chida	Chira	Sekoru	Limu Genet	Imdibir	Wolkite	Tercha	Danna_1
	2000	868.6	1621.9	991.9	1136.1	616.4	1364.1	1184.6	1442.1	1137.3	1665.8	924.1	703	1081	1359.9
	2001	1084.3	1771.4	1145.5	1021.2	536.9	1506	1695.5	2063.9	1370.9	1467.8	834.3	1279.3	1398.6	1302.5
	2002	808.7	1409.7	1346.4	1114.4	520.6	1057	1026.2	1596.4	1090.5	1535.8	793	1248.7	1624.2	1314.8
	2003	882.4	1285.3	1017	1175.4	851	1254.2	473.3	1569.4	1197.5	1667.1	681	1312.2	1382.3	1462.7
	2004	758.3	1468.1	800.2	1229.8	802.5	1204	1069.1	1842.1	1191	1379.5	1089.6	864.2	1396.2	1337.3
years	2005	933.1	1559.6	1179	1209.9	1000.7	1619.2	1086	1010.6	1653.6	1275.2	1879.1	1188.6	1434.2	1284.1
	2006	1128.4	1860.1	1201.7	1400	1032.4	1371.2	679.7	1524.8	2198.2	1415.4	1734.7	834.5	1191.9	1394.9
	2007	1141.1	1286.1	1175.3	1170.2	953.3	1621.6	1437.6	1363.6	1693.1	1241.8	1777.4	1101.2	1572.9	1736.3
	2008	850.5	1550.9	1202.8	1242.2	787	1436.4	1318.7	414.4	1927	1354.8	3036.5	1281.1	1221.3	1053
	2009	638.7	1581.3	1150.4	978.5	685.7	1090.9	976.8	834	1905.8	1804.1	1762.8	979.3	1233.3	841.9
	2010	1068.1	1550.1	1121.5	1383.7	1082.3	1341.2	1548.4	1620.6	1935.3	1109.5	2595.8	1336.9	1459.9	1209.6
	2011	748.8	1518.9	986.9	1135.8	805.7	1197.2	1124.2	942.6	1900.8	1235.9	2586.1	935	1295.8	987.7
	2012	1011.2	1442.9	988.3	955	564	1265.3	997.6	782.2	1465.3	981.7	1725.8	260.5	1134.2	1369.3
	2013	1061.1	1644.2	1175.3	863.7	1120.5	1245.6	1183.4	960.4	1688.3	1257.3	1736.6	208.1	1390.6	1617
	2014	866.2	1733	1334.5	1123.9	833.8	1705.9	1015.4	1462.8	1656.7	1596	2162.7	333.8	1235.4	1670.3
	2015	1121.3	1935	744.8	998.3	581	816	915.9	1079.1	1307.9	1278	2096.9	721.5	1485.5	1042.4
	2016	779.2	1748.9	1133.1	1066	676	1169.8	1066.3	1124.3	1783.3	1471	2404.7	589.5	1206.5	1030.5
	2017	752.6	1523.8	1038.7	384	635.1	716.8	846.7	1415.4	2075.1	1231.8	2253	206.4	1472	972.4
	2018	751.7	513	1314.2	1104.6	1089.8	1403	0	0	0	194.2	379.1	0	1187.6	643

Appendix -VII: Annual stream flow (Cumyr), and annual average runoff (mm)

No.	Station_Name	X	Y	Annual stream flow (Cu.m.per year)	Annual average runoff(mm) around GGIIID catchment		Mean annual rate erosion(t/ha) in GGIII dam catchment	
						Years		Year
1	Ghibe near Limu Genet	895931.9	272263.1	9.70E+10	3,354.6	2000-2013	1093.89	2001
2	Gilgel Gibe near Asendabo	857088.5	299652.2	4.56E+11	16,878.8	2000-2017	2647.44	2005
3	Gibe near Seka	840722.6	251754.2	6.37E+10	1,078.1	2000-2013	4589.4	2010
4	Wabi near Wolkite	912074.2	363560.3	1.22E+10	13,268.5	2000-2006	2518.23	2015
5	Sokie near Areka	781008.5	356661.3	1.49E+10	589.2	2000-2014	4222.67	2020
6	Gojeb near Shebe	820662.2	211152.7	7.22E+11	24,878.9	2000-2016		
7	Walga near Wolkite	911667.8	367069.7	8.27E+10	4,404.7	2000-2006		

Appendix - VIII: Daily recorded elevation of Gilgel Gibe III reservoir (m a.s.l) (Source: EEPOW)

Month of Year		2014/2015	2015/2016	2016/2017	2017/2018	2018/2019	2019/2020	2020/21
hamle 1	8-Jul		775.33	839.72	825.19	834.03	830.87	867.87
hamle 2	9-Jul		775.89	840.01	825.33	834.17	831.01	868.19
Nehase 13	19-Aug		808.16	854.27	840.31	847.29	853.47	887.4
Nehase 14	20-Aug		809.09	854.64	840.65	847.74	854.25	887.87
Nehase 15	21-Aug		810.17	855.1	840.91	848.1	854.97	888.22
Nehase 16	22-Aug		811.22	855.57	841.2	848.6	855.78	888.59
Nehase 17	23-Aug		812.08	855.88	841.58	849.24	856.41	888.9
Nehase 18	24-Aug		812.92	856.26	841.95	849.77	857.09	889.17
Nehase 19	25-Aug		813.87	856.62	842.25	850.22	858.03	889.31
Nehase 20	26-Aug		814.82	857.05	842.59	850.68	858.67	889.76
Nehase 21	27-Aug		815.63	857.35	843.05	851.12	859.47	890.08
Nehase 22	28-Aug		816.28	857.67	843.65	851.5	860.42	890.25
Nehase 23	29-Aug		816.89	857.97	844.75	851.89	861.1	890.17
Nehase 24	30-Aug		817.59	858.3	845.45	852.39	861.69	890.17
Nehase 25	31-Aug		818.2	858.57	846.16	852.94	862.37	890.03
Nehase 26	1-Sep		819	858.89	846.84	853.47	863.09	890
Nehase 27	2-Sep		819.66	859.18	847.5	853.97	863.82	890.08
Nehase 28	3-Sep		820.34	859.52	848.2	854.46	864.49	890.1
Nehase 29	4-Sep		820.9	859.89	849.11	854.83	865.03	889.98
Nehase 30	5-Sep		821.49	860.26	849.97	855.5	865.57	890.03
Pagume 1	6-Sep		822.19	860.52	850.79	855.87	866.16	890.08
Pagume 2	7-Sep		822.85	860.76	851.65	856.31	866.7	890.08
Pagume 3	8-Sep		823.4	860.96	852.32	856.63	867.33	890.3
Pagume 4	9-Sep		824.3	861.17	853.09	856.9	868.05	890.57
Pagume 5	10-Sep		825.32	861.37	853.91	857.13	868.5	890.66
Meskerem 1	11-Sep		826	861.56	854.42	857.35	868.87	890.8
Meskerem 2	12-Sep		826.74	861.75	854.93	857.58	869.31	890.99

Meskerem 3	13-Sep		827.37	861.96	855.46	857.8	869.9	890.97
Meskerem 4	14-Sep		828.08	862.11	856.13	858.1	870.31	891.2
Meskerem 5	15-Sep		828.9	862.31	856.98	858.42	870.58	891.16
Meskerem 6	16-Sep		829.79	862.52	856.98	858.71	870.98	891.16
Meskerem 7	17-Sep		830.56	862.73	858.49	858.85	871.21	891.16
Meskerem 8	18-Sep		831.25	862.98	859.15	859	871.57	891.29
Meskerem 9	19-Sep		832.05	863.18	859.87	859.5	871.8	891.16
Meskerem 10	20-Sep		832.75	863.41	860.57	859.7	871.98	891.38
Meskerem 11	21-Sep		833.35	863.65	861.39	859.93	872.3	891.47
Meskerem 12	22-Sep		834	863.82	862.04	860.11	872.52	891.52
Meskerem 13	23-Sep		834.62	863.94	862.58	860.33	872.84	891.56
Tahisas 8	17-Dec		848.68	859.46	867.7	854.74	880.87	889.35
Tahisas 9	18-Dec		848.73	859.27	867.64	854.64	880.87	889.26
Tahisas 10	19-Dec		848.81	859.12	867.5	854.42	880.69	889.13
Tahisas 11	20-Dec		848.9	859	867.3	854.15	880.55	888.99
Tahisas 12	21-Dec		848.96	858.83	867.19	853.97	880.28	888.9
Tahisas 13	22-Dec		849.02	858.64	867.01	853.74	880.26	888.72
Tahisas 14	23-Dec		849.06	858.44	866.87	853.47	880.24	888.63
Tahisas 15	24-Dec		849.11	858.3	866.66	853.25	880.1	888.54
Tahisas 16	25-Dec		849.15	858.1	866.6	852.93	879.87	888.36
Tahisas 17	26-Dec		849.2	857.92	866.42	852.75	879.78	888.18
Tahisas 18	27-Dec		849.26	857.76	866.25	852.52	879.65	888.13
Tahisas 19	28-Dec		849.28	857.6	866.1	852.26	879.47	888
Tahisas 20	29-Dec		849.33	857.42	865.88	852.07	879.33	887.9
Tahisas 21	30-Dec		849.37	857.22	865.7	852.07	879.38	887.8
Tahisas 22	31-Dec		849.41	857.05	865.53	851.71	879.24	887.64
Tahisas 23	1-Jan		849.46	856.88	865.34	851.44	879.11	
Tahisas 24	2-Jan		849.51	856.7	865.16	851.26	878.92	

Tahisas 25	3-Jan		849.53	856.55	864.93	851	878.75	
Tahisas 26	4-Jan		849.57	856.39	864.76	850.72	878.7	
Tahisas 27	5-Jan		849.61	856.21	864.62	850.59	878.57	
Tahisas 28	6-Jan		849.64	856.02	864.44	850.3	878.48	
Tahisas 29	7-Jan		849.67	855.85	864.3	850.09	878.34	
Tahisas 30	8-Jan		849.71	855.68	864.13	849.96	878.34	
Tir 24	1-Feb	700.88	850.43	850.92	859.34	844.1	875.72	
Tir 25	2-Feb	701.11	850.45	850.7	859.12	843.82	875.54	
Tir 26	3-Feb	701.15	850.38	850.51	858.89	843.64	875.46	
Tir 27	4-Feb	701.4	850.31	850.31	858.75	843.46	875.41	
Tir 28	5-Feb	701.69	850.24	850.1	858.53	843.23	875.27	
Tir 29	6-Feb	702	850.18	849.93	858.31	843.08	875.14	
Tir 30	7-Feb	702.25	850.11	849.71	858.07	842.87	875	
Yekatit 1	8-Feb	702.5	850.06	849.49	857.85	842.6	874.87	
Yekatit 2	9-Feb	702.66	849.99	849.26	857.63	842.33	874.77	
Yekatit 3	10-Feb	702.75	849.92	849.01	857.4	842.01	874.69	
Yekatit 4	11-Feb	703.06	849.88	848.78	857.22	841.61	874.55	
Yekatit 5	12-Feb	703.28	849.89	848.55	856.99	841.25	874.36	
Yekatit 6	13-Feb	703.51	849.83	848.33	856.77	841.1	874.24	
Yekatit 7	14-Feb	703.6	849.76	848.12	856.59	840.7	874.1	
Yekatit 8	15-Feb	703.66	849.7	847.94	856.36	840.48	873.96	
Yekatit 9	16-Feb	703.72	849.62	847.66	855.96	840.07	873.78	
Yekatit 10	17-Feb	703.6	849.55	847.47	855.73	839.89	873.69	
Yekatit 11	18-Feb	703.79	849.46	847.24	855.55	839.71	873.51	
Yekatit 12	19-Feb	703.96	849.35	847.06	855.28	839.35	873.37	
Yekatit 13	20-Feb	704	849.21	846.89	855.14	839.2	873.11	
Yekatit 14	21-Feb	703.97	849.05	846.67	854.97	838.86	873.02	
Yekatit 15	22-Feb	704	848.9	846.49	854.69	838.49	872.84	

Yekatit 16	23-Feb	703.92	848.75	846.26	854.46	838.27	872.65	
Megabit 13	22-Mar	702.64	845.22	840.65	847.5	830.24	868.15	
Megabit 14	23-Mar	703.05	845.08	840.47	847.16	830.01	867.96	
Megabit 15	24-Mar	703.3	844.94	840.27	846.9	829.73	867.78	
Megabit 16	25-Mar	703.7	844.83	840.08	846.62	829.47	867.68	
Megabit 17	26-Mar	704.23	844.7	839.94	846.4	829.2	867.52	
Megabit 18	27-Mar	704.55	844.54	839.78	845.9	828.88	867.33	
Megabit 19	28-Mar	704.89	844.27	839.6	845.62	828.61	867.15	
Megabit 20	29-Mar	705.05	844.27	839.41	845.27	828.3	867.01	
Megabit 21	30-Mar	705.16	844.13	839.16	845.04	828.06	866.88	
Megabit 22	31-Mar	705.26	843.95	839.05	844.72	827.8	866.7	
Megabit 23	1-Apr	705.45	843.74	838.86	844.5	827.66	866.47	
Megabit 24	2-Apr	705.59	843.04	838.69	844.18	827.34	866.43	
Megabit 25	3-Apr	705.64	843.38	838.54	843.9	827.08	866.11	
Megabit 26	4-Apr	705.64	843.2	838.35	843.59	826.85	866.06	
Megabit 27	5-Apr	705.43	843.04	838.17	843.41	826.63	865.93	
Megabit 28	6-Apr	705.34	842.86	837.98	843.23	826.36	865.66	
Megabit 29	7-Apr	705.1	842.66	837.78	842.92	826.1	865.48	
Megabit 30	8-Apr	704.93	842.49	837.64	842.83	826	865.35	
Miazia 1	9-Apr	704.76	842.29	837.42	842.7	825.72	865.16	
Miazia 2	10-Apr	704.81	842.11	837.15	842.42	825.5	864.99	
Miazia 3	11-Apr	704.72	841.95	836.93	842.19	825.18	864.71	
Miazia 4	12-Apr	704.64	841.79	836.7	841.93	824.96	864.53	
Miazia 5	13-Apr	704.66	841.58	836.46	841.6	824.7	864.38	
Miazia 6	14-Apr	704.54	841.44	836.25	841.42	824.6	864.17	
Miazia 7	15-Apr	704.75	841.34	836.04	841.2	824.41	864.08	
Miazia 8	16-Apr	706.07	841.21	835.87	840.93	824.19	864.09	
Miazia 9	17-Apr	708	841.12	835.68	840.61	824.01	863.9	

Miazia 10	18-Apr	709.18	841.08	835.52	840.44	823.82	863.76	
Miazia 11	19-Apr	709.83	840.98	835.35	840.12	823.57	863.99	
Miazia 12	20-Apr	710.16	840.87	835.18	839.89	823.47	863.85	
Miazia 13	21-Apr	710.46	840.76	834.98	839.63	823.2	863.76	
Miazia 14	22-Apr	710.74	840.81	834.79	839.4	822.85	863.94	
Miazia 15	23-Apr	710.96	840.7	834.6	839.17	822.6	863.72	
Miazia 16	24-Apr	711.04	840.55	834.45	838.9	822.37	863.67	
Miazia 17	25-Apr	711.12	840.4	834.21	838.59	822.2	863.58	
Sene 17	24-Jun	759.43	838.56	825.5	831.37	824.93	864.85	
Sene 18	25-Jun	760.61	838.61	825.37	831.5	825.35	864.85	
Sene 19	26-Jun	761.59	838.65	825.28	831.6	825.73	864.93	
Sene 20	27-Jun	762.98	838.65	825.19	831.77	826.03	865.12	
Sene 21	28-Jun	763.93	838.63	825.12	831.91	826.31	865.21	
Sene 22	29-Jun	765.18	838.58	825.09	832.13	826.63	865.39	
Sene 23	30-Jun	766.46	838.65	825.02	832.4	827.1	865.57	
Sene 24	1-Jul	768.19	838.65	825.1	832.67	827.49	865.74	
Sene 25	2-Jul	769.8	838.68	825.13	832.94	827.75	865.93	
Sene 26	3-Jul	771.13	838.7	825.27	833.17	828.41	866.2	
Sene 27	4-Jul	772.25	838.75	825.25	833.22	828.88	866.51	
Sene 28	5-Jul	773.19	838.9	825.2	833.3	829.45	866.7	
Sene 29	6-Jul	773.9	838.99	825.13	833.35	829.92	867.06	
Sene 30	7-Jul	774.71	839.43	825.12	833.48	830.42	867.29	